

博士論文

Investigation on the Formation of Active Site for deNO_x

Reactions over Cu-Zeolites with Several Topologies

(種々の骨格構造を有する銅ゼオライト上における

脱硝反応活性点の形成に関する研究)

Yusuke Ohata

大島 悠輔

The University of Tokyo

School of Engineering

Department of Chemical System Engineering

東京大学大学院

工学系研究科化学システム工学専攻

2021

Supervisor

Professor Masaru Ogura

*A Dissertation Submitted in Partial Fulfillment of the Requirements
for the Degree of Doctor of Philosophy*

Dissertation Committee:

Masaru OGURA, Ph. D. (Supervisor)
Professor, Department of Chemical System Engineering
Institute of Industrial Science
The University of Tokyo

Akira NAKAYAMA, Ph. D.
Professor, Department of Chemical System Engineering
The University of Tokyo

Toru WAKIHARA, Ph. D.
Professor, Department of Chemical System Engineering
Institute of Engineering Innovation
The University of Tokyo

Masashi OKUBO, Ph. D.
Associate Professor, Department of Chemical System Engineering
The University of Tokyo

Atsushi SATSUMA, Ph. D.
Department of Materials Chemistry
Nagoya University

Preface

Cu contained zeolite (Cu-zeolites) is a class of catalytic material that can effectively activate small molecular such as NO, O₂, and CH₄, and catalyze reactions with high difficulty without using rare elements. The reactions catalyzed by Cu-zeolites effectively can be listed such as direct decomposition of NO into N₂ and O₂, methane selective oxidation into methanol by O₂ as oxidant, selective catalytic reduction of NO_x by hydrocarbon as reducing agent (HC-SCR), and selective catalytic reduction of NO_x by ammonia as reducing agent (NH₃-SCR). The former two reactions are extremely difficult and sometimes called as “dream reactions”, and the last one is practically applied to the abatement of harmful NO_x from diesel engines owing to the distinguish reaction rates. Thus, the continuous studies on Cu-zeolites have been conducted as long as half a century with alteration of the targeted reactions.

The common origin of attractive reactivity of Cu-zeolites for several reactions has been thought as the redox property of Cu ion in the zeolite micropores between monovalent and divalent. The relationship between the reactivity and property of Cu species are relatively well understood. However, the effects of zeolites in the control of properties of Cu species are still missing. As a result, it is well known that the suitable zeolite topologies for each reaction are different, however, the origin of relationship between reactivity and zeolite structure is still missing. Thus, rational creation of the Cu-zeolite catalysts suitable for targeted reactions are quite difficult and guiding principles to cause the breakthrough to overcome the drawbacks in the current best catalysts are lacking.

In this context, this thesis presents a fundamental understanding on the role of zeolites for generation of the Cu species for several deNO_x reactions. To achieve the subject, the author first suggested a method to conduct the comparative study for model Cu-zeolites with including several topologies. Second, the author combined tuned reaction conditions and related *in situ* spectroscopic analysis, and successfully grasped the characteristic of Cu species on each model zeolite related to the reactivities. At last, it was shown that the origin of difference in the Cu species on each zeolite can be explained by the type and arrangement of ion-exchange sites of zeolites.

The present thesis has been conducted during 2016–2021 at Department of Chemical System Engineering, Graduate School of Engineering, The University of Tokyo under supervision of Professor Masaru Ogura. Part of this work was conducted under

direction of Professor Ken-ichi Shimizu at Hokkaido University and Associate Professor Toshiyuki Yokoi at Tokyo Institute of Technology.

At first, the author wishes to express his sincerest gratitude to Professor Masaru Ogura for his invaluable direction, profitable suggestions, flexible negotiation to co-working groups or companies, and continual encouragements. The author could have valuable experiences and become proficient at variable techniques during this work owing to his cheerful dispatch to experiments in several institutions and discussions with researchers working in several fields. The author thanks to Dr. Takeshi Ohnishi for guidances on the experiments and valuable comments during this study. The reaction tests and quantitative assessment of the reactants in Chapter 3 and 4 would be impossible without his coaching. The author is deeply grateful to Assistant Professor Takahiko Moteki for construction of pulse reactor used in Chapter 5, advices for writing and editing the articles, and valuable comments from experiences on zeolite synthesis and kinetic analysis. Construction of the discussion in Chapter 2 would be impossible without his comments in lab seminar. The author would like to thank secretary, Ms. Junko Torii for her warm encouragements, kind supports in daily life, and documental procedures during the work in the laboratory. The author appreciates to the former technical staffs, Mses. Yumiko Shimada and Naoko Ito for their guidances for the experiments and maintenance of the equipment. The author is grateful to all the students of the laboratory led by Professor Ogura. The author wishes to present special thank to Mr. Shohei Harada, who is a senior of the laboratory the author belongs to, for his comprehensive master works that construct the foundation of the present work and cheerful working as a colleague as the Ph. D student in the last 1 year. The author is indebted to Mr. Yuuki Koga for his assistance in CHNS elemental analysis. The author deeply thanks to Dr. Kiyoyuki Yamazaki and Dr. Choi Jihye, who were his senior as the Ph. D students in the laboratory, to gave some viewpoints on how to behave in doctoral course. The author also makes an acknowledgement to Messrs. Ken Watanabe, Kai Hidaka, Tatsuya Muramatsu, Naoto Tominaga, Tomohiro Imaseki, Tomohiro Sei, Jiachen Ge, Leo Takahashi, Takahiro Kimura, Shyunsuke Hayashi, Mses. Aisa Kawano, Jing Ma, and Chuang Liu for delightful times in the laboratory. The author would like to express his gratitude to the visiting researchers and students during the study, Dr. Sundaravel Balachandran, Dr. Yuxi Gao and Ms. Yanling Gan, for their co-working in the field of environmental catalysts. The author would like to give a gratitude to the alumni of the laboratory, especially Messrs. Keiichiro Watanabe, Taku Hasegawa, Koutarou Kawakami, Yutaro Furukawa, Kohei Kamatani, and Yasuhiro Kobatake

for their encouragements in the home coming days.

The author would like to express his appreciation to the dissertation committee members, Professor Akira Nakayama, Professor Toru Wakihara, Associate Professor Masashi Okubo, and Professor Atsushi Satsuma. Their fruitful comments and discussion gave the author new and wide viewpoints that improve the positioning of the present thesis.

The author is deeply grateful to all of the co-researchers in several institutions for their helps in accomplishment of the present work.

The author would like to thank Mr. Yutaka Yanaba in the Institute of Industrial Science, The University of Tokyo for the assistance in solid-state NMR measurements and analysis.

The author would like to express his appreciation to Assistant Professor Kenta Iyoki in the Okubo-Wakihara laboratory in the University of Tokyo for access to an ICP-AES measurement. His kind and cheerful attitudes always encourage the author to enjoy research. The author is indebted to Ms. Makiko Deguchi and Mr. Naomichi Hikichi for their assistance in ICP-AES measurement. The author is grateful for the members of the Okubo-Wakihara laboratory, Professor Tatsuya Okubo, Assistant Professor Zhendong Liu, Dr. Jie Zhu and Mr. Yuki Sada for their warm supports during the ICP-AES measurements or seminars.

The author thanks to Associate Professor Toshiyuki Yokoi and former Project Assistant Professor Toshiki Nishitoba (present affiliation: National Institute of Advanced Industrial Science and Technology) in the Institute of Innovative Research, Tokyo Institute of Technology, for the measurements of FT-IR spectra and fruitful discussions. Without their pleasant permission and kind supports in the continuous visiting experiments, the shape of present thesis would be completely different. The author also makes an acknowledgement to the members of the Yokoi group, Dr. Sungsik Park, Dr. Ryota Osuga, Dr. Yusuke Kunitake, Dr. Shuhei Yasuda, Messrs. Gakuji Sato, Willie Yang and Kengo Nakamura for their fruitful discussions in conferences, kind supports and joyful dinner during the visiting experiments.

The author would like to express his special appreciation to Professor Ken-ichi Shimizu in Institute for Catalysis, Hokkaido University for his kind and patient directions, continuous discussions, and various suggestions during the execution of Chapter 3. It's not too much to say he is a co-supervisor for the author. The author makes an acknowledgement to the members of the laboratory led by Professor Shimizu. The author owes his gratitude to Assistant Professor Takashi Toyao and Ms. Hiroe Kubota for their kind supports and fruitful discussions from the viewpoints of skilled researchers on *operando* measurements during

visiting experiments and editing the manuscript related to Chapter 3. The author would thank to the members in Shimizu group, Associate Professor Shinya Furukawa, Lecturer Zen Maeno, Dr. Grazia Malta, Messrs. Shunsaku Yasumura, Shingo Kayamori and Yuki Nakaya for kind supports, joyful dinner during the visiting experiments, and excellent works.

The author makes an acknowledgement to the members of the laboratory led by Professor Kazuya Yamaguchi, which is the previous affiliation of the author, at Department of Applied Chemistry, Graduate School of Engineering, The University of Tokyo. Without the training by Dr. Takuo Minato (present affiliation: Kyushu University) and Associate Professor Kosuke Suzuki during the period of undergraduate student for the author, accomplishment of this work would be impossible. The continuous warm and humorous on-line encouragements by Dr. Kento Taniguchi (present affiliation: Nippon Shokubai Co., Ltd.), who was a senior of both the laboratory and a preparatory school, raised the motivation to struggle the study. The author owes his gratitude to Assistant Professor Takafumi Yatabe and Professor Kazuya Yamaguchi for the fruitful discussions provided in a conference to gave the author some guidance to enrich the contents of this thesis (Especially in Chapter 4).

This work was supported, in part, by the Cooperative Research Program of Institute for Catalysis, Hokkaido University (grant no. 19B1020).

Finally, the author wish to thank his family for their enduring supports, warm encouragement and deep understandings on his works.

Yusuke Ohata

Meguro, Tokyo
December, 2020

Preface

1. General introduction ·····	1
1.1. NO _x abatement reactions·····	2
1.2. Application of metal zeolites as catalysts for NO _x abatement reactions·····	7
1.3. Application of Cu-zeolites·····	12
1.4. Objectives of this thesis·····	18
1.5. Outline of this thesis·····	20
References·····	21
2. Insight into ion-exchange property of zeolites ·····	29
2.1. Introduction·····	30
2.2. Methods·····	31
2.2.1. Definition of cation density in micropores·····	31
2.2.2. Selection of model zeolites with several topologies·····	32
2.3. Experimental·····	36
2.3.1. Materials·····	36
2.3.2. Na ion-exchange of zeolites·····	36
2.3.3. Cu ion-exchange of zeolites·····	36
2.3.4. Characterization of parent zeolites·····	36
2.4. Results and Discussion·····	38
2.4.1. Properties of parent zeolites in this work·····	38
2.4.2. Ion-exchange properties of the CHA zeolites·····	39
2.4.3. Cu ion-exchange properties of the zeolites in this work·····	41
2.5. Conclusions·····	46
References·····	47
3. Investigation on the formation of active site for NH₃-SCR over Cu-Zeolites with several topologies ·····	51
3.1. Introduction·····	52
3.2. Experimental·····	56
3.2.1. Catalytic activity test for NH ₃ -SCR·····	56
3.2.2. Quantitative analysis of reactants consumed during transient measurements··	56
3.2.3. <i>In situ</i> UV-Vis measurements·····	57

3.3.3. <i>In situ</i> IR measurements	58
3.3. Results and Discussion	59
3.3.1. Cu ion exchange level dependence of catalytic activities for NH ₃ -SCR	59
3.3.2. Reaction rates for low-temperature NH ₃ -SCR with similar cation densities in micropores	61
3.3.3. Reduction and oxidation behaviours of Cu ion species during transient reactions	64
3.3.4. Relationship between the Cu oxidation rate under transient conditions and the NH ₃ -SCR rate	76
3.3.5. Distribution of Cu ²⁺ species on zeolites	80
3.3.6. Nature of ion-exchange sites on zeolites	86
3.4. Conclusions	89
References	90

4. Dependence of reaction rates for NH₃-SCR over Cu-Zeolites with several topologies

on O₂	95
4.1. Introduction	96
4.2. Experimental	98
4.3. Results and Discussion	99
4.3.1. A dependence of O ₂ pressure on NH ₃ -SCR rates per Cu over a reference Cu-SSZ-13 catalyst	99
4.3.2. The dependence of O ₂ pressure on NH ₃ -SCR rates per Cu over Cu-zeolite catalysts with several topologies	102
4.3.3. The behavior of low pressure apparent O ₂ order for NH ₃ -SCR rates per Cu over Cu-zeolite catalysts with several topologies along with Cu density in micropores	106
4.4. Conclusions	108
References	109

5. Investigation on the formation of active site for NO direct decomposition over

Cu-Zeolites with several topologies	111
5.1. Introduction	112
5.2. Experimental	116

5.2.1. Catalytic activity test	116
5.2.2. <i>In situ</i> IR measurements	116
5.3. Results and Discussion	117
5.3.1. Correlation between ion-exchange level of Cu-zeolites and catalytic activity	117
5.3.2. NO probe IR measurement	119
5.3.3. Origin of Framework Effects on Active Site Formation	124
5.4. Conclusions	117
References	128
6. General conclusions and future perspectives	131
6.1. General Conclusions	131
6.2. Future Perspectives	137
Appendix	137
A1. Effect of Zeolite Topology on Reaction Rate for NH ₃ -SCR at 473 K	
– MOR and CHA Zeolites with a Similar Si/Al Ratio	140
A2. Effect of Si/Al Ratio on Reaction Rate for NH ₃ -SCR at 473 K	
– CHA, MFI, and *BEA Case	144
References	146
List of Publications	147

Chapter 1

General Introduction

1.1. NO_x abatement processes

Nitrogen Oxides (NO_x) are one of the most major air pollutants that cause photochemical smog and acid rain^[1]. Moreover, they can harm human respiratory^[1]. NO_x forms in combustion processes with high temperature and pressure conditions because the O₂ can react with N₂ in air or nitrogen species in fuels^[2]. The majority of NO_x is NO that forms by the oxidation of N₂ by O₂ (Thermal NO_x)^[1]. Thus, unlike the formation of Sulfur Oxides (SO_x), which are also the major air pollutants generated from combustion processes but whose emission can be reduced by desulfurization of the fuels^[3], the formation of NO_x is unavoidable as long as the atmosphere of the earth contains N₂. Therefore, the formed NO_x should be purified by the post-treatments^[4]. A lot of processes to reduce the amount of NO_x emitted from the combustion processes have been developed. The backgrounds of such processes can be classified by two phenomena – adsorption and reaction.

The adsorption process is mainly adopted for low temperature NO_x abatement^[5]. The adsorption is an exothermic process. During the isothermal adsorption, the entropy of the system decreases ($\Delta S < 0$) due to the decrease of flexibility in molecular dynamism. Moreover, this process proceeds spontaneously; therefore, the change in Gibbs energy should be minus ($\Delta G < 0$). As a result, to make the following equation of thermodynamics work, the change in the enthalpy should be minus ($\Delta H < 0$).

$$\Delta G = \Delta H - T\Delta S$$

Due to the nature described above, the adsorption is a favorable process in low temperature condition. The complete purification of NO_x is impossible to achieve by adsorption itself. However, the catalysts for deNO_x reactions described in the following section do not function appropriately in the low temperature region. Therefore, application of the adsorption process to storage NO_x until a higher temperature is an effective way to reduce the emission of NO_x.

The reaction process needs relatively high temperature to achieve because it needs a certain extent of activation energy, although it can eliminate the harmful NO_x completely by converting to harmless compounds. Catalysts have played a central role in the reaction processes for NO_x abatement to facilitate the reactions by reducing the activation energy. The catalysts for such processes are in a family of “Environmental Catalysts”, which are used to reduce the emissions of environmentally harmful compounds^[6]. From the practical point of view, environmental catalysts should fulfill several requirements to maintain high reaction rate for a long period in wide reaction conditions (*e.g.*, temperature region, concentration of NO_x and other compounds, and space velocity) that match with the emission of targeted

combustion processes. Figure 1.1 summarizes the requirements for environmental catalysts proposed by Misono^[7].

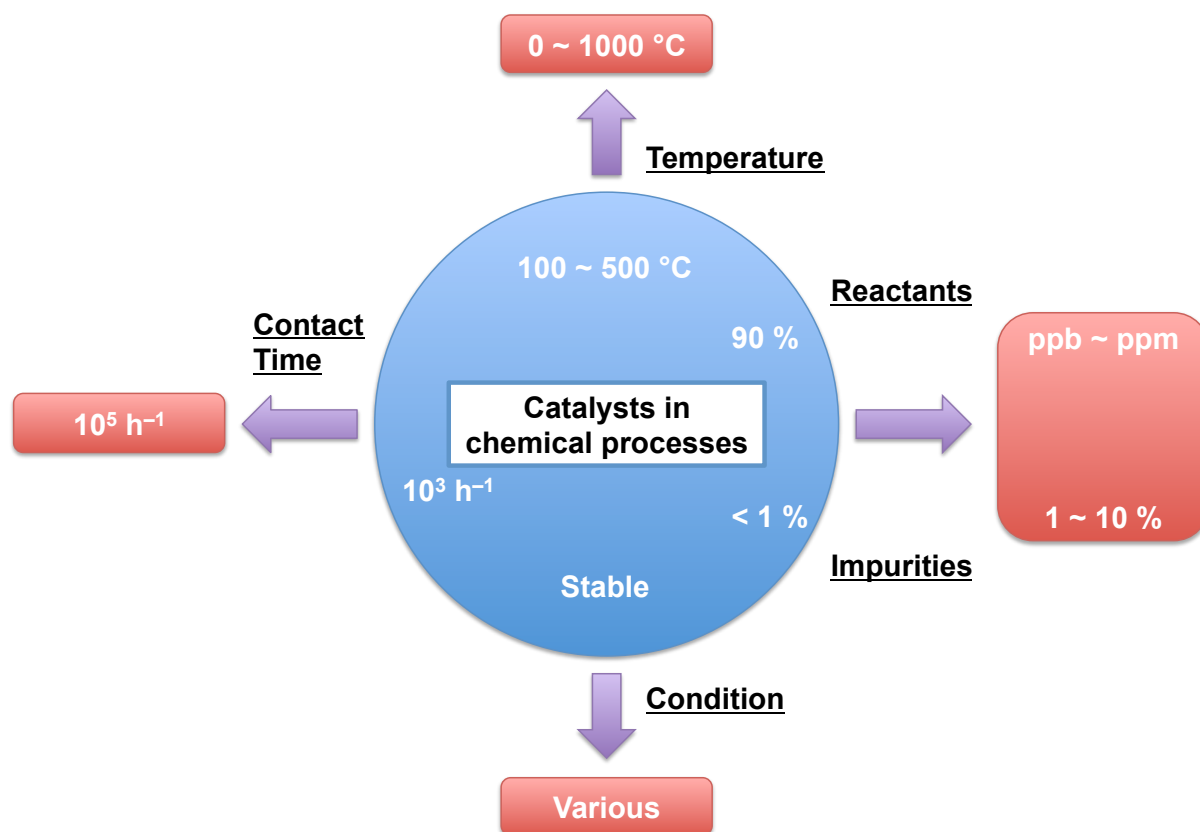


Figure 1.1. Reaction condition for environmental catalysts.^[7] The center blue cycle and outer red squares show the reaction condition for catalysts in chemical processes and environmental catalysts, respectively.

Moreover, considering the increasing demands for precious metals such as Pt, Pd, and Rh^[8], it has been desired to develop such the catalysts by using small or no amount of precious metals, whose supplement is unstable due to the small production amount or uneven distribution on earth. Therefore, continuous studies to develop the catalysts that fulfill social requests for several NO_x abatement reactions shown in the following sections have been conducted.

The main part of all reactions for NO_x abatement is to reduce the N atoms with positive oxidation numbers to the N₂ molecular with oxidation number of 0. Difference in the reactions occurs in the treatment of O atoms with oxidation number of -2.

The reaction that contains the oxidation of O atoms to O₂ with oxidation number of 0 is the direct decomposition of NO_x. Considering the large and positive enthalpy of

formation for NO ($\Delta H_{f(273\text{ K})}^0 = 90.2\text{ kJ mol}^{-1}$), the decomposition of unstable NOx into O₂ and N₂ is thermodynamically favorable^[9,10]. It is known that this reaction exhibits a highly negative Gibbs free energy change ($\Delta_r G_m = -86.6\text{ kJ mol}^{-1}$)^[9,10]. However, this reaction, which contains the formation of O₂ molecule with triplet ground spin state, is spin-forbidden and needs high activation energy ($\sim 335\text{ kJ mol}^{-1}$) without catalysts^[11,12]. Therefore, this reaction is kinetically slow and suitable catalysts are needed to make progress. This is the most desirable process to remove the NOx because no reducing agents are needed, however, the oxidative desorption of O atoms from the catalyst surface is difficult and the effective catalyst for this reaction is still missing. Toward the high and stable reaction rate, several catalysts including perovskite-type oxides, rare earth oxides, alkali or alkaline earth metal-doped cobalt oxide, barium supported rare earth oxides, precious metals supported metal oxides, and Cu-ZSM-5 zeolite have been reported.^[11,12] However, most catalysts suffer from high reaction temperature due to the slow reaction rate, inhibition by coexisting gasses such as O₂, H₂O, and SO₂, and low durability of the supports. Therefore, although the materials that proceed this reaction are known since the early 20th century^[13], it has not been applied to the real processes. Among the reported catalysts for the direct decomposition of NOx, Cu-ZSM-5 zeolite catalyst exhibits extremely high reaction rate in relatively low temperature region around 500 °C (Figure 1.2) though it suffers from deactivation by coexisting gasses and easy degradation of ZSM-5 zeolite at high temperature hydrothermal condition^[11].

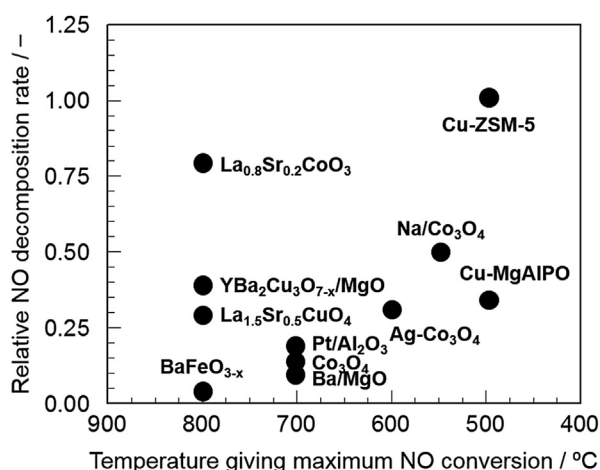


Figure 1.2. Comparison of the reaction rate over reported various catalysts for direct decomposition of NO.^[11]

Recently, as a suggestion for efficient use of high activity of Cu-ZSM-5 catalyst for NO direct decomposition and enhancement of its lifespan by reducing average surrounding temperature, a two-step catalytic system including low-temperature concentration of NO and reaction by rapid heating using microwave is reported.^[14,15] It is achieved by this catalytic system that reaction with low inhibition by O₂ or H₂O coexistence in reaction feed.^[14,15] It is needed to confirm the long-term activity or durability of catalyst on the system toward the real-world application, however, it is suggested that the designated reaction condition can expand the possibility of catalysts for NO direct decomposition toward the application.

In the real-world processes, the reactions that contain the emission of O atoms as a part of molecule such as H₂O or CO₂, with oxidation number keeping to -2. In these reactions, some reducing agents should be added for catalytic reduction of N atoms to N₂ molecular selectively and they are called “selective catalytic reaction (SCR)”. These reactions are classified by the added reducing agents such as H₂, unburned hydrocarbons (HC) contained in fuels, and NH₃^[16]. The SCR using NH₃ as a reducing agent (NH₃-SCR) is one of the oldest reaction that is in commercial application since 1977^[17]. The NH₃ had been thought as a unique reducing agent under coexistence of excess O₂ in the feeds and applied in real world for removal of NO_x emitted from stationary plants. As the catalyst in this process, vanadium and/or tungsten supported TiO₂ have been used^[2]. NH₃-SCR over proper catalysts exhibits reaction rate sufficient for application. However, unlike the stationary plants, application of this reaction to on-road vehicles had been avoided for a long time due to several problems. It is reported that approximately the 20 % of global NO_x emissions are from on-road diesel vehicles.^[18] The emission from diesel vehicles with lean-burn engine contains excess amount of O₂. Therefore, the application of NH₃-SCR can be regarded as a rational method for removal of NO_x. One problem to the application was the use of toxic NH₃^[19]. Moreover, the emission of vanadium with low hydrothermal durability and toxicity into atmosphere was also the concern for application of NH₃-SCR into on-road vehicles. However, current main process in the deNO_x reaction for diesel vehicle emission is urea-SCR that uses the non-toxic urea as NH₃ source and metal-zeolite as catalyst^[20]. The detail of such the catalysts for NH₃-SCR will be mentioned in the Section 1.3. In these backgrounds, development of the catalytic processes for removal of NO_x from exhausts of lean-burn automotive engine including diesel engine has been a large issue for a long time.

HC and CO can be used as reducing agents for NO_x in the absence of O₂, which is typical in the exhaust from the engines with stoichiometric combustion. For the NO_x

purification process from the exhausts with such composition, three-way catalysts (TWC) using noble metals have been adopted from 1970s^[21]. In the viewpoint of NO_x abatement, the reaction over TWC can be regarded as the selective reduction of NO_x into N₂ by HC and CO reducing agents. It is impossible for TWC to reduce NO_x efficiently in O₂ rich atmosphere, therefore, they can use only for the exhausts with stoichiometric combustion under support of O₂ concentration control systems. TWC consumes large amount of platinum group metals (PGMs; Pt, Pd, and Rh), therefore, autocatalysts have occupied the largest share in the demand of PGMs^[8]. Considering the increasing demand and insecurity supplement for PGMs, recent goal for development of TWC is to reduce or replace of PGMs with maintaining the catalytic activity and durability (*i.e.*, “intelligent catalyst” using Pd-perovskite^[22]).

In the case of the exhausts containing excess amount of O₂, HC have been recognized as the non-selective reducing agent for NO_x. However, in 1990, Iwamoto *et al.*^[23] and Held *et al.*^[24] independently reported that selective catalytic reduction of NO with HC in an O₂ rich atmosphere proceeds over Cu-zeolite catalysts. Since the breakthrough findings, HC-SCR catalysts by using several HCs have been studied until early 2000s^[25]. This process has advantage that no additional reducing agents from outlet are required, however, there were drawbacks on durability of catalysts and reaction rates in low temperature region; therefore, application in real-world was limited^[26].

Lean NO_x trap (LNT) technology by combination of storage materials using alkali elements (typically Ba²⁺ or CeO₂) and oxidation catalysts using PGMs^[27] can be regarded as one derivation of HC-SCR in non-steady-state reaction condition. This family of catalysts oxidates NO_x into NO₃⁻ over oxidation catalysts and concentrates NO₃⁻ on storage materials in lean condition with excess O₂ flow. The stored NO₃⁻ exhibits higher reactivity than NO_x. Therefore, they react with unburned fuel remaining in exhausts during the rich conditions and reducible removal is achieved.

Hydrogen (H₂) is the reducing agent that can react with NO at low temperature as low as 373 K and can be contained in exhausts from rich-burn combustion processes^[28]. Therefore, the SCR using H₂ as a reducing agent (H₂-SCR) has advantage in low temperature activity and no additional reducing agents from outlet. As the catalysts for this reaction, precious metal loaded catalysts on which the dissociative adsorptions of H₂ easily occur^[28,29]. However, in the presence of excess O₂, the selectivity can be decreased by the combustion of H₂ by O₂. Moreover, the selectivity of products into N₂ is low due to the formation of N₂O. Because of these drawbacks, H₂-SCR is not applied in real-world process.

1.2. Application of metal zeolites as catalysts for NOx abatement reactions

Zeolites are crystalline porous materials with high surface area and cation exchange properties^[30,31]. Metal-loaded zeolites (Metal zeolites) are prepared by ion-exchange of metal cation into the extraframework or introduction of metal species into the innerframework^[32]. Metal zeolites can contain highly depressed active metal species on the surface of stable solid oxides with high surface area. Moreover, the micropore of the zeolites with molecular size (Å order) makes it easy to concentrate the small molecular such as NOx or reducing agents (*e.g.*, NH₃, HC). These features make the metal zeolites one of the most promising catalyst or adsorbent materials for the NOx abatement processes described above. Therefore, the metal zeolites for deNOx application have been studied for as long as half a century^[16]. However, the highlighted process has been changed with progress of the period.

Since the mid 1980s to late 1990s, the NO direct decomposition over Cu-zeolites was deeply investigated. It was shown that Cu-Y zeolite with FAU topology desorbs large amount of O₂ in relatively low temperature region (~ 573 K) by O₂-TPD technique^[33]. By using this feature of Cu-zeolites, the application of Cu-Y zeolite as catalyst for NO direct decomposition was first reported in 1981^[34]. Later, Cu-MFI zeolites with excessively ion-exchanged ones have been shown to exhibit quite high catalytic activity in the wide temperature region (623–873 K)^[35]. However, due to the low stability of the MFI zeolites, their application in the real-world was not achieved. Moreover, the deactivation of the catalyst caused by cofeed of O₂, H₂O, and SO₂ was known^[35]. Since the effective ways to overcome these drawbacks were not found, the main issue for studies on metal zeolites as deNOx catalysts were gradually changed to HC-SCR.

A lot of metal zeolites were studied intensively toward the application for the HC-SCR catalyst^[25,36]. Before the discovery of the HC-SCR over Cu-zeolite catalysts^[13,14], HC was thought as the non-selective reductant for NOx. This reaction was first reported by Iwamoto *et al.*^[23] and Held *et al.*^[24] independently. It was reported that by coexistence of NOx, the oxidation rates of the HCs increased in temperature region and the reduction rate of NOx increased by coexistence of O₂^[23]. This reaction was expected as an application to the deNOx process in O₂ rich exhausts without additional reducing agents, because the HCs contained in fuel can be used as reducing agents for NOx. Not only the Cu-zeolites, but also the other metal zeolites could be used as catalysts for this reaction and it was revealed that the different reactivity to the several HCs could be achieved by the alteration of metal species. Additional to the metal species, several oxides for catalyst supports were tested and it was

revealed that the HC-SCR proceeds over various types of metal oxides other than zeolites.^[37] Among the catalysts, it was shown that the zeolite-based catalysts exhibit high catalytic activity in wide temperature window and high selectivity of reducing agents into the NO_x reduction compared to the other oxide-based catalysts^[25,38]. Figure 1.3 summarizes the NO_x reduction performance of various catalysts for HC-SCR.^[25]

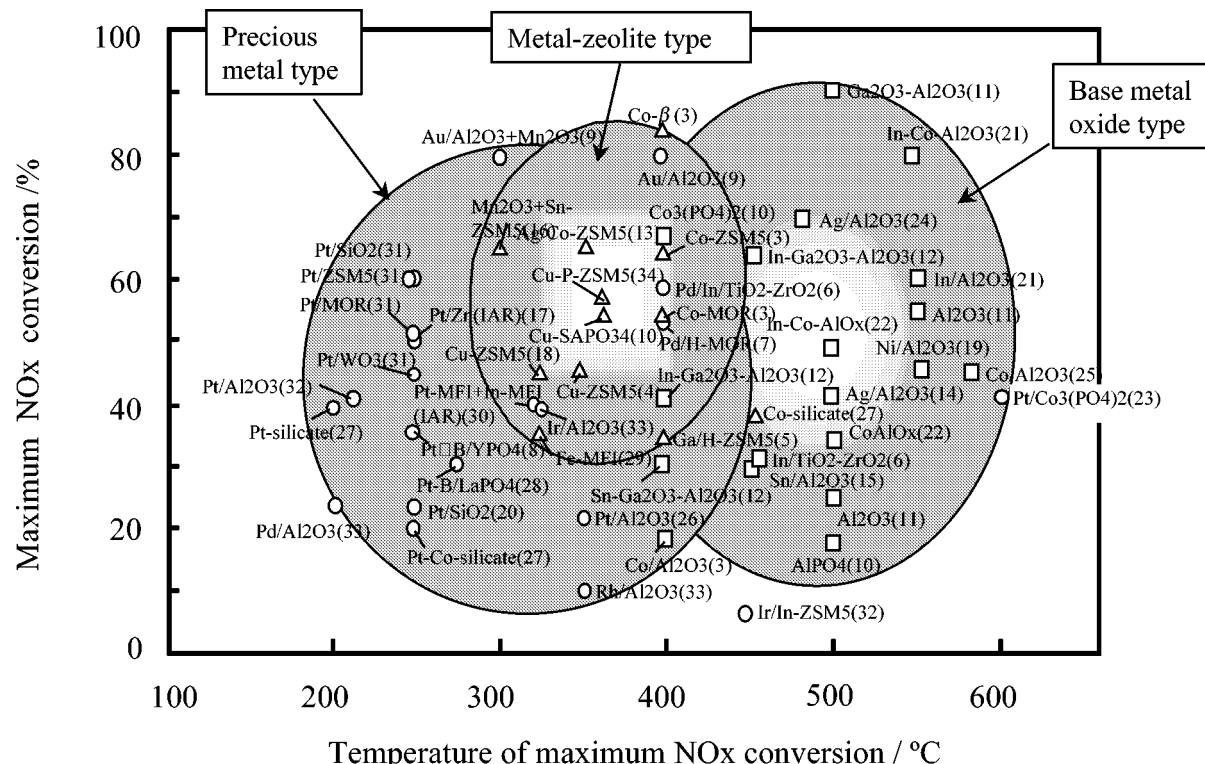


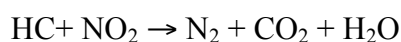
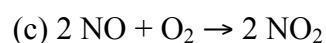
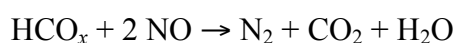
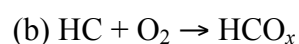
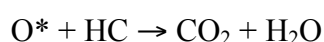
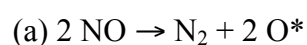
Figure 1.3. NO_x reduction performances of various catalysts for HC-SCR.^[25]

Table 1.1 shows the studied metal zeolites and main HCs used as reductant over them. As highlighted process, CH₄-SCR by Co^[39], Ga^[40], In^[40], and Pd^[41] contained zeolite catalysts can be explained. CH₄ is the HC with the lowest reactivity because of its high stability. It was shown that even such a stable reducing agent could be activated by the selection of metal species on zeolites.

Table 1.1. Active metal species on zeolites and their catalytic property for HC-SCR.

Element	HC	Positive feature	Negative feature	Ref.
H	C ₃ H ₈ , C ₃ H ₆	High selectivity to SCR	Poisoning by H ₂ O vapor	42
			Low activity	43
Mn	CH ₄	Low temperature activity	Low temperature window	44
Fe	<i>i</i> -C ₄ H ₁₀	Resistance to H ₂ O vapor	Difference in preparation	45
		Resistance to SO ₂ poisoning		
Co	CH ₄ , C ₃ H ₈	Resistance to H ₂ O vapor	Low activity	39
		Resistance to SO ₂ poisoning (C ₃ H ₈ -SCR)	Poisoning by H ₂ O vapor (CH ₄ -SCR)	46
Ni	CH ₄	Low temperature activity	Low hydrothermal stability	44
Cu	C ₂ H ₄	High availability of reductants	Low hydrothermal stability	23
		Wide temperature window		
Zn	C ₂ H ₄	High selectivity to SCR	Poisoning by H ₂ O	47
Ga	CH ₄ , C ₃ H ₈	High selectivity to SCR	Poisoning by H ₂ O	40
Rh	CH ₄	Low temperature activity	Low selectivity to N ₂	48
			Low hydrothermal stability	
Pd	CH ₄	Low temperature activity	Low hydrothermal stability	41
		Resistance to H ₂ O vapor		
Ag	C ₂ H ₄	Resistance to H ₂ O vapor	Requirement for NO oxidation	49
In	CH ₄	High selectivity to SCR	Poisoning by H ₂ O vapor	40
			Low activity in low temperature region	
Ce	C ₃ H ₆	High selectivity to SCR	Poisoning by H ₂ O vapor	50
Ir	C ₃ H ₆	High hydrothermal stability	Low selectivity to SCR	51
		High selectivity to N ₂		
Pt	C ₂ H ₄	Low temperature activity	Poisoning by H ₂ O vapor	52
		Resistance to H ₂ O vapor		

There are several mechanisms suggested for HC-SCR. When it is limited over the Cu-zeolites, the mechanisms can be listed as the following three categories: (a) N₂ formation and subsequent regeneration of the active site occurs by decomposition of NO and reaction with the HC, respectively, (b) reactive intermediates formation over active sites and subsequent reduction of NO occurs by partial oxidation of HC by O₂ and further oxidation of intermediates by NO, respectively, and (c) strong oxidant (*e.g.*, NO₂) formation over active sites and subsequent oxidation of HC by the oxidant occurs by oxidation of NO by O₂ and preferential reaction of HC with the oxidant compared with O₂. Scheme 1.1 summarizes the proposed mechanisms^[53].



Scheme 1.1. Suggested mechanisms for HC-SCR.^[53]

In those mechanisms, it is generally thought that the metal species work as active center playing a role in the formation of reactive intermediates to facilitate some reactions prefer to HC oxidation by O₂. Based on the screening and characterization studies, significant efforts were conducted to obtain the catalysts with practical activity and durability since the mid 1990s until mid 2000s. However, the application of HC-SCR over metal zeolites in real-world process was limited because of the low selectivity of HCs into the reaction, narrow temperature window around 573–673 K, inhibition by water vapor, and the low hydrothermal stability of zeolites available in this era^[38]. These features were not match to the condition of the exhausts from diesel engine.

The application of the metal zeolites for the deNO_x catalysts was achieved in Urea-SCR, which is the part of NH₃-SCR that uses the non-toxic urea as NH₃ source^[20]. At first, Fe-zeolite catalysts were applied^[54] because they used no metal whose emission to the air was regulated^[55]. In the standard-SCR condition (NO/NO_x ~ 1), Fe-zeolite catalysts exhibit low reaction rate in the temperature region of exhausts of diesel engine (423–573 K), however, they exhibit high catalytic activity in wide temperature region for the fast-SCR

reaction ($\text{NO}/\text{NO}_2 \sim 1$) and high resistance to the sulfur poisoning^[54]. To achieve high reaction rates, SCR system for Fe-zeolite catalysts required oxidation catalyst for oxidation of the NO to achieve the fast-SCR condition. To overcome the low ion-exchange efficiency of Iron, several preparation procedures were tested. As a noteworthy procedure, the method to synthesis the Fe-beta zeolite with high crystallinity and large amount of Fe directly introduced into framework should be mentioned^[56–58]. In contrast to the Fe-zeolites, Cu-zeolites exhibit high catalytic activity for standard-SCR in low temperature region (423–573 K)^[54]. Due to this feature and the improvement of hydrothermal stability by application of small pore CHA zeolites^[59,60], application of the Cu-zeolites for NH_3 -SCR catalysts in real-world was achieved since early 2010s. Figure 1.4 shows the typical catalysts for the NH_3 -SCR and their features.

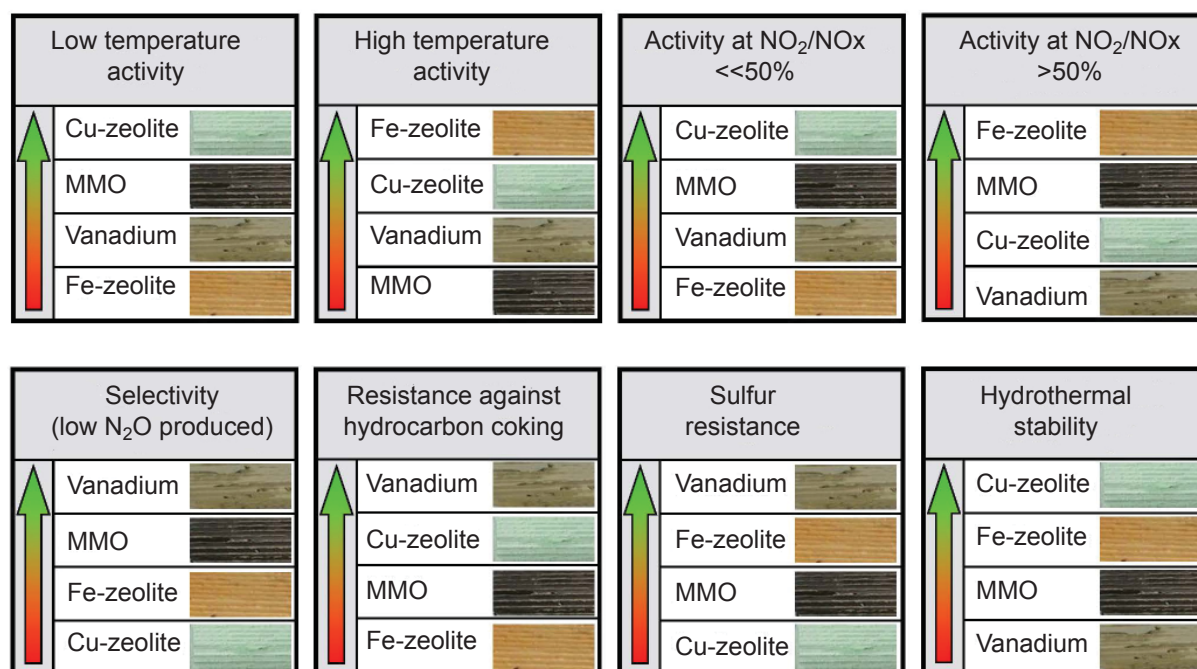


Figure 1.4. Typical catalysts for the NH_3 -SCR and their feature (MMO = mixed metal oxides)^[19].

Typically, the deNO_x catalysts such as TWC or NH_3 -SCR catalysts have light-off temperatures above 473 K^[54]. Therefore, achievement of enough NO_x conversion rate around 423 K is still difficult only by the reactions (cold-start problem). Moreover, it is difficult to form the NH_3 from the thermal decomposition of urea in this temperature region in the Urea-SCR technique. Therefore, to reduce the amount of NO_x emission in exhaust temperature region as low as 423 K, development of a novel technique using the adsorption

process called passive NO_x adsorber (PNA) is in progress since late 2010s. For the PNA material, Pd/zeolites with small pore structure are used^[61]. Pd species depressed in the zeolites adsorb NO_x even in the coexistence of CO or H₂O, which generally have higher affinity to the metal species with Lewis acidity^[62]. In the preparation procedure of Pd/zeolites, there is difficulty in introduction of the Pd cation with large ionic radii into the micropore of zeolites with small pore window and the creation of enough amounts of adsorption sites is challenging. Therefore, the development of introduction procedure is ongoing^[63].

Figure 1.5 summarizes the historical trends on application of metal zeolites for NO_x abatement processes.

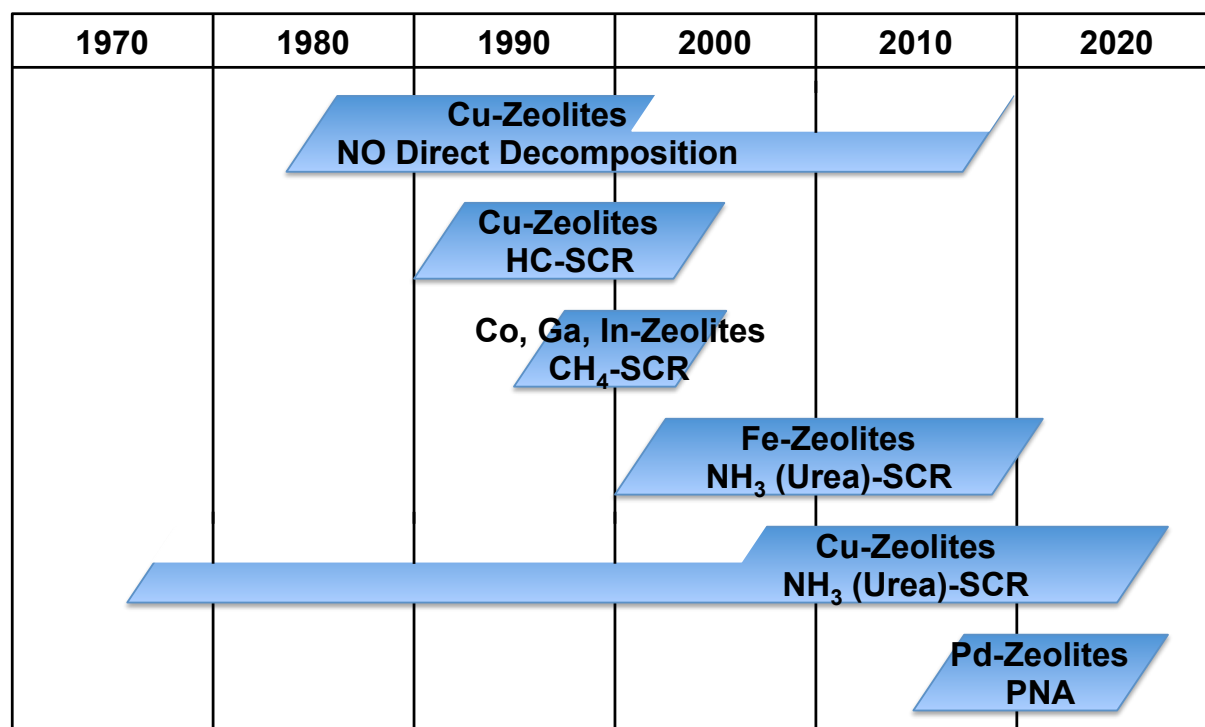
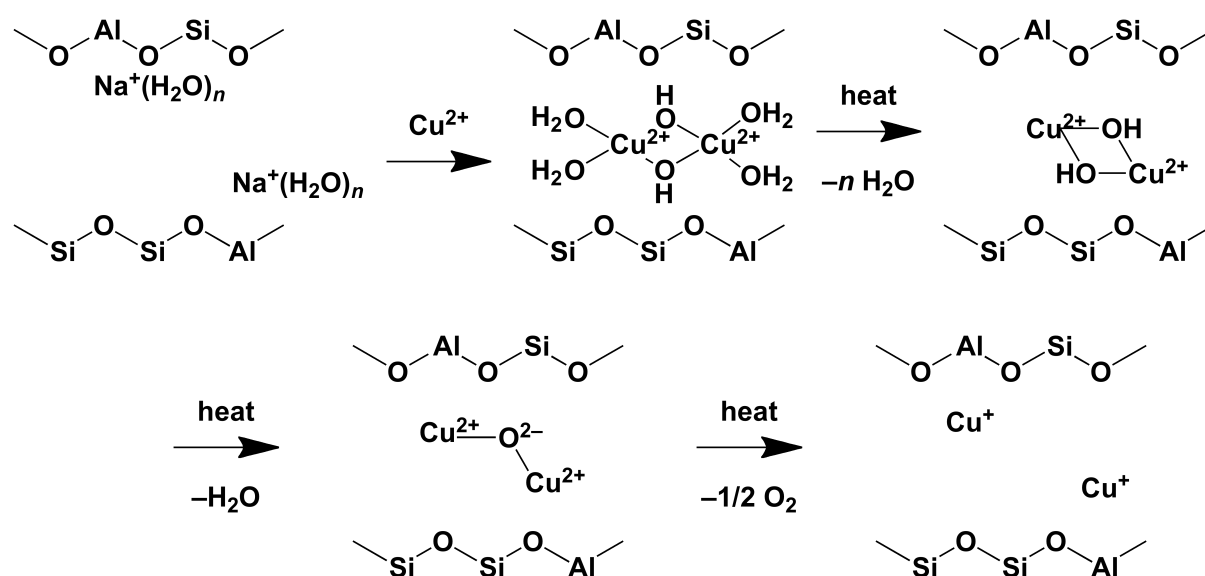


Figure 1.5. Historical trends of metal zeolites and their application to the NO_x abatement processes.

1.3. Application of Cu-zeolites

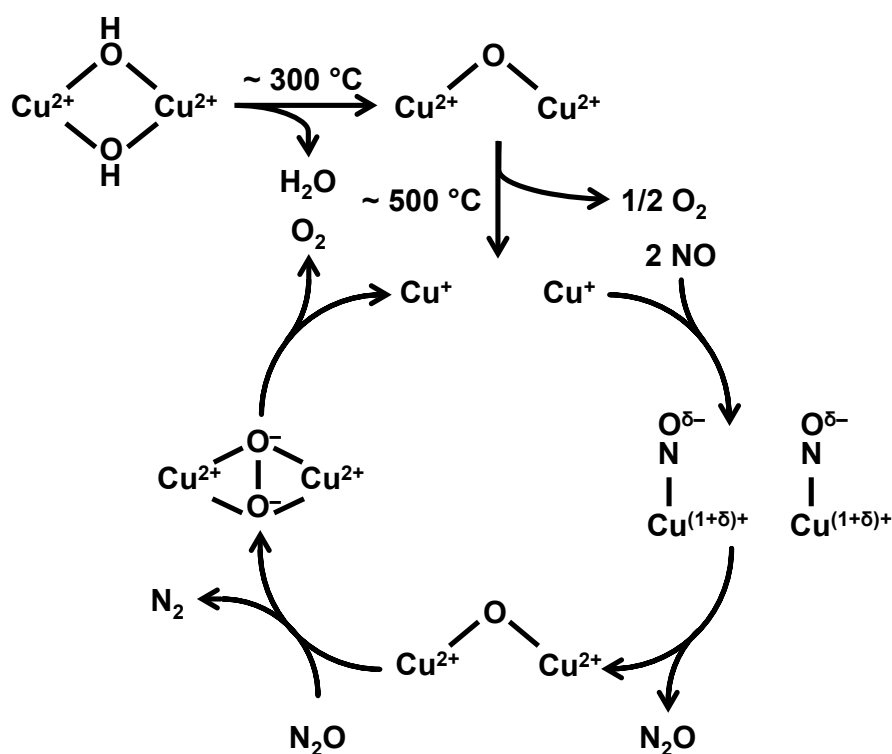
Among the metal zeolites, Cu-zeolites are one of the most fascinating materials. The active center of Cu-zeolites is copper, which is one of the most frequently applied metal in real-world. By the high dispersion of Cu species on zeolites, the catalytic activities of Cu-zeolites can be achieved by Cu content of less than 10 wt.%. Moreover, Cu-zeolites can catalyze a variety of redox reactions with high difficulty that sometimes called as “dream

ion-exchanged zeolites was suggested as Scheme 1.3.^[70]



Scheme 1.3. The total reaction mechanisms for the formation of dimeric Cu active species in zeolites speculated by Kuroda *et al.*^[70]

The contribution of Cu⁺ in the reaction was confirmed by the study using NO adsorbed IR spectroscopy combined with an isotopic tracer method^[71]. Existence of anionic NO adspecies on Cu⁺ and intensity decrease of the species with the reaction time according to the second order rate equation accompanying formation of N₂ was observed^[71]. Therefore, the active intermediates for NO direct decomposition was suggested as anionic NO adspecies on Cu⁺. By using *in situ* UV-Vis-NIR and EXAFS techniques, the formation of O-bridged Cu dimer species over MFI zeolites during NO direct decomposition was reported by Groothaert *et al.* and their role in rate-determining O₂ desorption step was suggested^[72]. The O-bridged Cu dimer species were observed by *in situ* UV-Vis spectroscopy as a characteristic adsorption band at 22700 cm⁻¹ ^[72]. Considering these things, the overall mechanism for NO direct decomposition over Cu-zeolites was proposed as Scheme 1.4.^[73]



Scheme 1.4. The overall mechanisms for the formation of dimeric Cu active species and NO direct decomposition over the site in zeolites proposed by Iwamoto and Kuroda.^[73]

Methane partial oxidation into methanol over Cu-MFI and Cu-MOR zeolites was reported in 2005^[74]. The application of Cu-zeolites to the reaction is introduced by the structural similarity of O-bridged Cu dimer on zeolites during NO direct decomposition^[72] with the active site of methane monooxygenase (MMO) enzyme. The *in situ* UV-vis absorption spectroscopy detected characteristic absorption feature around 22700 cm⁻¹ when the Cu-zeolites with high Cu loading were activated in O₂ flow above 450 °C^[75]. They were observed not only over MFI zeolites, but also over MOR zeolites^[75]. Consumption of the band observed in CH₄ oxidation in lower temperature, therefore, they were assigned to the O-activated Cu species with some similarity with the active site for NO direct decomposition^[72]. Typically, this reaction is non-catalytic stepwise process including 1) activation of Cu-zeolites by oxidants such as O₂ or N₂O at high temperatures (above 723 K), 2) methane oxidation at lower temperatures (~ 473 K), and 3) extraction of methanol from the surface of Cu-zeolites by water at ambient temperature or by steaming at an elevated temperature. In the case of this reaction, such as MOR^[74,76], CHA^[77], and MAZ^[78] zeolites have been applied and the application of new zeolites are ongoing to make the productivity of

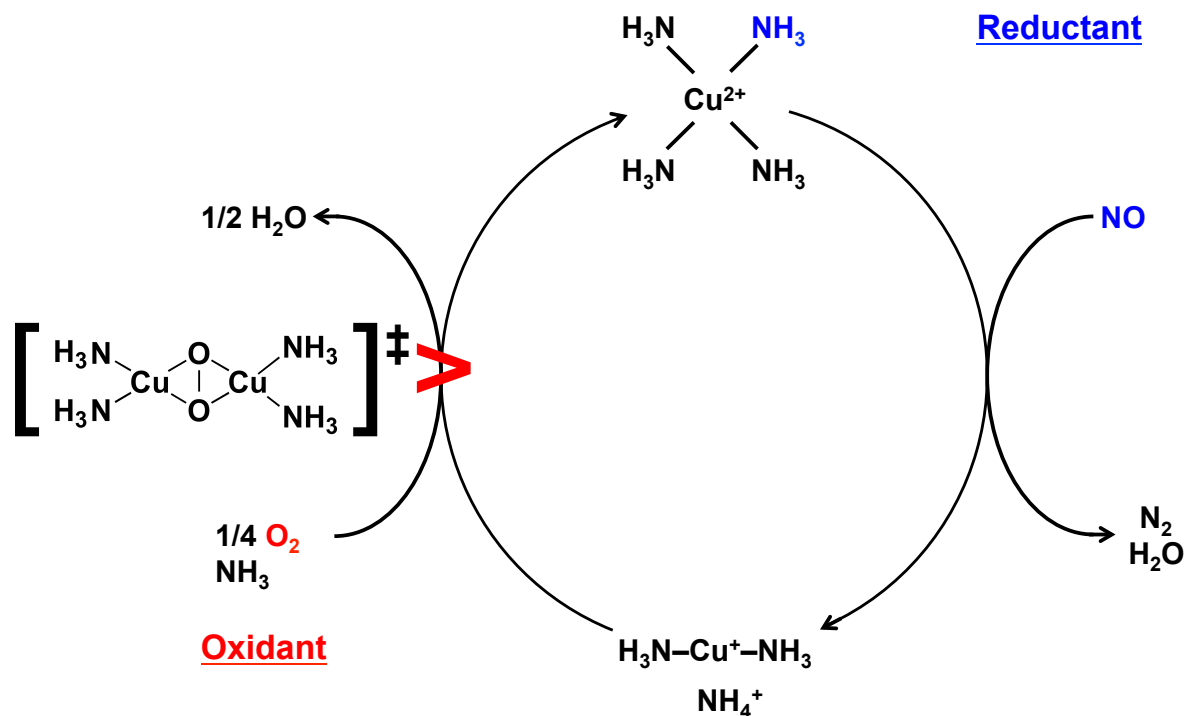
methanol increase^[79–82]. Interestingly, the discovery of this process was originated from the investigation of the structure of active sites for NO direct decomposition, the MFI zeolite typically used for NO direct decomposition is hardly applied for this process because of the relatively low productivity of methanol compared to the zeolites described above.

The studies on application of Cu-zeolites to the NH₃-SCR have relatively independent to the former studies. The first reports on NH₃-SCR over Cu-zeolite catalysts were using Y zeolite with FAU topology in mid 1970s, which is even earlier than the first report on NO direct decomposition over Cu-Y zeolite^[83,84]. However, NH₃-SCR has the disadvantage requiring the addition of toxic reducing agents compared with the NO direct decomposition or HC-SCR processes. Therefore, NH₃-SCR over Cu-zeolites received limited attention until the early 2000s and only a few studies using MOR^[85,86] or MFI^[87] zeolites were reported. However, Cu-zeolite catalysts were finally commercialized in a deNO_x process for diesel engines involving urea-SCR, which is a type of NH₃-SCR that uses a nontoxic urea solution as an NH₃ source^[20], as the reaction rate was higher than those for the direct decomposition of NO and HC-SCR in the temperature range of diesel engine exhausts around 473 K.

A large pore *BEA (12 membered ring; MR) zeolite that provides superior hydrothermal stability to the medium pore MFI (10 MR) zeolite was tested in early studies^[54], however, *BEA zeolite also suffered from problems on hydrothermal stability and deactivation by hydrocarbons^[88]. Finally, Cu-SSZ-13 zeolite catalysts with CHA topology (8 MR) were found to overcome these drawbacks, and the commercialization for the diesel engine automobile was achieved^[59,60]. The Cu-CHA catalyst exhibits high activity and selectivity in wide temperature region and high hydrothermal durability compared with so far investigated Cu-MFI, Cu-*BEA, and Cu-FAU zeolite catalysts^[60,89]. After development of Cu-CHA zeolite, a lot of zeolites with a variety of topology and composition, have been tested for the NH₃-SCR application. As the zeolite topologies that have been applied to the NH₃-SCR successfully, such as AEI^[90–92], LTA (high-silica)^[93], UFI^[94], KFI^[94], MSE^[95], RTH^[92,96], AFX^[97–99], and ERI^[100] can be listed. Not only the variety in topologies, but also in preparation procedures such as OSDA free synthesis^[101,102], ultrafast flow synthesis^[99,100,103], synthesis using different OSDAs^[98,99,104], P modification^[97,105–108], and addition of second metal cation^[109–113] have been developed and various zeolites have been adopted for NH₃-SCR with the main consideration of high hydrothermal stability. The zeolite topologies mainly adopted for the NH₃-SCR are different from them applied to the two reactions

described above.

The great applicability of Cu-zeolites with various topologies to NH₃-SCR is supported by the following widely accepted reaction mechanism for the reaction over Cu-zeolites around 473 K^[114]. This reaction mechanism has been suggested based on studies of Cu-CHA zeolites with a simple structure. The active center for NH₃-SCR over Cu-CHA zeolites is suggested to be an isolated Cu ion in a zeolite micropore, located in either a 6 MR as a bare Cu²⁺ balanced by two negative charges of the zeolite framework^[115,116] or in an 8 MR as a Cu²⁺-OH⁻ complex balanced by a negative charge of the zeolite framework^[117]. Under steady state NH₃-SCR conditions, the isolated Cu ions have a mixture of monovalent and divalent states^[118]. From electron paramagnetic resonance spectra and the linear dependence of the NH₃-SCR kinetics on the square of Cu loading at low Cu loading levels, a high mobility of Cu ions and the existence of transient dimeric Cu species as active sites were suggested, respectively^[119]. The reduction of Cu²⁺ to Cu⁺ was suggested to occur via reaction with NO + NH₃^[120,121]. Moreover, X-ray absorption spectroscopy (XAS) spectra and *ab initio* molecular dynamics simulations suggested that both Cu²⁺ and Cu⁺ are coordinated to NH₃ molecules, not by zeolite framework oxygen, in the temperature region around 473 K^[122]. The Cu⁺ to Cu²⁺ oxidation pathways is proposed to proceed by the reaction of a pair of highly mobile linear H₃N-Cu⁺-NH₃ complexes with O₂ molecules.^[123,124] This oxidation process is thought to be the rate-determining step for NH₃-SCR over commercial Cu-CHA catalysts with relatively low Cu/Al ratios^[125] under on-road reaction conditions at low O₂ pressures (5–20 kPa).^[114,126] In this case, the formation of dimeric Cu intermediates would be an important step, with the NH₃-SCR rate depending on the square of the Cu loading^[123] or the Cu volumetric density in zeolites,^[124] and being independent of the zeolite structure except for the channel dimensions^[92,122]. More recently, further studies on the structure of suggested important intermediates such as O-bridging Cu dimeric or nitrosamine species are conducted by using advanced spectroscopic techniques and DFT calculations^[127–129]. The overall suggested mechanism for the reaction is summarized as Scheme 1.5.



Scheme 1.5. The overall picture for widely accepted reaction mechanisms of the NH₃-SCR over Cu-zeolites involving redox between Cu⁺ and Cu²⁺ around 473 K.^[122,124]

1.4. Objectives of this thesis

This work aims to find the key factors of zeolite topology that govern the formation of Cu active sites for the NO_x abatement reactions with scientific and industrial importance. The author presented the NO direct decomposition and NH₃-SCR as targeted reactions. NO direct decomposition is the most desirable way for NO_x removal. It has been revealed that Cu-zeolites, especially Cu-ZSM-5 zeolite with MFI topology, exhibit excellent activity in relatively low temperature region, however, the applicability of zeolites is limited in this application and the improvement both in activity and durability has been inhibited. Instead, commercial application of the NH₃-SCR over Cu-zeolites with much higher reaction rate in practical temperature region (~ 473 K) has been realized as deNO_x reaction for on-road diesel vehicles. Practical application of Cu-zeolites for NH₃-SCR was achieved by adoption of zeolites with high durability with maintaining high activity. The feature of Cu-zeolites as NH₃-SCR catalyst is the high standard-SCR rate with low NO₂/NO_x ratio. This feature is preferable to gain low temperature activity because it is difficult to increase the population of NO₂ with high reactivity in low temperatures.

In the deNO_x system for diesel engine, improvement of the current technologies or development of new technologies are desired from decreasing exhaust temperature by improvement of fuel efficiency of internal combustion engines and becoming stricter emission regulations^[88,130]. Moreover, it is reported that excess NO_x emissions are generated from diesel vehicles in several major vehicle markets than expected from the regulations currently operated in the regions^[18]. Considering these things, further efforts to improve the catalytic activity of Cu-zeolites are still with importance.

The progress of Cu-zeolites has been conducted by application of new zeolite topology preferable for the targeted reactions. The mechanism of the targeted reactions in this work is relatively well understood by the study on representative zeolites shown in Scheme 1.4 or Scheme 1.5. It is pointed out that redox between Cu⁺ and Cu²⁺ and formation of dimeric Cu species are playing role in both reactions. However, the zeolites used for both reactions are different, and impacts of zeolites on the suggested mechanisms are still missing due to lack of the systematic comparative studies. The author attempted to find the key factors in structural feature of zeolites related to the formation of active sites for the reactions by using the model zeolite catalysts with topologies frequently applied to some reactions. As the topologies for model zeolites, MFI, *BEA and CHA, and MOR zeolites were adopted as the typical catalysts for NO direct decomposition, NH₃-SCR, and methane partial oxidation, respectively (Figure 1.6). The author chose the compositions of the model zeolites with consideration of the suggested mechanisms shown in Scheme 1.4 or Scheme 1.5 to avoid as many the considerable factors other than zeolite topologies. As the parameter for comparison among the zeolites, the behavior of catalytic activity along with the ion-exchange level of Cu was chosen. In the comparison among zeolites, the author focused especially on difference in redox steps between Cu⁺ and Cu²⁺ on zeolites relevant to the targeted reactions.

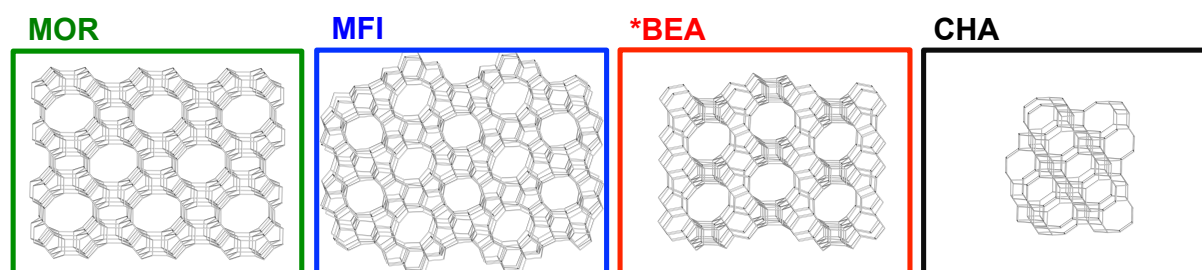


Figure 1.6. Structure of the model zeolites adopted in this thesis.

1.5. Outline of this thesis

Figure 1.7 shows the structure of this doctoral thesis. In chapter 1, a general background on deNO_x processes and the association of zeolites to the processes was described. Chapter 2 presents a discussion on the construction of a methodology to compare among the catalytic activity over zeolites with different topologies and the preparation of catalysts used in this study. In Chapter 3, the explanation of the active site formation for NH₃-SCR over the model zeolites and the suggestion on their origin is described. Chapter 4 presents an expansion of the key finding on the redox behavior of Cu ion over zeolites described in Chapter 3. The explanation of the active site formation for NO direct decomposition over the model zeolites and the investigation on their origin is discussed in Chapter 5. In Chapter 6, the author presents the general conclusions of this thesis and future perspectives on the science of Cu-zeolites.

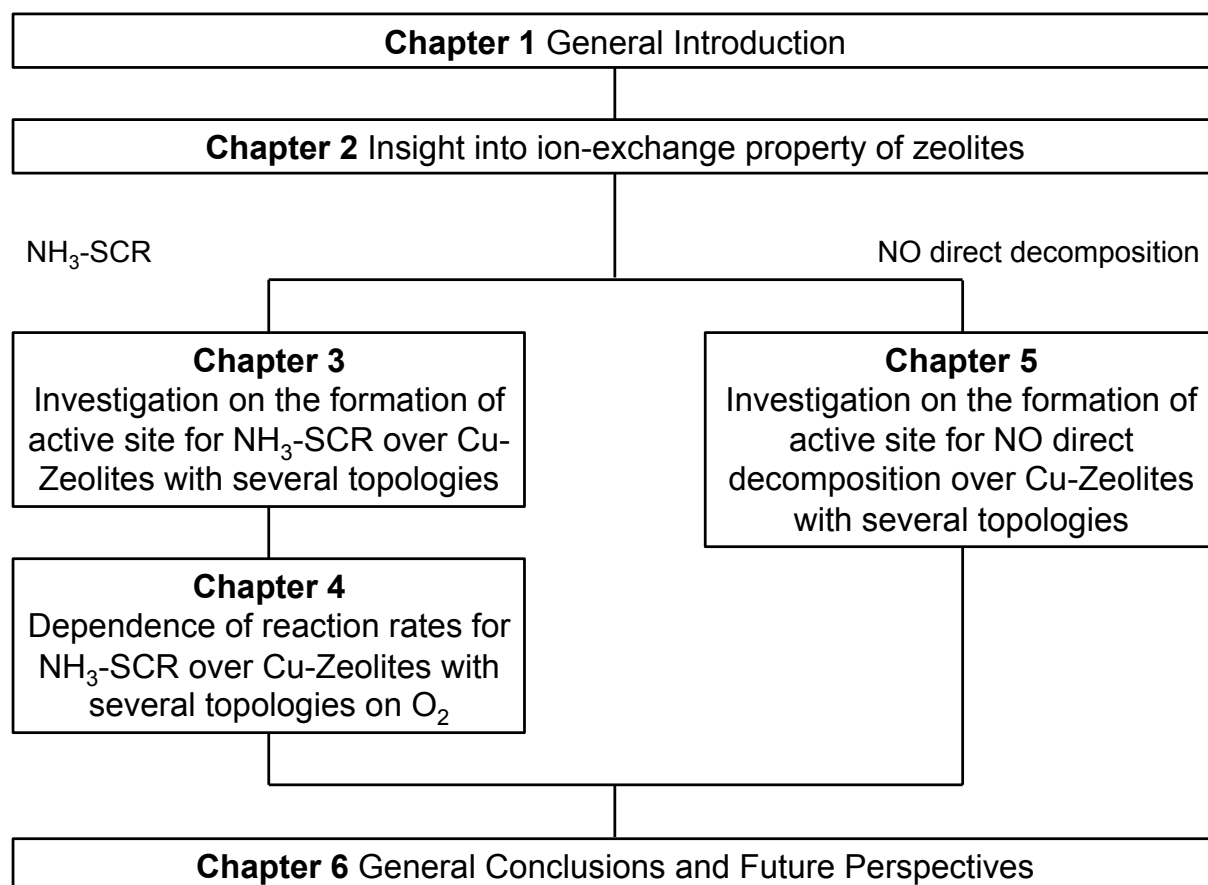


Figure 1.7. Structure of this thesis.

References

- [1] M. Misono, *Modern Chemical Science and Technology for the Environment – Its Understanding and Improvement*, Shokabo, Tokyo, **2017**.
- [2] H. Bosch, F. J. J. G. Janssen, *Catal. Today* **1988**, *2*, 369.
- [3] R. Abro, A. A. Abdeltawab, S. S. Al-Deyab, G. Yu, A. B. Qazi, S. Gao, X. Chen, *RSC Adv.* **2014**, *4*, 35302.
- [4] Z. R. Ismagilov, M. A. Kerzhentsev, *Catal. Rev.* **1990**, *32*, 51.
- [5] J. Lee, J. R. Theis, E. A. Kyriakidou, *Appl. Catal. B* **2019**, *243*, 397.
- [6] G. Centi, P. Ciambelli, S. Perathoner, P. Russo, *Catal. Today* **2002**, *75*, 3.
- [7] M. Misono, *Chemical Science and Technology for the Environment*, Shokabo, Tokyo, **2007**.
- [8] A. Cowley, *May 2020 Pgm Market Report*. <http://www.platinum.matthey.com/documents/new-item/pgm%20market%20reports/pgm-market-report-may-2020.pdf>, (accessed 16 December 2020) (Johnson Matthey, 2020).
- [9] H. Wise, M. F. Frech, *J. Chem. Phys.* **1952**, *20*, 22.
- [10] F. Garin, *Appl. Catal. A* **2001**, *222*, 183.
- [11] M. Haneda, H. Hamada, *C. R. Chimie* **2016**, *19*, 1254.
- [12] Q. Sun, Z. Wang, D. Wang, Z. Hong, M. Zhou, X. Li, *Catal. Sci. Technol.* **2018**, *8*, 4563.
- [13] K. Jellinek, *Z. Anorg. Allg. Chem.* **1906**, *49*, 229.
- [14] T. Ohnishi, K. Kawakami, M. Nishioka, M. Ogura, *Catal. Today* **2017**, *281*, 566.
- [15] S. Harada, T. Ohnishi, M. Ogura, *Chem. Lett.* **2016**, *45*, 1283.
- [16] R. Zhang, N. Liu, Z. Lei, B. Chen, *Chem. Rev.* **2016**, *116*, 3658.
- [17] F. Nakajima, I. Hamada, *Catal. Today* **1996**, *29*, 109.
- [18] S. C. Anenberg, J. Miller, Ray Minjares, L. Du, D. K. Henze, F. Lacey, C. S. Malley, L. Emberson, V. Franco, Z. Klimont, C. Heyes, *Nature* **2017**, *545*, 467.
- [19] C. Görsmann, *Johnson Matthey Technol. Rev.* **2015**, *59*, 139.
- [20] *Urea-SCR Technology for deNOx After Treatment of Diesel Exhausts*, ed. I. Nova, E. Tronconi, Springer Science+Business Media, New York, **2014**.
- [21] J. T. Kummer, *J. Phys. Chem.* **1986**, *90*, 4747.
- [22] Y. Nishihata, J. Mizuki, T. Akao, H. Tanaka, M. Uenishi, M. Kimura, T. Okamoto, N. Hamada, *Nature* **2002**, *418*, 164.
- [23] M. Iwamoto, H. Yahiro, Y. Yu-u, S. Shundo, N. Mizuno, *Shokubai* **1990**, *32*, 430.
- [24] W. Held, A. Konig, T. Richter, L. Puppe, *SAE Transaction* **1990**, *99*, Section 4, 209.

- [25] H. Akama, K. Matsushita, *Catal. Surv. Jpn.* **1999**, *3*, 139.
- [26] A. Takami, T. Takemoto, H. Iwakuni, F. Saito, K. Komatsu, *SAE Technical Paper* **1995**, 950746.
- [27] N. Takahashi, H. Shinjoh, T. Iijima, T. Suzuki, K. Yamazaki, K. Yokota, H. Suzuki, N. Miyoshi, S. Matsumoto, T. Tanizawa, T. Tanaka, S. Tateishi, K. Kasahara, *Catal. Today* **1996**, *27*, 63.
- [28] H. Hamada, M. Haneda, *Appl. Catal. A* **2012**, *421-422*, 1.
- [29] Z. Liu, J. Li, S. I. Woo, *Energy Environ. Sci.* **2012**, *5*, 8799.
- [30] D. W. Breck, *Zeolite Molecular Sieves: Structure, Chemistry, and Use*, Wiley–Interscience publication, New York, **1974**.
- [31] *Handbook of Zeolite Science and Technology*, ed. S. M. Auerbach, K. A. Carrado, P. K. Dutta, Marcel Dekker, New York, **2003**.
- [32] N. Kosinov, C. Liu, E. J. M. Hensen, E. A. Pidko, *Chem. Mater.* **2018**, *30*, 3177.
- [33] M. Iwamoto, K. Maruyama, N. Yamazoe, T. Seiyama, *J. Phys. Chem.* **1977**, *81*, 622.
- [34] M. Iwamoto, S. Yokoo, K. Sakai, S. Kagawa, *J. Chem. Soc., Faraday. Trans. 1* **1981**, *77*, 1629.
- [35] M. Iwamoto, H. Yahiro, K. Tanda, N. Mizuno, Y. Mine, S. Kagawa, *J. Phys. Chem.* **1991**, *95*, 3727.
- [36] Y. Traa, B. Burger, J. Weitkamp, *Microporous Mesoporous Mater.* **1999**, *30*, 3.
- [37] H. Hamada, *Catal. Today* **1994**, *22*, 21.
- [38] S. Namba, M. Niwa, *Shokubai* **1994**, *36*, 289.
- [39] Y. Li, J. N. Armor, *Appl. Catal. B* **1992**, *1*, L31.
- [40] K. Yogo, S. Tanaka, M. Ihara, T. Hishiki, E. Kikuchi, *Chem. Lett.* **1992**, 1025.
- [41] Y. Nishizaka, M. Misono, *Chem. Lett.* **1993**, 1295.
- [42] H. Hamada, Y. Kintaichi, M. Sasaki, T. Ito, M. Tabata, *Appl. Catal.* **1990**, *64*, L1.
- [43] A. Satsuma, K. Yamada, T. Mori, M. Niwa, T. Hattori, Y. Murakami, *Catal. Lett.* **1995**, *31*, 367.
- [44] Y. Li, P. J. Battavio, J. N. Armor, *J. Catal.* **1993**, *142*, 561
- [45] X. Feng, W. K. Hall, *J. Catal.* **1997**, *166*, 368.
- [46] T. Tabata, M. Kokitsu, H. Ohtsuka, O. Okada, L.M.F. Sabatino, G. Bellussi, *Catal. Today* **1996**, *27*, 91.
- [47] M. Iwamoto, T. Zengyo, *Chem. Lett.* **1997**, 1283.
- [48] R. Burch, S. Scire, *Appl. Catal. B* **1994**, *24*, 295.

- [49] S. Sato, Y. Yu-u, H. Yahiro, N. Mizuno, M. Iwamoto, *Appl. Catal.* **1991**, *70*, L1.
- [50] C. Yokoyama, M. Misono, *J. Catal.* **1994**, *150*, 9.
- [51] B. H. Engler, J. Leyrer, E. S. Lox, K. Ostgathe, *SAE Transaction* **1993**, *930735*, Section 4, 535.
- [52] H.K. Shin, H. Hirabayashi, H. Yahiro, M. Watanabe, M. Iwamoto, *Catal. Today* **1995**, *26*, 13.
- [53] M. Iwamoto, H. Yahiro, *Catal. Today* **1994**, *22*, 5.
- [54] S. Brandenberger, O. Kröcher, A. Tissler, R. Althoff, *Catal. Rev.-Sci. Eng.* **2008**, *50*, 492.
- [55] http://www.mlit.go.jp/jidosha/jidosha_fr1_000032.html
- [56] Y. Naraki, K. Ariga and T. Sano, *Adv. Porous Mater.* **2016**, *4*, 125.
- [57] Y. Naraki, K. Ariga, H. Oka, H. Kurashige, T. Sano, *Adv. Porous Mater.* **2016**, *4*, 91.
- [58] Y. Naraki, K. Ariga, H. Oka, H. Kurashige, T. Sano, *J. Nanosci. Nanotechnol.* **2018**, *18*, 11.
- [59] I. Bull, W.-M. Xue, P. Burk, R.S. Boorse, W.M. Jaglowski, G.S. Koermer, A. Moini, J. A. Patchett, J. C. Dettling, M. T. Caudle, *US Patent* **2009**, *7*, 610, 662.
- [60] J. H. Kwak, R. G. Tonkyn, D. H. Kim, J. Szanyi, C. H. F. Peden, *J. Catal.* **2010**, *275*, 187.
- [61] H.-Y. Chen, J. E. Collier, D. Liu, L. Mantarosie, D. Duran-Martin, V. Novak, R. R. Rajaram, D. Thompsett, *Catal. Lett.* **2016**, *146*, 1706.
- [62] Y. Zheng, L. Kovarik, M. H. Engelhard, Y. Wang, Y. Wang, F. Gao, J. Szanyi, *J. Phys. Chem. C* **2017**, *121*, 15793.
- [63] K. Khivantsev, N. R. Jaegers, L. Kovarik, J. C. Hanson, F. Tao, Y. Tang, X. Zhang, I. Z. Koleva, H. A. Aleksandrov, G. N. Vayssilov, Y. Wang, F. Gao, J. Szanyi, *Angew. Chem. Int. Ed.* **2018**, *57*, 16672.
- [64] M. Iwamoto, H. Furukawa, S. Kagawa, *Stud. Surf. Sci. Catal.* **1986**, *28*, 943.
- [65] M. Iwamoto, H. Yahiro, K. Tanda, *Stud. Surf. Sci. Catal.* **1988**, *37*, 219.
- [66] J. Dědeček, O. Bortnovsky, A. Vondrová, B. Wichterlová, *J. Catal.* **2001**, *200*, 160.
- [67] M. Y. Kustova, A. Kustov, S. E. Christiansen, K. T. Leth, S. B. Rasmussen, C. H. Christensen, *Catal. Commun.* **2006**, *7*, 705.
- [68] M. Y. Kustova, S. B. Rasmussen, A. L. Kustov, C. H. Christensen, *Appl. Catal. B* **2006**, *67*, 60.
- [69] Y. Kuroda, A. Kotani, H. Maeda, H. Moriwaki, T. Morimoto, M. Nagao, *J. Chem. Soc.*

Faraday Trans **1992**, *88*, 1583.

[70] Y. Kuroda, R. Kumashiro, M. Nagao, *Appl. Surf. Sci.* **2002**, *196*, 408.

[71] M. Iwamoto, H. Yahiro, N. Mizuno, W.-X. Zhang, Y. Mine, H. Furukawa, S. Kagawa, *J. Phys. Chem.* **1992**, *96*, 9360.

[72] M. H. Groothaert, J. A. Bokhoven, A. A. Battiston, B. M. Weckhuysen, R. A. Schoonheydt, *J. Am. Chem. Soc.* **2003**, *125*, 7629.

[73] Y. Kuroda, M. Iwamoto, *Top. Catal.* **2004**, *28*, 111.

[74] M. H. Groothaert, P. J. Smeets, B. F. Sels, P. A. Jacobs, R. A. Schoonheydt, *J. Am. Chem. Soc.* **2005**, *127*, 1394.

[75] P. J. Smeets, M. H. Groothaert, R. A. Schoonheydt, *Catal Today* **2005**, *110*, 303.

[76] S. Grundner, M. A.C. Markovits, G. Li, M. Tromp, E. A. Pidko, E. J. M. Hensen, A. Jentys, M. Sanchez-Sanchez, J. A. Lercher, *Nat. Commun.* **2015**, *6*, 1.

[77] M. J. Wulfers, S. Teketel, B. Ipek, R. F. Lobo, *Chem. Commun.* **2015**, *51*, 4447.

[78] A. J. Knorpp, A. B. Pinar, M. A. Newton, V. L. Sushkevich, J. A. van Bokhoven, *ChemCatChem* **2018**, *10*, 5593.

[79] B. Ipek, M. J. Wulfers, H. Kim, F. Göttl, I. Hermans, J. P. Smith, K. S. Booksh, C. M. Brown, R. F. Lobo, *ACS Catal.* **2017**, *7*, 4291.

[80] A. R. Kulkarni, Z.-J. Zhao, S. Siahrostami, J. K. Nørskov, F. Studt, *Catal. Sci. Technol.* **2018**, *8*, 114.

[81] M. A. Newton, A. J. Knorpp, V. L. Sushkevich, D. Palagin, J. A. van Bokhoven, *Chem. Soc. Rev.* **2020**, *49*, 1449.

[82] J. Zhu, V. L. Sushkevich, A. J. Knorpp, M. A. Newton, S. C. M. Mizuno, T. Wakihara, T. Okubo, Z. Liu, J. A. van Bokhoven, *Chem. Mater.* **2020**, *32*, 1448.

[83] T. Seiyama, T. Arakawa, T. Matsuda, Y. Takita, N. Yamazoe, *J. Catal.* **1977**, *48*, 1.

[84] W. B. Williamson, J. H. Lunsford, *J. Phys. Chem.* **1976**, *80*, 2664.

[85] J. G. M. Brandin, L. A. H. Andersson, C.U.I. Odenbrand, *Catal. Today* **1989**, *4*, 187.

[86] E. Y. Choi, I.-S. Nam, Y. G. Kim, J. S. Chung, J. S. Lee, M. Nomura, *J. Mol. Catal.* **1991**, *69*, 247.

[87] T. Komatsu, M. Nunokawa, I. S. Moon, T. Takahara, S. Nanba, T. Yashima, *J. Catal.* **1994**, *148*, 427.

[88] C. H. F. Peden, *J. Catal.* **2019**, *373*, 384.

[89] J. H. Kwak, D. Tran, S. D. Burton, J. Szanyi, J. H. Lee, C. H. F. Peden, *J. Catal.* **2012**, *287*, 203.

- [90] M. Moliner, C. Franch, E. Palomares, M. Grillb, A. Corma, *Chem. Commun.* **2012**, *48*, 8264.
- [91] N. Martín, C. R. Boruntea, M. Moliner, A. Corma, *Chem. Commun.* **2015**, *51*, 11030.
- [92] J. D. Albarracin-Caballero, I. Khurana, J. R. Di Iorio, A. J. Shih, J. E. Schmidt, M. Dusselier, M. E. Davis, A. Yezerets, J. T. Miller, F. H. Ribeiro, R. Gounder, *React. Chem. Eng.* **2017**, *2*, 168.
- [93] D. Jo, T. Ryu, G. T. Park, P. S. Kim, C. H. Kim, I.-S. Nam, S. B. Hong, *ACS Catal.* **2016**, *6*, 2443.
- [94] J. Kim, S. J. Cho, D. H. Kim, *ACS Catal.* **2017**, *7*, 6070.
- [95] J. H. Lee, Y. J. Kim, T. Ryu, P. S. Kim, C. H. Kim, S. B. Hong, *Appl. Catal. B* **2017**, *200*, 428.
- [96] Y. Shan, X. Shi, J. Du, Y. Yu, H. He, *Catal. Sci. Technol.* **2019**, *9*, 106.
- [97] S. V. Priya, T. Ohnishi, Y. Shimada, Y. Kubota, T. Masuda, Y. Nakasaka, M. Matsukata, K. Itabashi, T. Okubo, T. Sano, N. Tsunoji, T. Yokoi, M. Ogura, *Bull. Chem. Soc. Jpn.* **2018**, *91*, 355.
- [98] N. Nakazawa, S. Inagaki, Y. Kubota, *Adv. Porous Mater.* **2016**, *4*, 219.
- [99] A. Chokkalingam, W. Chaikittisilp, K. Iyoki, S. H. Keoh, Y. Yanaba, T. Yoshikawa, T. Kusamoto, T. Okubo, T. Wakihara, *RSC Adv.* **2019**, *9*, 16790.
- [100] J. Zhu, Z. Liu, L. Xu, T. Ohnishi, Y. Yanaba, M. Ogura, T. Wakihara, T. Okubo, *J. Catal.* **2020**, *391*, 346.
- [101] L. Xu, C. Shi, Z. Zhang, H. Gies, F.-S. Xiao, D. De Vos, T. Yokoi, X. Bao, M. Feyen, S. Maurer, B. Yilmaz, U. Müller, W. Zhang, *Microporous Mesoporous Mater.* **2014**, *200*, 304.
- [102] Y. Wang, T. Nishitoba, Y. Wang, X. Meng, F.-S. Xiao, W. Zhang, B. Marler, H. Gies, D. De Vos, U. Kolb, M. Feyen, R. McGuire, A.-N. Parvulescu, U. Müller, and T. Yokoi, *Ind. Eng. Chem. Res.* **2020**, *59*, 7375.
- [103] Z. Liu, T. Wakihara, K. Oshima, D. Nishioka, Y. Hotta, S. P. Elangovan, Y. Yanaba, T. Yoshikawa, W. Chaikittisilp, T. Matsuo, T. Takewaki, Tatsuya Okubo, *Angew. Chem. Int. Ed.* **2015**, *54*, 5683.
- [104] R. Ransom, R. Moulton, D. F. Shantz, *J. Catal.* **2020**, *382*, 339.
- [105] T. Sonoda, T. Maruo, Y. Yamasaki, N. Tsunoji, Y. Takamitsu, M. Sadakane, T. Sano, *J. Mater. Chem. A* **2015**, *3*, 857.
- [106] Y. Kakiuchi, Y. Yamasaki, N. Tsunoji, Y. Takamitsu, M. Sadakane, T. Sano, *Chem. Lett.* **2016**, *45*, 122.

- [107] E. Mitani, Y. Yamasaki, N. Tsunoji, M. Sadakane, T. Sano, *Microporous Mesoporous Mater.* **2018**, *267*, 192.
- [108] Y. Kakiuchi, T. Tanigawa, N. Tsunoji, Y. Takamitsu, M. Sadakane, T. Sano, *Appl. Catal. A* **2019**, *575*, 357.
- [109] F. Gao, Y. Wang, N. M. Washton, M. Kollaf, J. Szanyi, C. H. F. Peden, *ACS Catal.* **2015**, *5*, 6780.
- [110] T. Usui, Z. Liu, S. Ibe, J. Zhu, C. Anand, H. Igarashi, N. Onaya, Y. Sasaki, Y. Shiramata, T. Kusamoto, T. Wakihara, *ACS Catal.* **2018**, *8*, 9165.
- [111] Z. Zhao, R. Yu, C. Shi, H. Gies, F.-S. Xiao, D. De Vos, T. Yokoi, X. Bao, U. Kolb, R. McGuire, A.-N. Parvulescu, S. Maurer, U. Müller, W. Zhang, *Catal. Sci. Technol.* **2019**, *9*, 241.
- [112] Y. Cui, Y. Wang, D. Mei, E. D. Walter, N. M. Washton, J. D. Holladay, Y. Wang, J. Szanyi, C. H. F. Peden, F. Gao, *J. Catal.* **2019**, *378*, 363.
- [113] Y. Cui, Y. Wang, E. D. Walter, J. Szanyi, Y. Wang, F. Gao, *Catal. Today* **2020**, *339*, 233.
- [114] C. Paolucci, J. R. Di Iorio, W. F. Schneider, R. Gounder, *Acc. Chem. Res.* **2020**, *53*, 1881.
- [115] D. W. Fickel, R. F. Lobo, *J. Phys. Chem. C* **2010**, *114*, 1633.
- [116] S. T. Korhonen, D. W. Fickel, R. F. Lobo, B. M. Weckhuysen, A. M. Beale, *Chem. Commun.* **2011**, *47*, 800.
- [117] R. Zhang, J.-S. McEwen, M. Kollar, F. Gao, Y. Wang, J. Szanyi, C. H. F. Peden, *ACS Catal.* **2014**, *4*, 4093.
- [118] V. F. Kispersky, A. J. Kropf, F. H. Ribeiro, J. T. Miller, *Phys. Chem. Chem. Phys.* **2012**, *14*, 2229.
- [119] F. Gao, E. D. Walter, M. Kollar, Y. Wang, J. Szanyi, C. H. F. Peden, *J. Catal.* **2014**, *319*, 1.
- [120] C. Paolucci, A. A. Verma, S. A. Bates, V. F. Kispersky, J. T. Miller, R. Gounder, W. N. Delgass, F. H. Ribeiro, W. F. Schneider, *Angew. Chem. Int. Ed.* **2014**, *53*, 11828.
- [121] T. V. W. Janssens, H. Falsig, L. F. Lundegaard, P. N. R. Vennestrom, S. B. Rasmussen, P. G. Moses, F. Giordanino, E. Borfecchia, K. A. Lomachenko, C. Lamberti, S. Bordiga, A. Godiksen, S. Mossin, P. Beato, *ACS Catal.* **2015**, *5*, 2832.
- [122] C. Paolucci, A. A. Parekh, I. Khurana, J. R. Di Iorio, H. Li, J. D. A. Caballero, A. J. Shih, T. Anggara, W. N. Delgass, J. T. Miller, F. H. Ribeiro, R. Gounder, W. F. Schneider, *J.*

Am. Chem. Soc. **2016**, *138*, 6028.

[123] F. Gao, D. Mei, Y. Wang, J. Szanyi, C. H. F. Peden, *J. Am. Chem. Soc.* **2017**, *139*, 4935.

[124] C. Paolucci, I. Khurana, A. A. Parekh, S. Li, A. J. Shih, H. Li, J. R. Di Iorio, J. D. Albarracin-Caballero, A. Yezerets, J. T. Miller, W. N. Delgass, F. H. Ribeiro, W. F. Schneider, R. Gounder, *Science* **2017**, *357*, 898.

[125] J. Luo, D. Wang, A. Kumar, J. Li, K. Kamasamudram, N. Currier, A. Yezerets, *Catal. Today* **2016**, *267*, 3.

[126] C. B. Jones, I. Khurana, S. H. Krishna, A. J. Shih, W. Nicholas Delgass, J. T. Miller, F. H. Ribeiro, W. F. Schneider, R. Gounder, *J. Catal.* **2020**, *389*, 140.

[127] A. G. Greenaway, A. Marberger, A. Thetford, I. Lezcano-González, M. Agote-Arán, M. Nachtegaal, D. Ferri, O. Kröcher, C. R. A. Catlow, A. M. Beale, *Chem. Sci.* **2020**, *11*, 447.

[128] C. Negri, T. Selleri, E. Borfecchia, A. Martini, K. A. Lomachenko, T. V. W. Janssens, M. Cutini, S. Bordiga, G. Berlier, *J. Am. Chem. Soc.* **2020**, *142*, 15884.

[129] A. Oda, H. Shionoya, Y. Hotta, T. Takewaki, K. Sawabe, A. Satsuma, *ACS Catal.* **2020**, *10*, 12333.

[130] S. Zhang, L. Pang, Z. Chen, S. Ming, Y. Dong, Q. Liu, P. Liu, W. Cai, T. Li, *Appl. Catal. A* **2020**, *607*, 117855.

Chapter 2
Insight into ion-exchange property of
zeolites

2.1. Introduction

In the zeolites with same topology, the preparation condition such as synthesis methods or post-synthetic treatment can affect the properties such as composition, size and morphology of the particle, hydrophobicity, position of Al atoms in frameworks^[1-5]. These properties can alter the catalytic property of the zeolites such as ion-exchange properties for metal cation, the diffusion for the reactants, and durability^[6-10]. In the comparative study on metal zeolites with different topologies, it is the often case that the discussions are conducted on the results from a few representatives on each topology with consideration of a simple parameter (*e.g.* metal loading or composition) or no parameter^[11-16]. Therefore, it is difficult to obtain the reasonable description for the difference related to the suggested mechanism for the targeted reaction.

In this chapter, it was objected to establish the methodology for fundamental comparative study on metal zeolite catalysts with different topologies. Toward the objective described above, it was attempted to minimize the contributions of considerable factors other than the topology that can affect the activities for the targeted reactions by choosing the reasonable representatives on each topology. The targeted reaction in this work, NH₃-SCR and NO direct decomposition, is suggested in the reaction mechanism that the Cu dimeric intermediates^[17,18] or active sites^[19], respectively, have important role in the rate-determining steps. Therefore, the volumetric density of Cu ion in the zeolites is suggested as a key descriptor for formation of the species described above^[18]. Considering these backgrounds, a descriptor named “cation density in micropores” for zeolites with a variety of topologies was determined based on the composition and crystallographic amounts on zeolite frameworks at first. This parameter is determined to describe the quantitative index of the cation exchange capacity per micropores, which is the valid space for the exchanged cation to exist. Next, a representative zeolites with similar and large “cation density in micropores” was chosen on each topology to suppress the effect of localized Al atoms distribution in zeolite frameworks as much as possible. The selected zeolites were subjected to copper ion-exchange with same ion-exchange procedure to obtain the Cu-zeolites with several ion-exchange level (\approx volumetric density of Cu ion in the micropores).

2.2. Methods

2.2.1. Definition of cation density in micropores

It has been suggested that Cu ions coordinated to NH₃ are the active sites for NH₃-SCR over Cu-CHA zeolites at low temperatures (<523 K), resulting in a semihomogeneous reaction mechanism^[17,18,20]. Moreover, it has been suggested that the rate-determining step for Cu⁺ to Cu²⁺ oxidation in commercial catalysts under on-road conditions involves the formation of O-bridging Cu dinuclear intermediates^[17,18]. Thus, the key descriptor has been suggested to be the mean Cu density in a certain volume, as calculated from the zeolite framework density of tetrahedral framework atoms (Si and Al; T atoms) and the Si/Al and Cu/Al molar ratios:^[18]

$$(\text{Cu density} / (1000 \text{ \AA}^3)^{-1}) = (\text{Cu/Al}) \times (1/(\text{Si/Al} + 1)) \times (\text{T}/1000 \text{ \AA}^3)$$

This approach is valid for comparisons among CHA zeolites with different compositions. However, the Cu density is problematic for comparisons among zeolites with different topologies owing to variations in the framework densities (*e.g.*, the number of T atoms per 1000 Å³)^[21]. The framework density of a zeolite is calculated from the number of T atoms contained in the unit cell, but the number of T atoms per unit cell is not comparable among zeolites because the unit cell volume is affected by topologies with different crystallographic cell parameters. However, comparisons can be made when the number of T atoms per unit cell is normalized to the number of T atoms in a certain volume unit (*e.g.*, 1000 Å³). The differences in framework density cause the framework atoms (Si, Al, and O atoms) to have different occupancies in a certain volume. Conversely, the available micropore volume in a certain volume unit is also affected by the zeolite topology. As an indicator of the available micropore volume in a certain volume unit, the term “accessible volume”, has been defined^[22] and registered in a database^[21]. The accessible volume is determined as the portion of the volume within the unit cell that the center of a spherical water molecule with a radius of 1.4 Å can access and that has continuity between all unit cells.^[21,22] Note, although the accessible volume is calculated based on the unit cell, it is normalized to a percentage and is a comparable among zeolites.

It can be assumed that the exchanged Cu ions that contribute to NH₃-SCR within a zeolite can only exist in the space not occupied by the zeolite framework atoms. Zeolites with the same composition (*e.g.*, Cu/Si/Al ratio) but different topologies have different numbers of

Cu ions per micropore volume. Even when the mean Cu density^[18] is the same, the number of Cu ions per micropore volume differs for different zeolites. Figure 2.1.a shows a simplified schematic for zeolites with the same Si/Al ratio and different topologies with a Cu²⁺ ion exchange level of 100%. The volumetric density of the cation can vary considerably, even with the same composition. For example, for an MFI zeolite (9.81% accessible volume^[21]) and a CHA zeolite (17.27% accessible volume^[21]) with the same Cu density,^[18] the number of Cu ion per micropore volume is approximately two times larger in the MFI zeolite than in the CHA zeolite.

In this study, instead of the well-defined Cu density,^[18] the “cation density in micropores” was determined for each zeolite using the T atoms per volume, the Si/Al ratio, and the accessible volume, as follows:

$$\begin{aligned} & (\text{cation density in micropores} / (1000 \text{ \AA}^3)^{-1}) \\ & = 1/(\text{Si/Al} + 1) \times (\text{T}/1000 \text{ \AA}^3) / ((\text{accessible volume} / \%) / 100) \end{aligned}$$

This value indicates the density of cation-exchangeable Al atoms in the zeolite framework per available reaction volume within the zeolite microspaces. In other words, the cation density in micropores is a quantitative index of the cation exchange capacity per micropore.

The mean Cu density in micropores was calculated based on the cation density in micropores and the Cu/Al ratio using the following equation.

$$\begin{aligned} & (\text{Cu density in micropores} / (1000 \text{ \AA}^3)^{-1}) \\ & = (\text{Cu/Al}) \times (\text{cation density in micropores} / (1000 \text{ \AA}^3)^{-1}) \end{aligned}$$

The Cu density per micropore of the CHA zeolites in this work is about 6 times larger than the Cu density reported by Paolucci *et al.*^[18] owing to the difference in the definition of volume. Moreover, it should be noted that the calculated Cu density in micropores reflects the mean density normalized by the bulk zeolite composition and not necessarily the composition of local sites.

2.2.2. Selection of model zeolites with several topologies

In this work, representative zeolites with various topologies were selected based on the definition of the cation density in micropores. At a constant bulk Si/Al ratio, which is an

indicator of the ion-exchange capacity, the maximum Cu density in micropores varies depending on the zeolite topology (Figure 2.1.a). Therefore, the Si/Al ratio of each model zeolite was chosen to obtain similar cation densities in micropores. Moreover, if the Al content is insufficient, the Al atoms in the zeolite framework and the exchanged cations, which are located around the Al sites, can be localized in a specific part of the micropore^[23–25]. Therefore, to achieve delocalized distributions of exchanged cations, the as large as possible cation density in micropores was chosen. Figure 2.1.b shows a simplified schematic for zeolites with different topologies and a Cu²⁺ ion exchange level of 100% with modified Si/Al ratios to achieve the same cation densities in micropores. Table 2.1 shows the Si/Al ratios and cation densities in micropores for the zeolites used as model catalysts in this work. As shown in Table 2.1, cation densities in micropores similar to that of the MFI zeolite, which has the highest Si/Al ratio, were achieved by increasing the Al contents of zeolites with low framework densities and high accessible volumes, thus accounting for the limitations in the volumetric density of the cation. The Cu ion exchange level is approximately equal to the number of Cu ions per available micropore volume in the prepared zeolite catalysts with similar cation densities in micropores.

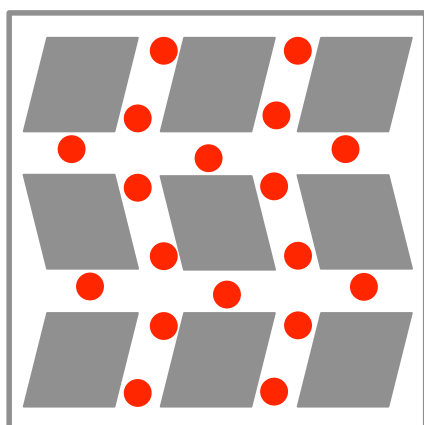
It is known that the amount and location of Al contained in the zeolite frameworks are determined by the counter cation such as hydrated sodium or OSDAs, contained in the zeolite synthesis conditions.^[8,23–29] The proportion of micropore not occupied by the atoms contained in the zeolite frameworks are affected by the framework density that is peculiar to the zeolite topology^[21]. It is reported on the OSDA-free zeolite synthesis, which is a method with tendency to obtain zeolites with low Si/Al ratio^[30], even obtained from similar synthesis gel, Si/Al ratio of obtained zeolites varied by zeolite topologies^[31, 32]. Moreover, it is observed on zeolites obtained in the works described above that zeolites with high framework density tend to have high Si/Al ratio. Then, the maximum “cation density in micropores” of each zeolite may be an amount characteristic of the structure determined by the maximum number of packable cation with the largest positive charge density contained in the zeolite synthesis conditions into the micropore of each zeolite.

Table 2.1. Si/Al ratio, parameters associated to the each topology, and the calculated “Cation Density in Micropore” of the zeolites used as the model catalysts in this work.

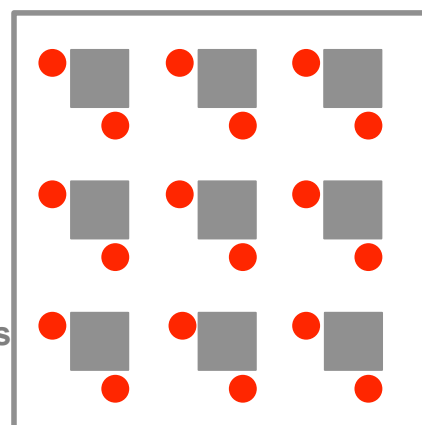
Topology	Si/Al	T / 1000 Å ³ [68]	Accessible Volume / % ^[68]	“Cation Density in Micropore” / (1000 Å ³) ⁻¹
MOR	9	17	12.27	13.9
MFI	11.9	18.4	9.81	14.5
*BEA	5.6	15.3	20.52	11.3
CHA	6.9	15.1	17.27	11.1

a)

MFI

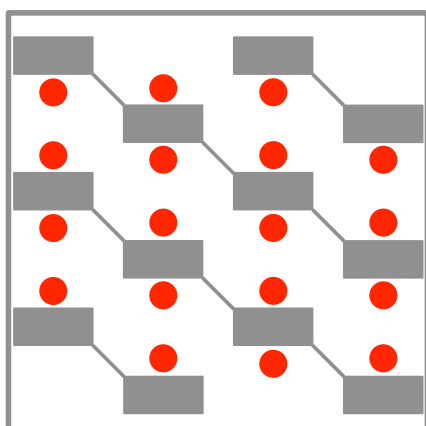


***BEA**

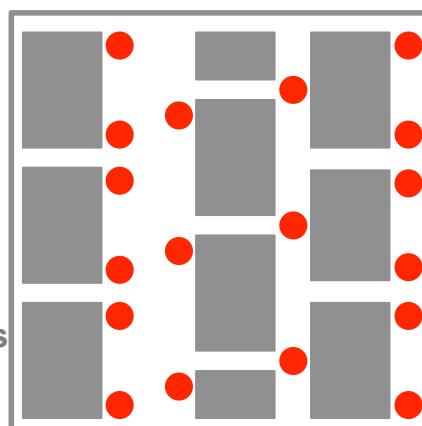


■ : Zeolite Walls
● : Cu²⁺ Cation

CHA



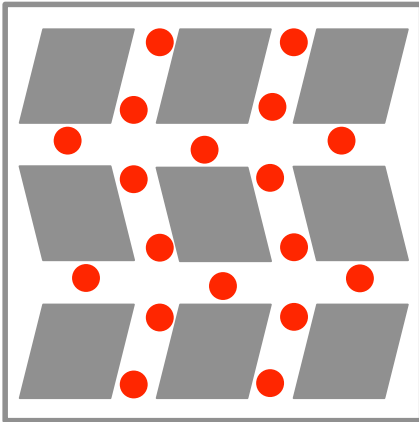
MOR



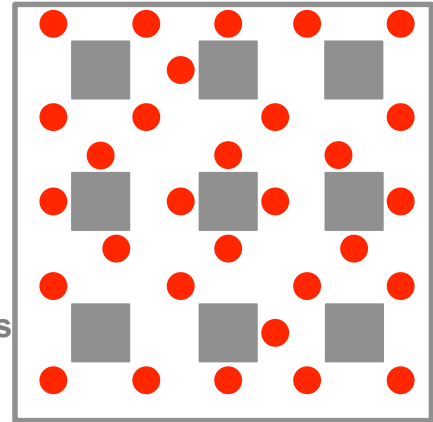
■ : Zeolite Walls
● : Cu²⁺ Cation

b)

MFI

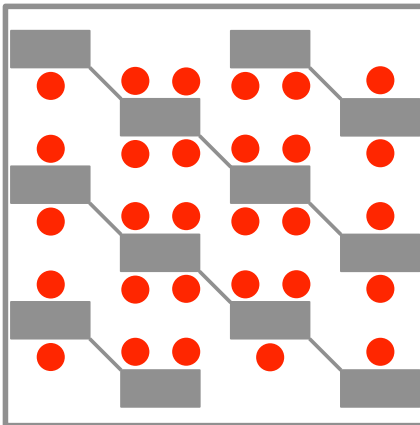


*BEA

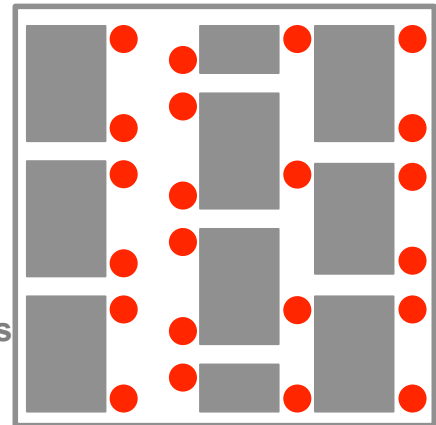


■ : Zeolite Walls
● : Cu²⁺ Cation

CHA



MOR



■ : Zeolite Walls
● : Cu²⁺ Cation

Figure 2.1. Simplified schematic depiction of the situation in zeolites with similar (a) Si/Al ratio and (b) similar “Cation Density in Micropore” and different topologies with 100 % ion-exchange level of Cu²⁺.

2.3. Experimental

2.3.1. Materials

Sodium-form *BEA (UniZeo Co., Ltd., Si/Al = 5.6),^[30] MFI (Tosoh Corp. Si/Al = 11.9), and MOR (Wako Chemical Co., Si/Al = 9) zeolites were supplied and used without calcination. Ammonium-form CHA (Si/Al = 6.9), proton-form *BEA (Si/Al = 14), ammonium-form MFI (Si/Al = 19.5), and sodium-form FAU (Si/Al = 2.8) zeolites were obtained from Tosoh Corp. Sodium-proton-form CHA (Si/Al = 9) zeolite was supplied by the Japan Zeolite Association. Sodium nitrate was obtained from Wako Pure Chemical Industries and copper acetate was obtained from Kanto Chemical and used as received.

2.3.2. Na ion-exchange of zeolites

Any zeolites that were not in the sodium form were ion exchanged to the sodium form before copper ion exchange. Briefly, 3 g of zeolite was suspended in an aqueous solution (300 mL) of sodium nitrate (25.5 g, 1 M) and stirred at room temperature (~300 K) for 24 h, and this procedure was repeated twice. In the case of ammonium-form CHA (Si/Al = 6.9), the temperature was maintained at 353 K. The products were filtered, washed with distilled water, and dried at 373 K for 12 h.

2.3.3. Cu ion-exchange of zeolites

In the experiment, 1.5 g of sodium-form zeolite was dispersed in a 100 mL aqueous copper acetate solution (3–45 mM) and stirred at room temperature for 24 h. The procedure was repeated 1–4 times^[33]. The products were filtered, washed with distilled water, and dried at 373 K overnight.

The chemical composition of the obtained products were determined by using ICP-AES (Thermo Fisher Scientific iCAP6300). Samples were dissolved in HF and HCl solution before the ICP-AES measurement. The carbon contents of the obtained products were analyzed by an elemental analyzer (Elementar Analysensysteme GmbH Vario Micro Cube).

2.3.4. Characterization of parent zeolites

²⁹Si solid-state MAS NMR spectra for the parent sodium-form zeolites were recorded at room temperature (~20 °C) in a ZrO₂ tube with a 4 mm diameter, using a JNM-ECA 500 spectrometer (JEOL). ²⁹Si DD MAS NMR spectra were recorded at a

spinning frequency of 10 kHz by collecting 512 scans at 99.37 MHz with a $\pi/2$ pulse length of 5.0 μs and a recycle delay of 120 s. ^{29}Si CP MAS NMR spectra were recorded at a spinning frequency of 6 kHz by collecting 2048 scans with a recycle delay of 1.5 s. Spectral curve fitting was carried out using the Voigt distribution in the Delta Software (JEOL RESONANCE Inc.).

2.4. Results and Discussion

2.4.1. Properties of patent zeolites in this work

Figures 2.2.a and 2.2.b show ^{29}Si DD and CP MAS NMR spectra of the sodium-formed zeolites used as the parent zeolites in this work, respectively. Table 2.2 shows the results of the peak fitting of the ^{29}Si DD MAS NMR spectra. In the ^{29}Si DD MAS NMR spectra of the zeolites, a large fraction of the peak assignable to the $\text{Q}^4(1\text{Al})$ species around -105 ppm was observed, and small fractions assignable to the $\text{Q}^4(2\text{Al})$ around -100 ppm were observed for all zeolites, even in the *BEA or CHA zeolites with high Al contents. It is shown from the results that the Al atoms contained in the zeolite frameworks are highly delocalized. In the ^{29}Si CP MAS NMR spectra on the zeolites, the Q^3 and Q^2 peaks were hardly observed. These results suggest that a defect site such as the Si–OH groups hardly exists. It is shown by the ^{29}Si MAS NMR spectra that the model zeolites selected in this work hold a relatively delocalized Al site in the framework with high crystallinity.

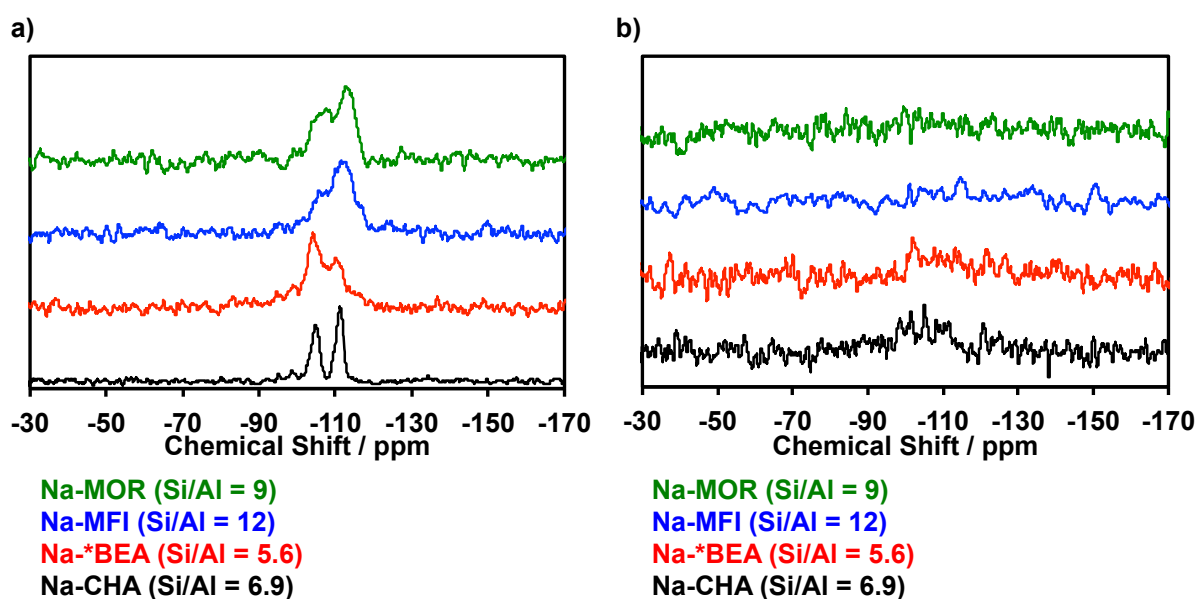


Figure 2.2. (a) ^{29}Si DD MAS NMR spectra and (b) ^{29}Si CP MAS NMR spectra of the sodium-formed zeolites used as the parent zeolites.

Table 2.2. Ratio of the each Si species obtained by the deconvolution of ^{29}Si DDMAS NMR spectra of zeolites.

Zeolite	Peak / ppm	Area ratio / %	Assignment
Na-MOR (Si/Al = 9)	-104.3	14.3	Q ⁴ (1Al)
	-107.6	38.4	Q ⁴ (1Al)
	-113.2	47.3	Q ⁴ (0Al)
Na-MFI (Si/Al = 12)	-105.7	24.8	Q ⁴ (1Al)
	-112.1	75.2	Q ⁴ (0Al)
Na-*BEA (Si/Al = 5.6)	-85.7	6.3	SiOH
	-94.8	4.6	SiOH
	-98.7	5.2	Q ⁴ (2Al)
	-104.3	45.4	Q ⁴ (1Al)
	-110.2	35.5	Q ⁴ (0Al)
	-115.9	3.1	Q ⁴ (0Al)
Na-CHA (Si/Al = 6.9)	-98.9	8.5	Q ⁴ (2Al)
	-103.0	5.0	Q ⁴ (1Al)
	-104.9	37.7	Q ⁴ (1Al)
	-109.8	9.5	Q ⁴ (0Al)
	-111.3	39.3	Q ⁴ (0Al)

2.4.2. Ion-exchange properties of the CHA zeolites

In this work, sodium-form zeolites were ion-exchanged in aqueous solution of copper acetate to prepare Cu ion-exchanged zeolite catalysts. It is often the case that Cu ion-exchanged zeolites for NH₃-SCR is prepared from Cu ion-exchange of its proton-form zeolites in aqueous solutions of copper nitrate^[34]. However, recent studies on CHA zeolites have shown that the sodium co-cation is more preferable than proton co-cation from the viewpoints of reaction rate at lower reaction temperatures and hydrothermal stability^[35-37]. The copper acetate solution (pH ≈ 6) applied in this study showed weaker acidity than copper nitrate solution (pH ≈ 5) and then undesirable sodium to proton ion-exchange during ion-exchange process can be suppressed. The Cu ion-exchange using the sodium-form zeolites and copper acetate solution for preparation has been adopted onto stoichiometry controlled Cu ion-exchange of zeolites until excessive region to utilize for NO direct decomposition.^[33] Zeolite MOR, MFI, and *BEA were supplied in a sodium form. The detail

of Cu ion-exchange of the MOR, MFI, and *BEA zeolites would be described in the following session. CHA zeolites were supplied in a Na/H form (Si/Al = 9) and a NH₄ form (Si/Al = 6.9). Then, they were ion-exchanged to sodium form, and Cu-zeolites were prepared by the following Cu ion-exchange. By the sodium ion-exchange, it was difficult to obtain the fully sodium form with Na/Al = 1. As the results of sodium ion-exchange, CHA zeolites with Si/Al = 9 and Si/Al = 6.9, Na/Al = 0.56 and Na/Al = 0.7 samples were obtained, respectively. It is suggested that the 8MR window of CHA cage is too small to defuse the hydrated sodium cation, or there exist specific Al sites that have small contribution in the ion-exchange process.

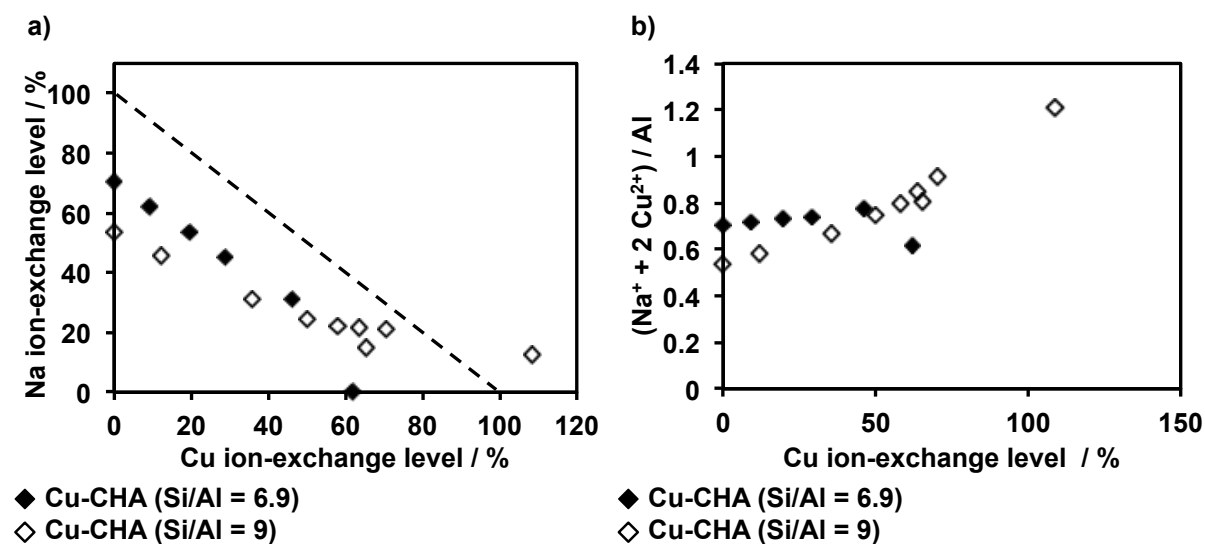


Figure 2.3. (a) Correlation between the Na ion-exchange level and Cu ion-exchange level, or (b) Cu ion-exchange level and $(\text{Na}^+ + 2 \text{Cu}^{2+})/\text{Al}$ of the CHA zeolites (Si/Al = 6.9; \blacklozenge , Si/Al = 9; \diamond). Na ion-exchange level were calculated at Na/Al = 1 as 100 % because the sodium ion is monovalent. Cu ion-exchange level were calculated at Cu/Al = 0.5 as 100 % because the copper ion is divalent.

Figure 2.3.a shows the profile for sodium to copper ion-exchange. Figure 2.3.b shows the correlation between $(2 \text{Cu}^{2+} + \text{Na}^+)/\text{Al}$ and Cu ion-exchange level. The value of $(2 \text{Cu}^{2+} + \text{Na}^+)/\text{Al}$ is an indicator of stoichiometry for sodium to copper ion-exchange. As shown in Figure 2.3.b, the values of $(2 \text{Cu}^{2+} + \text{Na}^+)/\text{Al}$ are almost constant for CHA zeolite with Si/Al = 6.9. This result suggests that a sodium to copper stoichiometric ion-exchange over this zeolite takes place in the process, and the ion-exchange sites available for the metal cation

ion-exchange are around 70 % to the total Al content in this CHA zeolite. On the other hand, for CHA zeolite with Si/Al = 9, the values of (2 Cu + Na)/Al increased gradually with the increase in Cu ion-exchange level (Figure 2.3.b). This result suggests that sodium to copper ion-exchange over this zeolite is not such a stoichiometric process, and indicates that CuOx species with extraframework oxygen might form at higher ion-exchange level region.

2.4.3. Cu ion-exchange properties of the zeolites in this work

The Cu ion-exchange of MOR, MFI, and *BEA zeolites were also conducted by the procedure using the sodium-form zeolites and copper acetate solution as precursor. This procedure was adopted for the stoichiometry controlled Cu ion-exchange until excessive region to utilize for both NH₃-SCR and NO direct decomposition.

It has been reported that among the Cu ion-exchanged zeolites, excessively ion-exchanged (molar ratio of Cu/Al > 0.5) Cu-MFI zeolites exhibit especially high catalytic activity for NO direct decomposition^[38]. The excessively ion-exchanged (Cu/Al > 0.5) Cu-MFI zeolites are generally prepared by repeated ion-exchange, using the aqueous solution of copper acetate^[33]. It has also been mentioned that excessively ion-exchanged zeolites other than MFI are difficult to prepare^[33]. Moreover, Cu ion-exchange of sodium form MFI zeolite with Si/Al = 12 in the aqueous solution of copper acetate is reported to be highly suitable for excessive Cu ion-exchange^[33]. However, more recently, the preparation of excessively ion-exchanged (Cu/Al > 0.5) MOR^[38], CHA^[39,14], and AEI^[39,14] zeolites and the application to catalyst or adsorbent have been reported.

Sodium-form zeolites with topologies other than MFI and modified Si/Al ratio to achieve the similar “cation density in micropores” to the MFI zeolite with Si/Al = 12 were ion-exchanged repeatedly in aqueous solution of copper acetate to prepare the excessively ion-exchanged Cu-zeolites, and their ion-exchange properties were compared to that of the MFI zeolite with Si/Al = 12. Table 2.3 shows the ion-exchange conditions and copper ion-exchange level of obtained samples, determined by inductively coupled plasma atomic emission spectrometry (ICP-AES). The ion-exchange level of copper was calculated by the following equation:

$$\text{Cu}^{2+} \text{ ion-exchange level} / \% = (\text{amount of Cu}) / (\text{amount of Al}) \times 200$$

This definition means that the ion-exchange level is 100 % at Cu/Al molar ratio is 0.5,

because the positive charge of divalent Cu cation is fully balanced by the negative charge of zeolite framework formed by the framework Al atoms. CHNS elemental analysis of excessively ion-exchanged *BEA and MOR zeolite samples (B12, M9) revealed that the carbon content was below 0.1 wt.%. This result suggests that the positive charge of loaded Cu species onto the zeolites are balanced only by the negative charge of the zeolite framework and that of Cu–Cu bridging extraframework oxygen or hydroxo ligands, not by that of residual acetate anion (AcO⁻) on the samples.

Table 2.3. Copper ion-exchange condition and ion-exchange level of the obtained samples.

Entry.	Precursor	Molarity / mmol L ⁻¹	Repeat / times	Cu Ion-Exchange Level ^(a) / %	Na Ion-Exchange Level ^(b) / %
Z1		0.94	1	12	91
Z1		1.8	1	33	69
Z2		4.2	1	54	48
Z3		7	1	78	31
Z4	Na-MFI	15	1	96	16
Z5	(Si/Al = 12)	30	1	109	9
Z6		10	2	110	4
Z6'		10	2	101	0
Z7		45	2	128	0
Z8		30	3	140	0
B1		0.91	1	5.3	88
B2		2.0	1	13	88
B3		3.6	1	21	74
B4		5.4	1	30	65
B5		5.9	1	39	66
B6	Na-*BEA	9.8	1	57	50
B7	(Si/Al = 5.6)	15	1	68	43
B8		30	1	86	30
B9		10	2	92	17
B10		45	2	119	6
B11		30	3	132	1
B12		30	4	141	0.1

M1		1.2	1	13	90
M2		3.6	1	36	72
M3		6	1	53	56
M4	Na-MOR (Si/Al = 9)	9.6	1	64	47
M5		15	1	70	42
M6		30	1	81	39
M7		10	2	87	31
M8		45	2	101	26
M9		30	3	106	24
C1		1.5	1	9.3	62
C2		3.0	1	20	53
C3	Na-CHA (Si/Al = 6.9)	4.5	1	29	45
C4		7.5	1	46	31
C5		12.1	1	62	0
C6		30	1	85	18
C901		1.3	1	12	46
C902		4.0	1	36	31
C903		6.7	1	50	25
C904	Na-CHA (Si/Al = 9)	10.7	1	58	22
C905		15	1	64	21
C906		30	1	70	21
C907		10	3	65	15
C908		30	3	109	12
B171	Na-*BEA (Si/Al = 17)	0.81	1	13	78
B172		2.4	1	41	55
B173		4.1	1	66	39
Z191	Na-MFI	1.8	1	31	66
Z192	(Si/Al = 19.5)	3.0	1	49	51
F1	Na-FAU (Si/Al = 2.8)	9.0	1	36	61

(a) Cu Ion-exchange level / % = (amount of Cu)/(amount of Al) × 200

(b) Na Ion-exchange level / % = (amount of Na)/(amount of Al) × 100

At the lower ion-exchange level (below ~ 80% ion-exchange level), the Cu/Al ratio of obtained samples was similar to the (Cu in solution)/(Al in zeolite) ratio of preparation conditions. This means that almost all Cu ion in the aqueous solution of copper acetate were ion-exchanged and loaded onto the zeolites in this region. By comparing the samples obtained by 30 mM, once ion-exchange and 10 mM, twice ion-exchange (*i.e.*, Z6–Z7, B8–B9, and M6–M7), it is revealed that the samples obtained in the latter condition have higher ion-exchange levels for all zeolites in spite of the smaller (Cu in solution)/(Al in zeolite) ratio of the preparation conditions. This result shows that repeated ion-exchange is more efficient to prepare the higher ion-exchanged samples than increasing copper concentration of the solution for ion-exchange. In the case of the repeated ion-exchange using high concentration (30–45 mM) of copper acetate solution, copper ion was successfully ion-exchanged excessively onto all zeolites. However, the ion-exchange level finally reached were dramatically different by the zeolites. MFI and *BEA zeolites were ion-exchanged upto around 140%. On the other hand, ion-exchange level of MOR zeolite was saturated below 110% in our ion-exchange conditions.

Correlation between copper and sodium ion-exchange level determined by the ICP-AES measurement is shown in Figure 2.4. The ion-exchange level of sodium, which is monovalent, was calculated by the following equation:

$$\text{Na}^+ \text{ ion-exchange level / \%} = (\text{amount of Na})/(\text{amount of Al}) \times 100$$

As is shown in Figure 2.4, it was revealed that in preparation of Cu-MFI and Cu-*BEA zeolite samples with higher ion-exchange level, almost all sodium ions were removed and replaced by the copper ions. On the other hand, on Cu-MOR samples, sodium ions remained over 20% of Na ion-exchange level even in the samples prepared by repeated ion-exchange using the aqueous solution of copper acetate with high concentration (30–45 mM). This result suggests that, in the micropore of MOR zeolite, a certain amount of sodium ions are difficult to be exchanged to copper ions even under repeated ion-exchange conditions. In any cases, not only MFI zeolite, but also MOR and *BEA zeolite, could be successfully ion-exchanged until excessively region, which is thought to be particularly suitable for NO direct decomposition.

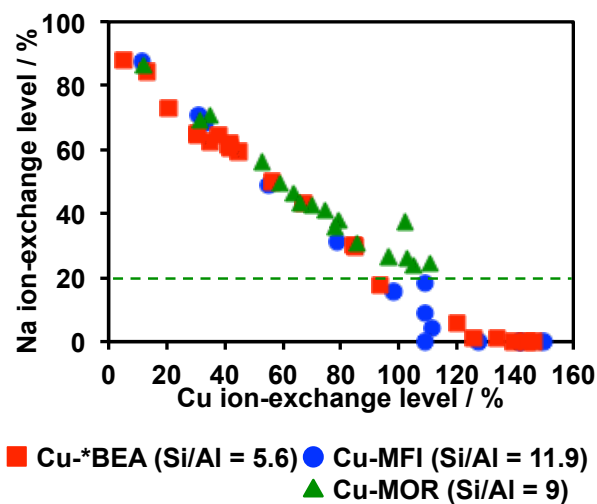


Figure 2.4. Correlation between the Cu ion-exchange level and Cu ion-exchange level on the Cu-zeolites with different framework structure. Na ion-exchange level were calculated at Na/Al = 1 as 100 % because the sodium ion is monovalent. Cu ion-exchange level were calculated at Cu/Al = 0.5 as 100 % because the copper ion is divalent.

2.5. Conclusions

As a descriptor for zeolites with several topologies, “cation density in micropores” was determined and the representative zeolite on each topology was selected with considering the parameter. The selected zeolites were subjected to the sodium to copper ion-exchange with same procedure except for the concentration to achieve the stoichiometry controlled Cu ion-exchange until excessive region. As a result, relatively well stoichiometry controlled sodium to copper ion-exchange was successfully achieved over all representative zeolites with similar “cation density in micropores”. Moreover, not only MFI zeolite, but also MOR and *BEA zeolite, could be successfully ion-exchanged until excessively region, which is thought to be particularly suitable for NO direct decomposition.

References

- [1] M. E. Davis, L. F. Lobo, *Chem. Mater.* **1992**, *4*, 756.
- [2] L. Tosheva, V. P. Valtchev, *Chem. Mater.* **2005**, *17*, 2494.
- [3] M. Ogura, *Catal. Surv. Asia* **2008**, *12*, 16.
- [4] J. Dědeček, Z. Sobalík, B. Wichterlová, *Catal. Rev.* **2012**, *54*, 135.
- [5] S. Li, J. Li, M. Dong, S. Fan, T. Zhao, J. Wang, W. Fan, *Chem. Soc. Rev.* **2019**, *48*, 885.
- [6] B.A. Williams, S.M. Babitz, J.T. Miller, R.Q. Snurr, H.H. Kung, *Appl. Catal. A* **1999**, *177*, 161.
- [7] M. Ogura, S. Shinomiya, J. Tateno, Y. Nara, M. Nomura, E. Kikuchi, M. Matsukata, *Appl. Catal. A* **2001**, *219*, 33.
- [8] J. R. Di Iorio, R. Gounder, *Chem. Mater.* **2016**, *28*, 2236.
- [9] S. Park, T. Biligetu, Y. Wang, T. Nishitoba, J. N. Kondo, T. Yokoi, *Catal. Today* **2018**, *303*, 64.
- [10] Y. Nakasaka, T. Kanda, K. Shimizu, K. Kon, G. Shibata, T. Masuda, *Catal. Today* **2019**, *332*, 64.
- [11] M. Iwamoto, H. Furukawa, S. Kagawa, *Stud. Surf. Sci. Catal.* **1986**, *28*, 943.
- [12] J. H. Kwak, D. Tran, S. D. Burton, J. Szanyi, J. H. Lee, C. H. F. Peden, *J. Catal.* **2012**, *287*, 203.
- [13] J. D. Albarracin-Caballero, I. Khurana, J. R. Di Iorio, A. J. Shih, J. E. Schmidt, M. Dusselier, M. E. Davis, A. Yezerets, J. T. Miller, F. H. Ribeiro, R. Gounder, *React. Chem. Eng.* **2017**, *2*, 168.
- [14] S. V. Priya, T. Ohnishi, Y. Shimada, Y. Kubota, T. Masuda, Y. Nakasaka, M. Matsukata, K. Itabashi, T. Okubo, T. Sano, N. Tsunoji, T. Yokoi, M. Ogura, *Bull. Chem. Soc. Jpn.* **2018**, *91*, 355.
- [15] V. L. Sushkevich, J. A. van Bokhoven, *ACS Catal.* **2019**, *9*, 6293.
- [16] M. De Prins, E. Verheyen, A. Hoffmann, G. Vanbutsele, S. Pulinthanathu Sree, S. Kerkhofs, L. Van Tendeloo, F.-W. Schütze, J. Martens, *J. Catal.* **2020**, *390*, 224.
- [17] F. Gao, D. Mei, Y. Wang, J. Szanyi, C. H. F. Peden, *J. Am. Chem. Soc.* **2017**, *139*, 4935.
- [18] C. Paolucci, I. Khurana, A. A. Parekh, S. Li, A. J. Shih, H. Li, J. R. Di Iorio, J. D. Albarracin-Caballero, A. Yezerets, J. T. Miller, W. N. Delgass, F. H. Ribeiro, W. F. Schneider, R. Gounder, *Science* **2017**, *357*, 898.
- [19] M. H. Groothaert, J. A. Bokhoven, A. A. Battiston, B. M. Weckhuysen, R. A. Schoonheydt, *J. Am. Chem. Soc.* **2003**, *125*, 7629.

- [20] C. Paolucci, A. A. Parekh, I. Khurana, J. R. Di Iorio, H. Li, J. D. A. Caballero, A. J. Shih, T. Anggara, W. N. Delgass, J. T. Miller, F. H. Ribeiro, R. Gounder, W. F. Schneider, *J. Am. Chem. Soc.* **2016**, *138*, 6028.
- [21] Database of Zeolite Structures, <http://www.iza-structure.org/databases/>.
- [22] M. D. Foster, I. Rivin, M. M. J. Treacy, O. Delgado Friedrichs, *Microporous Mesoporous Mater.* **2006**, *90*, 32.
- [23] T. Yokoi, H. Mochizuki, S. Namba, J. N. Kondo, T. Tatsumi, *J. Phys. Chem. C* **2015**, *119*, 15303.
- [24] T. Yokoi, H. Mochizuki, T. Biliget, Y. Wang, T. Tatsumi, *Chem. Lett.* **2017**, *46*, 798.
- [25] T. Biliget, Y. Wang, T. Nishitoba, R. Otomo, S. Park, H. Mochizuki, J. N. Kondo, T. Tatsumi, T. Yokoi, *J. Catal.* **2017**, *353*, 1.
- [26] Y. Román-Leshkov, M. Moliner, M. E. Davis, *J. Phys. Chem. C* **2011**, *115*, 1096.
- [27] J. Dedecek, V. Balgová, V. Pashkova, P. Klein, B. Wichterlová, *Chem. Mater.* **2012**, *24*, 3231.
- [28] K. Muraoka, W. Chaikittisilp, Y. Yanaba, T. Yoshikawa, T. Okubo, *Angew. Chem. Int. Ed.* **2018**, *57*, 3742.
- [29] J. R. Di Iorio, S. Li, C. B. Jones, C. T. Nimlos, Y. Wang, E. Kunkes, V. Vattipalli, S. Prasad, A. Moini, W. F. Schneider, R. Gounder, *J. Am. Chem. Soc.* **2020**, *142*, 4807.
- [30] Y. Kamimura, W. Chaikittisilp, K. Itabashi, A. Shimojima, T. Okubo, *Chem. Asian J.* **2010**, *5*, 2182.
- [31] K. Itabashi, Y. Kamimura, K. Iyoki, A. Shimojima, T. Okubo, *J. Am. Chem. Soc.* **2012**, *134*, 11542.
- [32] Y. Kubota, K. Itabashi, S. Inagaki, Y. Nishita, R. Komatsu, Y. Tsuboi, S. Shinoda, T. Okubo, *Chem. Mater.* **2014**, *26*, 1250.
- [33] H. Yahiro, M. Iwamoto, *How to Prepare Heterogeneous and Homogeneous Catalysts*, ed. M. Iwamoto, NTS, Tokyo, **2011**, Chap. 3, 246.
- [34] J. H. Kwak, R. G. Tonkyn, D. H. Kim, J. Szanyi, C. H. F. Peden, *J. Catal.* **2010**, *275*, 187.
- [35] F. Gao, Y. Wang, N. M. Washton, M. Kollaf, J. Szanyi, C. H. F. Peden, *ACS Catal.* **2015**, *5*, 6780.
- [36] Y. Cui, Y. Wang, D. Mei, E. D. Walter, N. M. Washton, J. D. Holladay, Y. Wang, J. Szanyi, C. H. F. Peden, F. Gao, *J. Catal.* **2019**, *378*, 363.
- [37] Y. Cui, Y. Wang, E. D. Walter, J. Szanyi, Y. Wang, F. Gao, *Catal. Today* **2020**, *339*,

233.

[38] Y. Kuroda, A. Kotani, H. Maeda, H. Moriwaki, T. Morimoto, M. Nagao, *J. Chem. Soc., Faraday Trans.* **1992**, 88, 1583.

[39] M. Moliner, C. Franch, E. Palomares, M. Grillb, A. Corma, *Chem. Commun.* **2012**, 48, 8264.

Chapter 3

Investigation on the formation of active site for NH₃-SCR over Cu-Zeolites with several topologies

3.1. Introduction

Nitrogen oxides (NO_x) formed during combustion processes by unavoidable reactions between oxygen (O₂) and nitrogen (N₂) are harmful to the environment and human health. Therefore, NO_x emissions, as hydrocarbon (HC) and carbon monoxide (CO) emissions, have been strictly regulated by governments in several regions. Lean-burn engines in automobiles, such as diesel engines, emit exhaust gases in the presence of high concentrations of O₂ owing to the high air-to-fuel ratio. Therefore, the removal of NO_x by reduction to N₂ is difficult because reducing agents such as HCs and CO are consumed. The selective catalytic reduction of NO_x using ammonia as the reducing agent (NH₃-SCR) is one of the most promising processes for reducing NO_x in O₂-rich exhausts. Among the catalysts for NH₃-SCR, Cu ion-exchanged zeolite (Cu-zeolite) catalysts exhibit high conversions in a wide temperature range from 423 to 723 K^[1]. Considering the on-road reaction conditions, the most important temperature region is around 473 K, and Cu-zeolite catalysts have been attracted great attention owing to their remarkable catalytic activities at this temperature region.

NH₃-SCR over Cu-zeolite catalysts was first reported using Y zeolites with FAU topology.^[2,3] However, until the late 1990s, studies on deNO_x processes using Cu-zeolite catalysts mainly focused on the direct decomposition of NO into N₂ and O₂,^[4-7] which requires no reducing agent. In addition, SCR using hydrocarbons as reducing agents (HC-SCR) has been considered desirable,^[8,9] as this process exploits HCs already present in the exhaust, thus avoiding the further addition of reducing agents. Nevertheless, the low activities of Cu-zeolite catalysts for the direct decomposition of NO and HC-SCR have hindered commercialization and interest in such reactions over Cu-zeolite catalysts has declined. Unlike these two processes, NH₃-SCR requires the addition of toxic reducing agents; therefore, NH₃-SCR over Cu-zeolites received limited attention until the early 2000s and only a few studies using MOR^[10,11] or MFI^[12] zeolites have been reported. However, Cu-zeolite catalysts were finally commercialized in a deNO_x process for diesel engines involving urea-SCR, which is a type of NH₃-SCR that uses a nontoxic urea solution as an NH₃ source^[13], as the reaction rate was higher than those for the direct decomposition of NO and HC-SCR in the temperature range of diesel engine exhausts.

A large-pore *BEA (12-membered ring; MR) zeolite that has greater hydrothermal stability than the medium-pore MFI (10 MR) zeolite was tested in early studies of practical catalysts for NH₃-SCR.^[13,14] However, *BEA zeolites also suffer from hydrothermal

instability and deactivation by HCs^[14]. The commercialization of Cu-zeolite catalysts in a deNO_x process for diesel engines was achieved using Cu-SSZ-13 zeolite catalysts with CHA topology (8 MR)^[15]. The Cu-CHA catalyst exhibits high activity and selectivity in a wide temperature region and high hydrothermal durability as compared to Cu-MFI, Cu-*BEA, and Cu-FAU catalysts^[16,17].

Since the development of Cu-CHA zeolites, many zeolites with a variety of topologies and compositions have been tested for NH₃-SCR applications. Various zeolite topologies have been successfully applied to NH₃-SCR including AEI,^[18–20] LTA (high silica),^[21] UFI,^[22] KFI,^[22] MSE,^[23] RTH,^[20,24] AFX^[25–27], and ERI^[28]. In addition, numerous preparation procedures such as organic structure-directing agent (OSDA)-free synthesis,^[29,30] ultrafast flow synthesis,^[26,28,31] synthesis using different OSDAs,^[26,27,32] P modification,^[25,33–36] and the addition of a second metal cation^[37–41] have been developed. When adopting zeolites for NH₃-SCR, the main consideration has been a high hydrothermal stability because the catalytic activities for NH₃-SCR are less affected by zeolite topology than those for other reactions catalyzed by Cu-zeolites such as NO direct decomposition^[5] or methane partial oxidation into methanol^[42].

The great applicability of Cu-zeolites with various topologies to NH₃-SCR is supported by the following widely accepted reaction mechanism for the reaction over Cu-zeolites around 473 K. This reaction mechanism has been suggested based on studies of Cu-CHA zeolites, with have simple structures. The active centre for NH₃-SCR over Cu-CHA zeolites is suggested to be an isolated Cu ion in a zeolite micropore, located in either a 6 MR as a bare Cu²⁺ balanced by two negative charges of the zeolite framework^[43,44] or in an 8 MR as a Cu²⁺–OH[–] complex balanced by a negative charge of the zeolite framework^[45]. Under steady state NH₃-SCR conditions, the isolated Cu ions have a mixture of monovalent and divalent states^[46]. From electron paramagnetic resonance spectra and the linear dependence of the NH₃-SCR kinetics on the square of Cu loading at low Cu loading levels, a high mobility of Cu ions and the existence of transient dimeric Cu species as active sites were suggested, respectively^[47]. The reduction of Cu²⁺ to Cu⁺ was suggested to occur via reaction with NO + NH₃^[48,49]. Moreover, X-ray absorption spectroscopy (XAS) spectra and *ab initio* molecular dynamics simulations suggested that both Cu²⁺ and Cu⁺ are coordinated to NH₃ molecules, not by zeolite framework oxygen, in the temperature region around 473 K^[50]. The Cu⁺ to Cu²⁺ oxidation pathways is proposed to proceed by the reaction of a pair of highly mobile linear H₃N–Cu⁺–NH₃ complexes with O₂ molecules^[51,52]. This oxidation process is thought to be the

rate-determining step for NH₃-SCR over commercial Cu-CHA catalysts with relatively low Cu/Al ratios^[53] under on-road reaction conditions at low O₂ pressures (5–20 kPa)^[54,55]. In this case, the formation of dimeric Cu intermediates would be an important step, with the NH₃-SCR rate depending on the square of the Cu loading^[51] or the Cu volumetric density in zeolites,^[52] and being independent of the zeolite structure except for the channel dimensions^[20,50]. Therefore, it has been thought that the preparation of the catalysts with high Cu loading are necessary to achieve high reaction rates. However, the formation of Cu²⁺–OH[−] active site with low stabilities has been observed on Cu-CHA catalysts with high Cu loadings.⁵⁶ During high-temperature hydrothermal treatment, the Cu²⁺–OH[−] active sites easily agglomerate into CuO_x clusters, the diffusion of which is suggested to be the primary cause of zeolite destruction that leads to the deterioration of catalytic activity^[57]. Accordingly, Cu-CHA zeolites with relatively low Si/Al ratios (≈ 10) and low Cu/Al ratios (≈ 0.3) have been used as commercial catalysts to maintain a balance between catalytic activity and hydrothermal stability^[53,57]. However, it is theoretically predicted that a certain amount of Cu²⁺–OH[−] species with low stability will form over the catalysts with such compositions^[52]. Therefore, it is desirable to obtain Cu-zeolite catalysts with both high reaction rates for NH₃-SCR and low Cu loadings.

However, guiding principles for obtaining such catalysts are lacking, mainly because there is no universal understanding of NH₃-SCR over Cu-zeolites. Although some efforts have been made to find new Cu-zeolite catalysts, they have focused on durability without sufficiently considering reaction rates. Therefore, the development of improved catalysts requires large-scale screening^[25,58]. Considering this background, this chapter focused on the relationship between zeolite topology and the reaction rate for NH₃-SCR. Some older reports have suggested that the turnover frequency^[17] or the dependence of the reaction rate on Cu loading^[12] is affected by zeolite topology, which indicates that the NH₃-SCR rate should also be affected by zeolite topology. Therefore, investigating the effect of zeolite topology on NH₃-SCR activity may provide a rational way to develop appropriate design principles.

The aim of this chapter was to determine the key factors of zeolite topology that affect low-temperature NH₃-SCR activity. Model zeolites with various topologies, namely, MFI (a typical NO direct decomposition catalyst)^[7,59], MOR (a typical methane partial oxidation catalyst)^{60,61}, and *BEA and CHA (typical NH₃-SCR catalysts)^[16,17] zeolites were selected, all of which are thought to have dimeric Cu active sites^[51,52,59–62]. As zeolites with

different topologies have different proportions of micropore in a fixed zeolite cell volume, to compare the catalytic activities, a suitable Si/Al ratio was chosen for each zeolite so that the cation-exchange-site densities in the micropore were similar. Then, the dependence of the reaction rate at 473 K on the mean “Cu density in micropores” determined in the previous chapter was used as an indicator of the effect of zeolite topology on NH₃-SCR, whose rate-determining step under on-road reaction condition is thought to be the oxidation of Cu⁺ to Cu²⁺ by O₂ molecules through dimeric Cu intermediates^[51,52]. Recently, it has been shown that a combination of *operando* and intrinsic kinetic measurements is critical for understanding the rate-determining step and the most abundant reactive intermediates^[63]. As an *operando* method, time-resolved UV-Vis measurements^[59,64], which can provide information about the coordination environment of Cu²⁺ species, were conducted. Finally, the relationship between the dynamic Cu redox properties, as observed by time-resolved UV-Vis measurements, and the reaction rates was evaluated.

3.2. Experimental

3.2.1. Catalytic activity test for NH₃-SCR

The catalytic activity for NH₃-SCR was measured using a fixed-bed flow reactor. The component gas mixtures were prepared using mass flow controllers and then introduced into the reactor. The Cu-zeolite catalyst (20 mg) was mixed with 280 mg of SiC (100 mesh) and packed in a quartz tube (7 mm i.d.). Prior to the test, the catalyst was pretreated with 5% O₂ in dried N₂ at a total flow rate of 200 cm³ min⁻¹ at 873 K for 10 min. The catalytic test was conducted using a mixture of 500 ppm NO, 500 ppm NH₃, and 5% O₂ in dried N₂ with a total flow rate of 200 cm³ min⁻¹ (50,000 h⁻¹ GHSV). H₂O was excluded from the reaction gas to determine the reaction rates under conditions that minimized the factors that could affect the Cu species and thus reflect the nature of Cu species observed using the characterization techniques. During the test, the temperature was decreased from 873 K and the outlet concentrations of NH₃, NO, and N₂O were detected with a VA-3000 Gas Analyzer connected to a VS-3000 Rack-Mounted Sample Gas Conditioning System (Horiba, Ltd.).

For the kinetic measurements of the reaction rates over the catalysts at 473 K, the contact time was adjusted by reducing the amount of catalyst (2–20 mg) or increasing the total flow rate to 300 cm³ min⁻¹ to achieve a NO conversion of less than 40% at 473 K. The reaction rates were calculated by determining the moles of NO converted to N₂ per second by the weight of the packed catalyst (per g_{cat}) or the moles of Cu atoms in the catalyst (per Cu).

3.2.2. Quantitative analysis of reactants consumed during transient measurements

The equipment used for the catalytic tests was also used for the transient measurements. Pretreatment was conducted under a feed of 5% O₂ in dried N₂ at a total flow rate of 200 cm³ min⁻¹ at 873 K for 10 min, followed by cooling to 473 K and O₂ purging under a N₂ flow.

Scheme A: NH₃ adsorption was conducted by switching the feed from dried N₂ to 500 ppm NH₃ in dried N₂. To model the Cu ion reduction step, the feed was switched from 500 ppm NH₃ in dried N₂ to 500 ppm NO + 500 ppm NH₃ in dried N₂ at 473 K, and the transient response was measured. The amounts of NH₃ and NO consumed during the transient reactions over Cu-zeolites were obtained from the breakthrough and elution curves recorded by the gas analyzer at 473 K. The parent sodium-form zeolites were used as the background to obtain the amounts reacted per Cu. The amount of Cu ions reducible to Cu⁺ was estimated from the amount of NO consumed, and the state of Cu⁺ was estimated from the total amount

of NH_3 consumed during NH_3 adsorption and the response upon switching from NH_3 to $\text{NH}_3 + \text{NO}$. The state of Cu^{2+} in the NH_3 flow was estimated by the amount of NH_3 consumed during NH_3 adsorption and the amount of Cu ions reducible to Cu^+ .

Scheme B: NH_3 adsorption was conducted by switching the feed from dried N_2 to 500 ppm NH_3 and 5% O_2 in dried N_2 . The transient response upon switching the feed from 5% O_2 in dried N_2 to 500 ppm NO and 5% O_2 in dried N_2 at 473 K after purging NH_3 from the feed was measured. The amount of Cu^{2+} in the Cu-zeolites was quantified using the amount of NO . The parent sodium-form zeolites were used as the background to account for the reversible adsorption of reactants on the zeolites.

3.2.3. *In situ* UV-Vis measurements

Diffuse reflectance UV-Vis measurements were performed using a JASCO V-670 UV-Vis spectrometer equipped with an integrating sphere, an optical fiber unit, and an *in situ* diffuse reflectance flow cell attached to a quartz window^[65]. The *in situ* cell was connected to a gas flow system with mass flow controllers for He, O_2 , 4% NO/He , and 4% NH_3/He . Gas mixtures were prepared using the mass flow controllers and then introduced into the *in situ* cell. The spectra were recorded in reflectance mode and converted to pseudo absorbance by the Kubelka–Munk (KM) function using the JASCO Spectra Manager Suite. The spectrum of leveled BaSO_4 powder at room temperature (~ 20 °C) was used as the background. For these measurements, a 15–19 mg sample was leveled on a stainless steel dish (6 mm i.d.) and placed in the center of the *in situ* flow cell. Pretreatment was conducted using a feed of 5% O_2 in He at a total flow rate of $100 \text{ cm}^3 \text{ min}^{-1}$ at 873 K for 10 min, followed by cooling to 473 K and purging with He. The required gas mixtures, as described in the following schemes, were fed to the *in situ* cell at a total flow rate of $100 \text{ cm}^3 \text{ min}^{-1}$ at 473 K. The relative concentration of N_2 in the outlet gas was monitored using a quadrupole mass spectrometry (MS; BELMASS, Microtrac BEL).

Scheme 1: After pretreatment, NH_3 adsorption was conducted using a feed of 500 ppm NH_3 in He at 473 K. To model the reduction step, the feed was switched from 500 ppm NH_3 to 500 ppm $\text{NO} + 500$ ppm NH_3 in He at 473 K, and the transient response was measured. To model the reoxidation of Cu ions, the transient reaction under a feed of 5% $\text{O}_2 + 500$ ppm NH_3 in He at 473 K was monitored after purging NO from the *in situ* cell using a feed of 500 ppm NH_3 .

Scheme 2: To model the reduction step, the transient response under a feed of 500 ppm $\text{NO} + 500$ ppm NH_3 in He at 473 K was monitored after pretreatment. To model the reoxidation of

Cu ions, the transient reaction under a feed of 5% O₂ in He at 473 K was monitored after purging of NO and NH₃ from the *in situ* cell using a feed of He.

3.3.3. *In situ* IR measurements

Fourier transform infrared (FT-IR) spectra were recorded at a resolution of 4 cm⁻¹ using a JASCO FT-IR 4600 spectrometer equipped with a triglycine sulfate detector. Each zeolite sample (20–40 mg) was pressed into a thin self-supporting wafer with a diameter of 20 mm and placed into an IR cell with CaF₂ windows attached to a closed gas-circulation system. The samples were pretreated under vacuum at 773 K for 1 h and then under 15 kPa O₂ at the same temperature for 10 min, followed by evacuation at room temperature. The NO adsorption spectra were recorded after NO dosage at increasing pressure from 5 to 250 Pa at room temperature. The IR spectra obtained by the subtraction of the background spectra from the NO adsorption spectra were shown. Spectra curve fitting was carried out using the Voigt distribution in the JASCO Spectra Manager Suite.

3.3. Results and Discussion

3.3.1. Cu ion exchange level dependence of catalytic activities for NH₃-SCR

All the Cu-ion-exchanged zeolite catalysts exhibited activity for a steady-state standard NH₃-SCR reaction. Figure 3.1 shows the results as a function of reaction temperature over Cu-ion-exchanged MOR, MFI, *BEA, and CHA zeolites with a Cu ion exchange level of ~30% as a representative example. The H₂O feed was omitted in this catalytic activity test to obtain the reaction rates under reaction conditions that directly reflect the nature of the Cu species observed using the characterization techniques were directly reflected. For all the Cu-ion-exchanged zeolites, both the NO and NH₃ conversions increased from 423 to 573 K, and the NO conversion decreased over 673 K with almost complete consumption of NH₃. It has been suggested that NH₃ oxidation by O₂ occurs as a side reaction over 573 K and the selectivity for NH₃ in NH₃-SCR decreases,^[79] which explains the phenomena observed at high reaction temperatures in this chapter. In the low-temperature region around 473 K, the NH₃ and NO conversions over each zeolite were similar, meaning that NH₃ selectivity during SCR in this temperature region is almost 100% (Figure 3.1). However, the Cu-zeolites with different topologies exhibited obviously different conversions for NO and NH₃.

Figure 3.2a shows the dependence of the catalytic activity over the MOR, MFI, *BEA, and CHA zeolites at 473 K on the Cu ion-exchange level. Each zeolite showed a different slope for NO conversion to N₂, decreasing in the following order: *BEA > CHA > MFI > MOR, which is the same as the Cu loading order (Figure 3.2b). As shown in Figure 3.2, the catalytic activity of each zeolite increased with an increase in the Cu ion exchange level, but the relationship clearly differed for the different zeolites. This finding indicates that the observed order is not simply explained by the Cu loading. Figure 3.3 shows the dependence of NH₃ selectivity during SCR at 873 K on the Cu ion-exchange level. As shown in Figure 3.3, there was no significant decrease in NH₃ selectivity during SCR at 873 K over all zeolites. The CuO_x cluster species have been suggested to be inactive for SCR but to cause the NH₃ selectivity during SCR to decrease^[66]. Therefore, a significant increase in CuO_x clusters along with an increase in the ion-exchange level of Cu²⁺ can be ruled out. Note that the NO conversion to N₂ over the *BEA zeolite decreased at high Cu ion exchange levels; however, 100% NO conversion was achieved over all catalysts and the decrease in N₂ formation was mainly due to an increase in N₂O formation. In summary, these results clearly demonstrate that the catalytic activity of Cu-zeolites for NH₃-SCR is strongly affected by the zeolite framework.

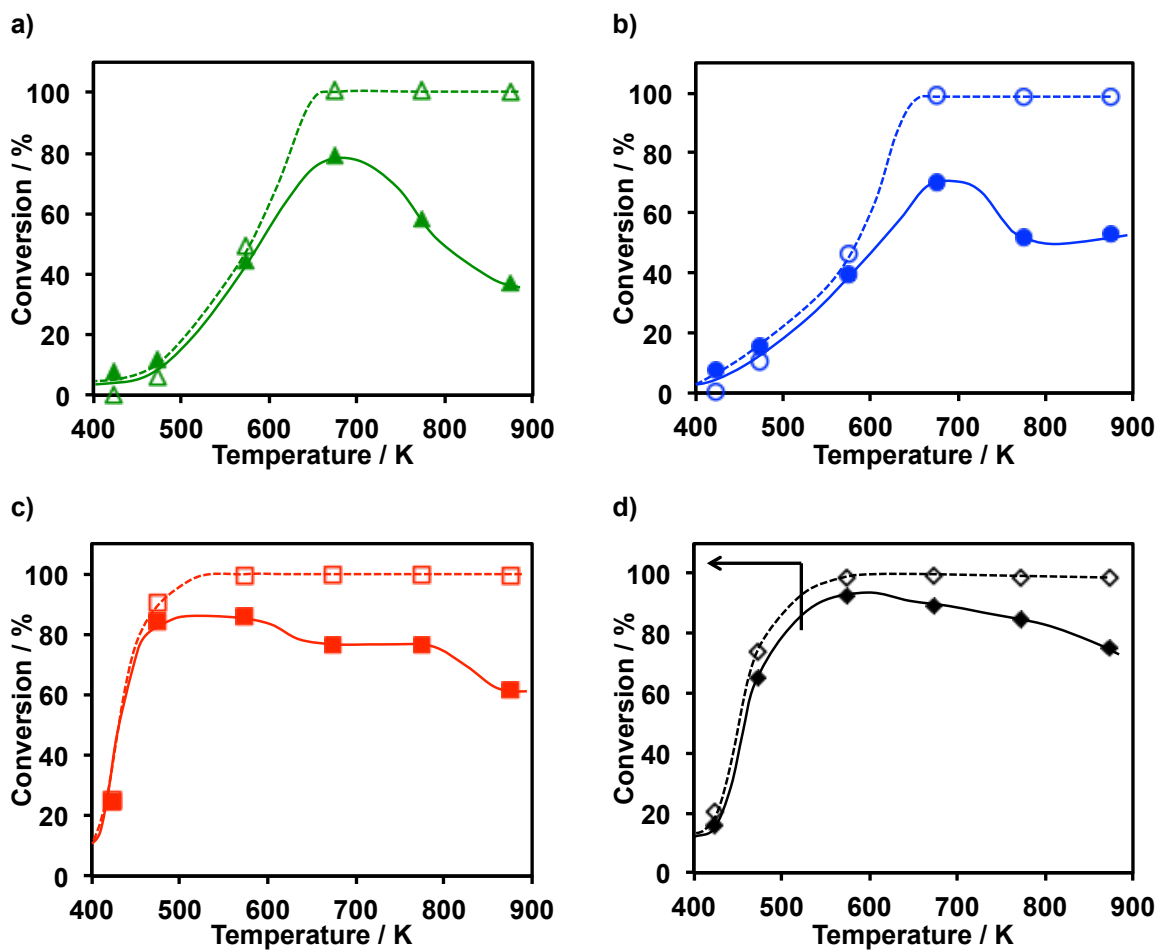


Figure 3.1. The catalytic activities for NH_3 -SCR of the (a) Cu-MOR (36 % Cu ion-exchange level), (b) Cu-MFI (33 % Cu ion-exchange level), (c) Cu-*BEA (39 % Cu ion-exchange level), and (d) Cu-CHA (29 % Cu ion-exchange level) zeolite catalysts as function of reaction temperature. The filled and hollow symbols show the conversion of NO and conversion of NH_3 , respectively.

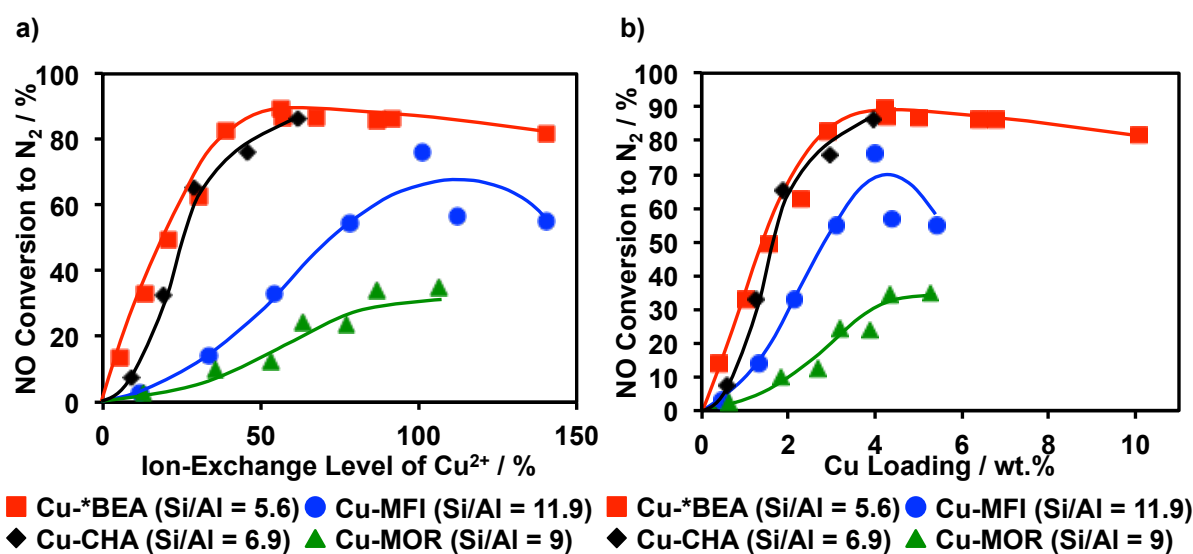


Figure 3.2. Correlation between the NO conversion into N₂ in the NH₃-SCR at 473 K and (a) Cu ion-exchange level or (b) Cu loading over the MOR (▲), MFI (●), *BEA (■), and CHA(◆) zeolites.

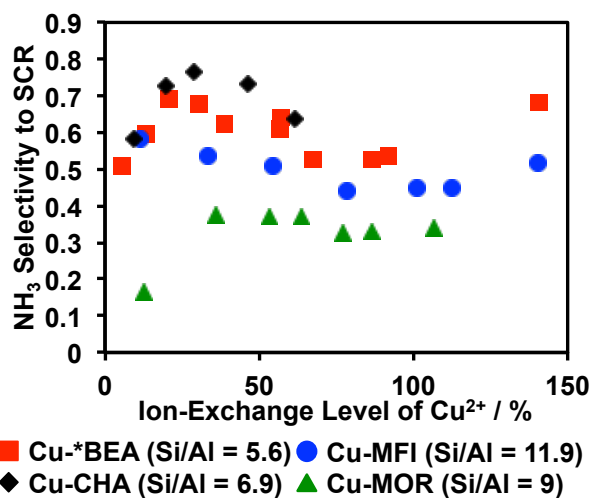


Figure 3.3. Correlation between the NH₃ selectivity to SCR in the NH₃-SCR at 873 K and Cu ion-exchange level over the MOR (▲), MFI (●), *BEA (■), and CHA(◆) zeolites.

3.3.2. Reaction rates for low-temperature NH₃-SCR with similar cation densities in micropores

Figure 3.4 shows the reaction rates per g_{cat} over the Cu-ion-exchanged zeolites as a function of the Cu loading of the zeolites or the Cu density in micropores (approximately proportional to the Cu ion exchange level) at 473 K. The reaction rates were calculated based

on kinetic measurements under approximate differential reaction conditions. As shown in Figure 3.4, the reaction rate depends strongly on both the Cu loading and the Cu density in micropores of the zeolite structure. Over the *BEA or CHA zeolites, the reaction rates per g_{cat} increased more rapidly with the increase in Cu loading (Figure 3.4a) or Cu density in micropores (Figure 3.4b) than over the MFI or MOR zeolites. In the low Cu density region, the reaction rates per g_{cat} for the same Cu densities in micropores and Cu loadings decrease in the following order: *BEA \geq CHA $>$ MFI $>$ MOR. As the Cu ion exchange level increased, the reaction rates per g_{cat} over CHA zeolites increased more rapidly than those over *BEA zeolites. This result indicates that the catalytic activities of the Cu species for NH_3 -SCR are strongly affected by the zeolite topology, even though the reaction is thought to occur on Cu ions mobilized in the micropores and weakly bound to the zeolite frameworks at this temperature^[50–52].

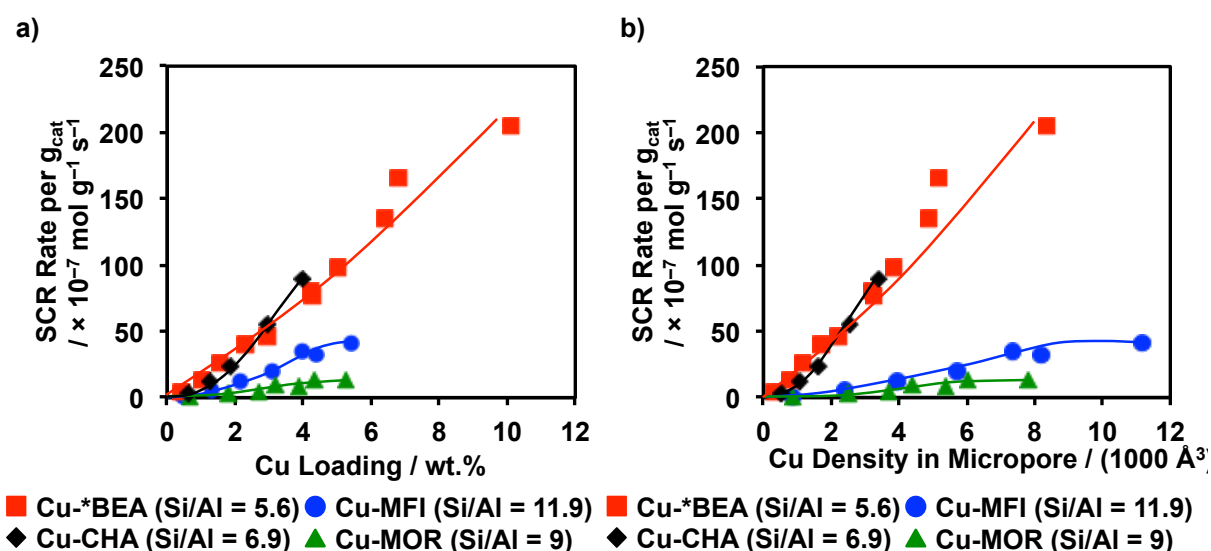


Figure 3.4. Correlation between the standard NH_3 -SCR rate per g_{cat} at 473 K and (a) Cu loading or (b) Cu density in micropores over the MOR (▲), MFI (●), *BEA (■), and CHA(◆) zeolites.

Similarly, the reaction rates per Cu for NH_3 -SCR over the Cu-zeolites with various topologies are shown as a function of Cu loading or Cu density in micropores in Figure 3.5. Note that the effects of different Cu loadings on the reaction rates are eliminated in these plots, even in the plots for the Cu density in micropores, because the reaction rate is normalized by the Cu loading of the catalyst. The plots for the reaction rates per Cu revealed the tendency

over each zeolite more clearly than those for the reaction rate per g_{cat} . Reflecting the high reaction rates per g_{cat} in the low Cu ion-exchange region and the gradual increase with increasing Cu loading, extremely high reaction rates per Cu were observed over the *BEA zeolites. An obvious increase in the reaction rate per Cu with the increase in the Cu ion-exchange level was observed for the CHA zeolite. Compared with the CHA zeolite, the increases in the reaction rates per Cu over the *BEA and MFI zeolites with the increase in the Cu ion exchange level were moderate. The Cu ion exchange level hardly affected the reaction rate per Cu over the MOR zeolite.

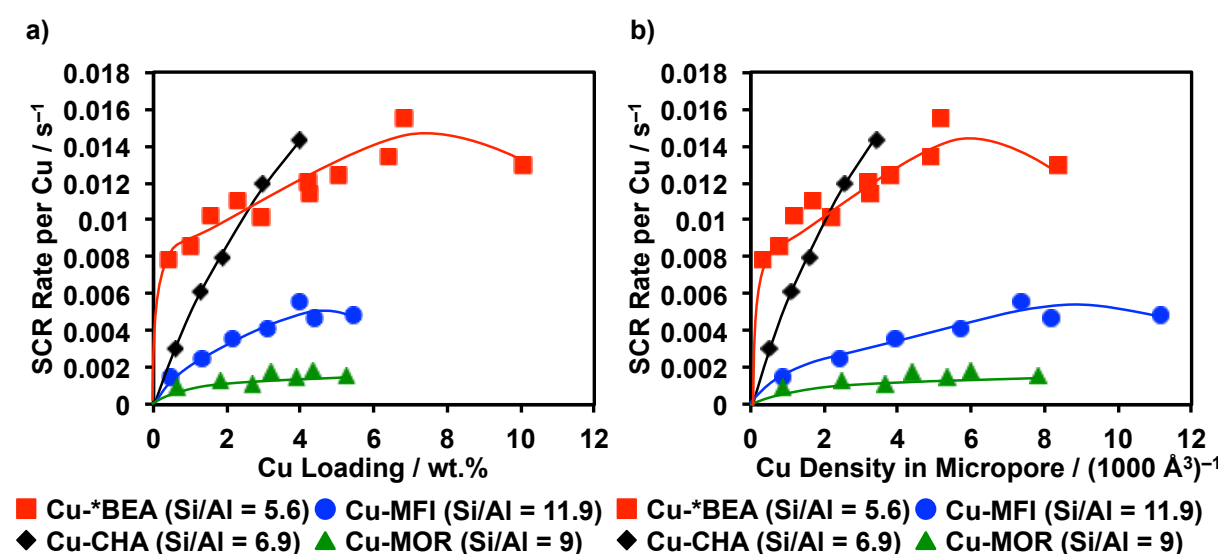


Figure 3.5. Correlation between the standard NH_3 -SCR rate per Cu at 473 K and (a) Cu loading or (b) Cu Density in Micropore over the MOR (▲), MFI (●), *BEA (■), and CHA(◆) zeolites.

Water vapor can cause the agglomeration of Cu species through the hydrolysis of Cu cations, which has recently been suggested to cause the damage zeolite frameworks^[57]. However, existence of the water vapor has been shown to have no effect on the reaction rates^[52]. In these tests, no water was present in the reaction stream and the reaction rate was recorded as soon as the reaction temperature reached a steady-state. Therefore, it can be assumed that the reaction rates were measured under the reaction conditions that minimized the factors that could change the properties of the Cu species observed using the characterization techniques. Thus, both the volumetric density of Cu ions, and the structure of the parent zeolite govern the reaction rates at low temperatures (~ 473 K) for NH_3 -SCR over

Cu-zeolite catalysts.

3.3.3. Reduction and oxidation behaviors of Cu ion species during transient reactions

The dynamics of Cu ions during the redox steps of NH₃-SCR were investigated by time-resolved UV-Vis measurements. It has been suggested that the reduction–oxidation cycle during NH₃-SCR over Cu-zeolite catalysts involves Cu⁺ coordinated to two NH₃ molecules and Cu²⁺ coordinated to three or four NH₃ molecules^[50]. Further, it has been shown that the reduction step from Cu²⁺ to Cu⁺ occurs via reaction with NO + NH₃, whereas the oxidation step from Cu⁺ to Cu²⁺ occurs via reaction with O₂^[52]. To observe the redox cycle between [Cu^{II}(NH₃)₄]²⁺ or [Cu^{II}(OH)(NH₃)₃]²⁺ and [H₃N–Cu^I–NH₃]⁺, transient response measurements were conducted according to Scheme 1. Figure 3.6 shows the UV-Vis spectra of the *BEA zeolite with a Cu²⁺ ion exchange level of 21% in various atmospheres at 473 K. Following pretreatment in a feed of 5% O₂ at 873 K, the peak below 400 nm, assigned to ligand-to-metal charge transfer (LMCT) from the oxygen atoms of the zeolite framework (O_Z) to Cu, increases in intensity with a red shift of the peak edge. This phenomenon, which has been observed previously^[67], likely results from an increase in the degree of covalency in the metal–ligand bond. Moreover, the single broad peak centered at 760 nm, which is typical of the d–d transition (²E_g → ²T_{2g}) of octahedral Cu²⁺^[68] attached to H₂O or zeolite framework oxygen atoms, obviously increases in intensity with a slight blue shift following the high-temperature dehydration pretreatment (hydrated: 780 nm, dehydrated: 740 nm). A similar increase in the d–d transition band due to dehydration was reported by Giordanino *et al.*^[80] and explained as being the result of a weakened Laporte forbidden transition owing the formation of Cu²⁺ in a coordination environment with high tetragonal distortion.

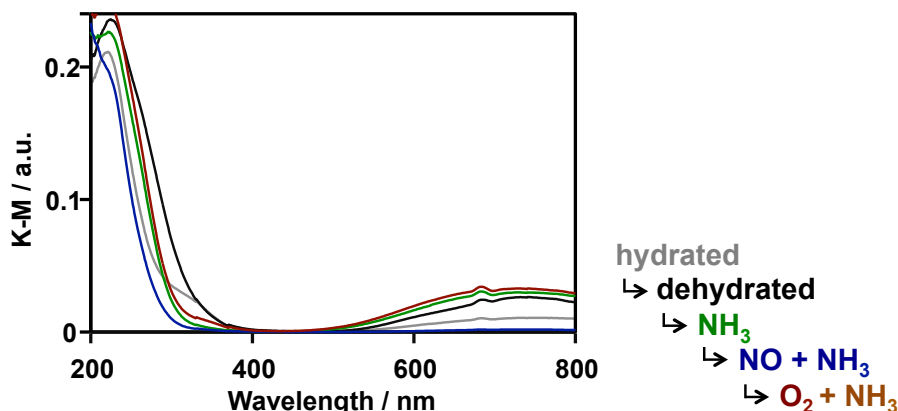


Figure 3.6. *In-situ* UV-Vis spectra of Cu-*BEA (21 % Cu ion-exchange level) during Scheme 1. Gray, black, green, blue, and brown line show the spectrum in hydrated condition under He ($100 \text{ cm}^3 \text{ min}^{-1}$) flow at room temperature, after dehydrated by 5 % O_2/He at 873 K under He ($100 \text{ cm}^3 \text{ min}^{-1}$) flow, after NH_3 adsorption by 500 ppm NH_3/He ($100 \text{ cm}^3 \text{ min}^{-1}$) flow, after reduction by 500 ppm $\text{NO} + 500 \text{ ppm NH}_3/\text{He}$ ($100 \text{ cm}^3 \text{ min}^{-1}$) flow, and after reoxidation by 5 % $\text{O}_2 + 500 \text{ ppm NH}_3/\text{He}$ ($100 \text{ cm}^3 \text{ min}^{-1}$) flow, respectively. In the measurement, temperature was kept at 473 K other than the hydrated condition, and the flow gas was same as the treatment condition unless otherwise noted.

N_2 formation was not observed by MS analysis of the outlet gas during NH_3 flow over dehydrated Cu-*BEA, suggesting that the reduction of Cu^{2+} does not occur during this process (Figure 3.7). An obvious blue shift of the LMCT band and an increase in intensity of the d–d transition band with a slight blue shift to 730 nm was observed following NH_3 adsorption. It has been reported that d–d transition bands of Cu^{2+} –ammonia complexes shift to lower wavelengths upon ligand exchange from OH_2 to NH_3 (1 NH_3 : 745 nm, 2 NH_3 : 680 nm, 3 NH_3 : 645 nm, 4 NH_3 : 590 nm) in aqueous solution,^[69] whereas the bands shift to slightly higher wavelengths with increasing temperature^[70]. The dominant species in the observed d–d transition band for NH_3 adsorbed by Cu^{2+} in the zeolite was similar to $[\text{Cu}^{\text{II}}(\text{NH}_3)(\text{H}_2\text{O})_5]^{2+}$ rather than a mixture of $[\text{Cu}^{\text{II}}(\text{NH}_3)_4]^{2+}$ and $[\text{Cu}^{\text{II}}(\text{OH})(\text{NH}_3)_3]^{2+}$. This result suggests that the majority of the ligands of Cu^{2+} in zeolites under NH_3 flow at 473 K can be assigned to O_Z , which is expected to be similar to H_2O with respect to order in the spectrochemical series. To confirm this suggestion, the outlet gas was analyzed quantitatively during the same transient reaction at 473 K, which revealed that the amount of NH_3 consumed was 1.5 times higher than the amount of Cu in the sample. The same measurement over the parent sodium-form zeolite gave a NH_3/Na ratio of ~ 0.1 , confirming that NH_3 on the parent sodium-form zeolite

is reversibly adsorbed because of the existence of few Brønsted acid sites. Moreover, it was confirmed that the final NH₃ concentrations of the breakthrough curve and elution curve over the Cu-ion-exchanged zeolite were similar to those over the parent sodium-form zeolite. Therefore, these measurements are considered to correctly quantify the amount of NH₃ consumed during the adsorption processes on Cu ions until saturation under NH₃ flow.

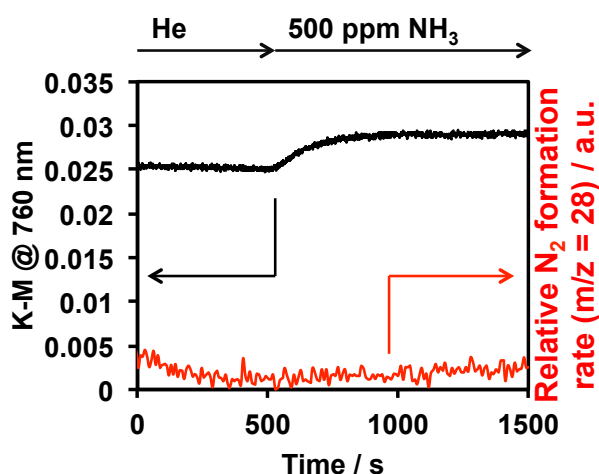
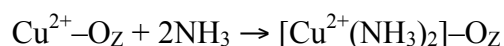


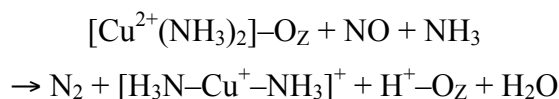
Figure 3.7. Time-resolved UV-Vis profiles for the KM at 760 nm (d-d transition band of Cu²⁺) and MS intensity of $m/z = 28$ (N₂) of Cu-*BEA (21 % Cu ion-exchange level) in the transition response switching to 500 ppm NH₃ flow.

When the NO + NH₃ feed was introduced, a blue shift of the LMCT band and a decrease in the d-d transition band were observed when compared to the spectra of the dehydrated and NH₃-adsorbed forms. This decrease in the d-d transition band indicates the disappearance of the vacant 3d orbital by the reduction of Cu²⁺ (3d⁹) to Cu⁺ (3d¹⁰). A quantitative analysis of the outlet gas revealed that the amounts NH₃ and NO consumed on the sample at 473 K were NH₃/NO \approx 0.72 and NO/Cu \approx 0.82. The amount of NO consumed can be considered to be the same as the amount of Cu ions reduced by NO + NH₃. The total amount of NH₃ consumed in the NH₃ feed and the subsequent NO + NH₃ feed can be considered as the amount of NH₃ attached to reduced Cu⁺ and consumed in the Cu ion reduction process. The amount of NH₃ consumed in these two processes was approximately 2.7 times that of NO. This behavior can be explained approximately by the stoichiometries of the following reactions.

NH₃ feed :



NH₃ to NH₃ + NO feed :



Thus, it is suggested that reduced Cu⁺ exists as a mobile complex with two NH₃ molecules.

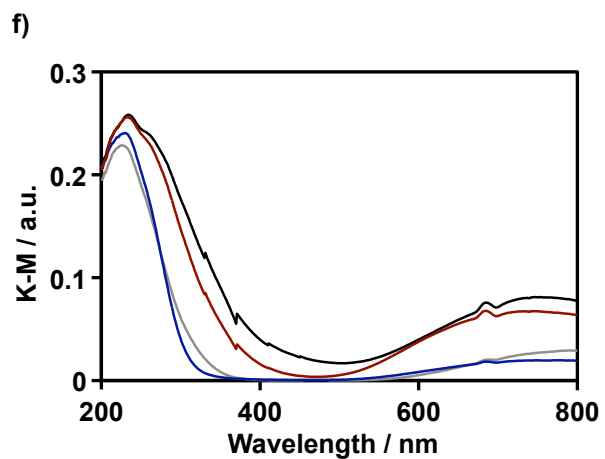
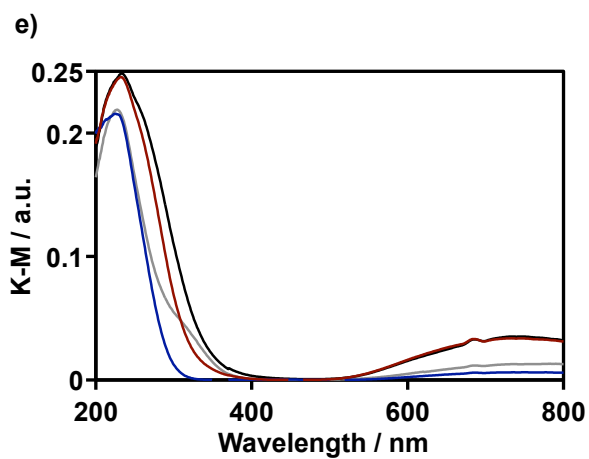
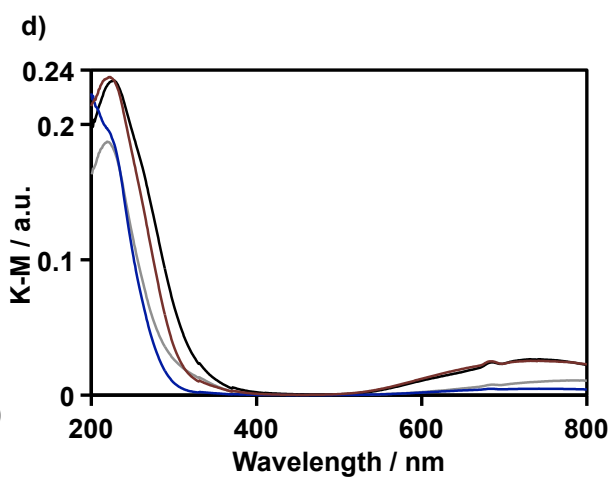
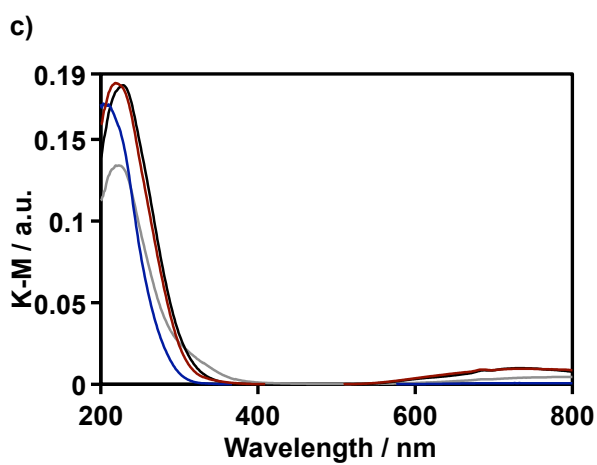
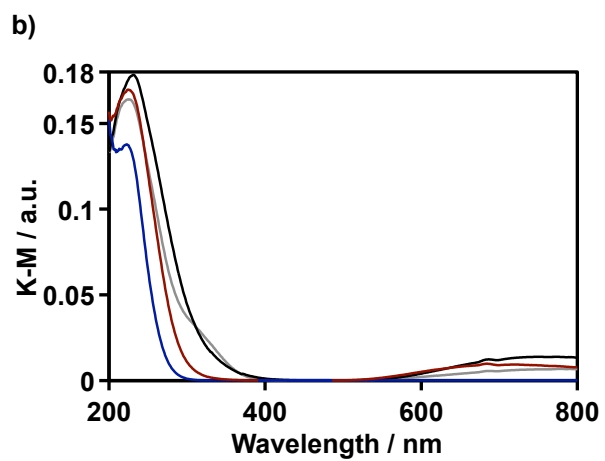
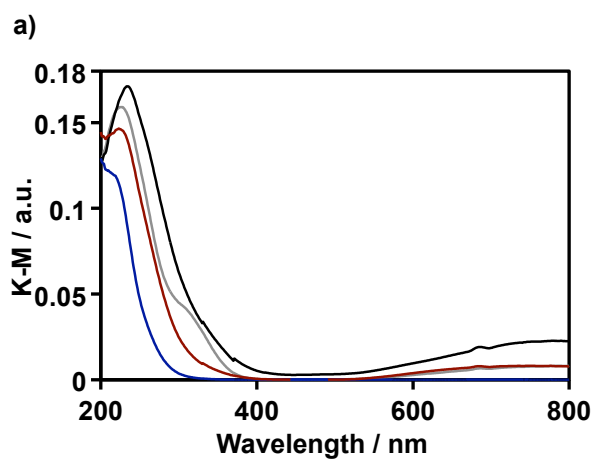
The intensities and positions of the d–d transition and LMCT bands after introducing the O₂ + NH₃ feed were similar to those after NH₃ adsorption. The absence of an additional peak around 400 nm shows that the majority of the observed species are isolated Cu²⁺ ions instead of O-bridged dimeric Cu²⁺ species^[59]. This result suggests that the final state following reoxidation by O₂ is isolated Cu²⁺, whereas the O-bridged dimeric Cu²⁺ species⁶⁵ is a rapidly consumed intermediate under the O₂ feed. Moreover, it is suggested that the Cu²⁺ after reoxidation is not fully coordinated by NH₃, which is similar to the state after NH₃ adsorption. The observed consumption of NH₃ when switching from the NH₃ feed to the NH₃ + NO feed also supports this assumption because if the Cu²⁺ were fully surrounded by NH₃, the stoichiometry would be as follows:

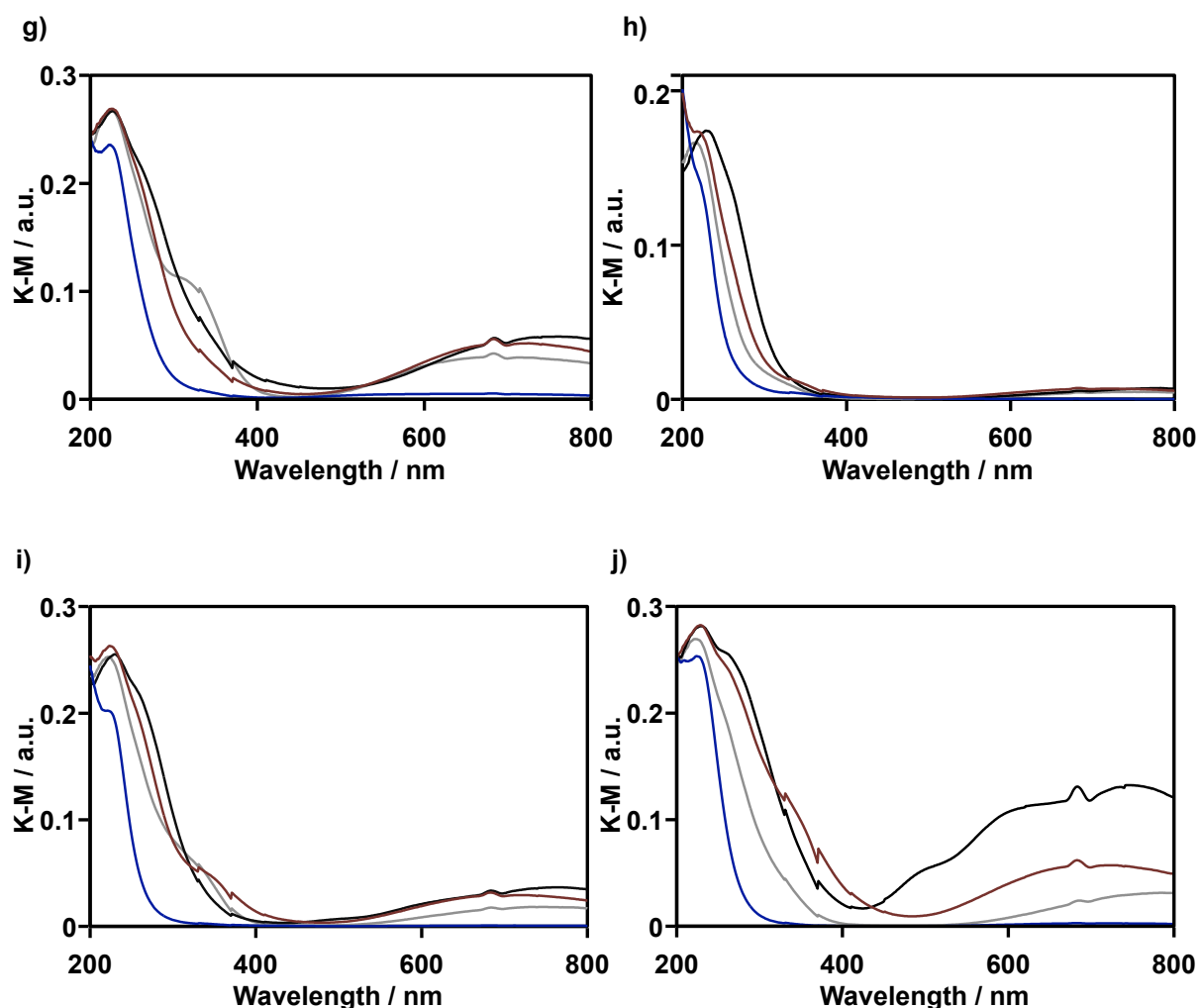


It has been reported that the d–d transition band was observed at 15800 cm⁻¹ (633 nm) when NH₃ was adsorbed on Cu²⁺ in a Y zeolite at room temperature^[71]. The band was assigned by complete active space self-consistent field second-order perturbation theory (CASPT2) calculations as [Cu^{II}(NH₃)₄]²⁺ with an additional axially coordinated zeolite lattice oxygen. The d–d transition bands after NH₃ adsorption and after reoxidation by the O₂ + NH₃ feed in this chapter, which are thought to correspond predominantly to NH₃ adsorbed by Cu²⁺, were observed in the lower energy region (maximum at 13700 cm⁻¹). Based on the UV-Vis spectra and the corresponding quantitative analysis of the outlet gas, the main ligand of Cu²⁺ is O_Z, comparable to the nitrogen belonging to NH₃, which has a stronger ligand field than oxygen donor ligands such as H₂O in the temperature region around 473 K, even after a reduction–reoxidation cycle. Therefore, it is suggested that in the working state of Cu-zeolites for NH₃-SCR, the majority of Cu²⁺ is coordinated to both a small number of NH₃ molecules (<2) and O_Z, which is not detached by ligand exchange to NH₃ until saturation (3 or 4 NH₃

molecules). Using *operando* XAS/XES during SCR, Lomachenko *et al.* proposed that the Cu^{2+} components in Cu-CHA catalysts exist as a complex mixture of residual Cu^{2+} bound to O_Z and mobile Cu^{2+} -ammonia complexes,^[72] which is in good agreement with the results of this study.

The behavior of different zeolites was compared using the transient reaction in Scheme 2. The d-d transition was observed as a single broad band at 730–780 nm for the MOR, MFI, *BEA, and CHA zeolites with a low Cu^{2+} ion exchange levels. A broad d-d transition band with a maximum at 781 and 775 (753) nm was observed for the dehydrated MOR and MFI zeolites with a Cu^{2+} ion exchange level of ~30% (Figure 3.8a and 3.8b, respectively). The d-d transition was observed as a broad band with a maximum at 730–750 nm for the dehydrated *BEA zeolites with various Cu^{2+} ion exchange levels (Figure 3.8c–f).





hydrated
 ↳ dehydrated
 ↳ NO + NH₃
 ↳ O₂

Figure 3.8. *In situ* UV-Vis spectra of (a) Cu-MOR (36 % Cu ion-exchange level), (b) Cu-MFI (33 % Cu ion-exchange level), (c) Cu-*BEA (13 % Cu ion-exchange level), (d) Cu-*BEA (21 % Cu ion-exchange level), (e) Cu-*BEA (39 % Cu ion-exchange level), (f) Cu-*BEA (93 % Cu ion-exchange level), (g) Cu-MFI (101 % Cu ion-exchange level), (h) Cu-CHA (9.3 % Cu ion-exchange level), (i) Cu-CHA (29 % Cu ion-exchange level) (j) Cu-CHA (62 % Cu ion-exchange level) during Scheme 2. Gray, black, blue, and brown line show the spectrum in hydrated condition under He (100 cm³ min⁻¹) flow at room temperature, after dehydrated by 5 % O₂/He at 873 K under He (100 cm³ min⁻¹) flow, after reduction by 500 ppm NO + 500 ppm NH₃/He (100 cm³ min⁻¹) flow, and after reoxidation by 5 % O₂/He (100 cm³ min⁻¹) flow, respectively. In the measurement, temperature was kept at 473 K other

than the hydrated condition, and the flow gas was same as the treatment condition unless otherwise noted.

The peak maximum shifted to higher wavelengths as the Cu^{2+} ion exchange level increased. It has been suggested that the most easily achieved state for Cu^{II} ions in zeolites is planar four-fold coordination at the planar 5 or 6 MR of zeolites^[73]. Moreover, planar arrangements with pyramidal features are known to be favorable for four-fold Cu^{II} complexes, and an increase in pyramidal features may be indicated by a red shift of the d–d transition bands in the UV-Vis spectra^[74]. Thus, the d–d transition bands observed for the dehydrated zeolites are assigned to four-fold Cu^{II} species on the zeolite framework with a structural diversity influenced by the local structure and Al distribution^[75]. The shifts of the band maxima depending on zeolite topology and the Cu ion exchange level provides a fingerprint of the distribution of planar-like Cu^{II} and pyramidal-like Cu^{II} . No clear shift of the band maximum was observed for the MFI zeolites (Figure 3.8b and 3.8g), possibly due to the structural complexity of this zeolite. Further investigations of the state of Cu^{2+} on zeolites with different topologies will be discussed later. In the case of the CHA zeolites, splitting of the d–d transition band was observed (Figure 3.8h–j) as the Cu^{2+} ion exchange level increased, which is in good agreement with the quadruplet d–d transition bands observed for CHA zeolites in previous reports^[67,76]. This splitting was not observed for the 10% ion-exchanged CHA zeolite (Figure 3.8h) but was obvious at higher Cu ion exchange levels (Figure 3.8j). Moreover, a comparison of the spectra of zeolite with similar Cu loading revealed that the split d–d transition bands had much higher intensities than the d–d transition bands without splitting. It is predicted that the population ratio between bare Cu^{II} and $[\text{Cu}^{\text{II}}\text{-OH}]^+$ is affected by both the Si/Al and Cu/Al ratios of the parent CHA zeolites, with the formation of the latter species being favorable at higher Si/Al and Cu/Al ratios^[50]. Considering the dependence on the Cu^{2+} ion exchange level, the high intensity, and previous findings,^[67,76] the d–d transition bands with splitting features can be assigned to a mixture of $[\text{Cu}^{\text{II}}\text{-OH}]^+$ and CuO_xH_y dimers or oligomers bridged by O or OH species^[76] with a highly distorted coordination environment^[90]. These findings suggest that Cu^{2+} species with a highly distorted coordination environment, which are frequently observed on CHA zeolites, are difficult to form on other zeolites, at least at the ion-exchange-site densities investigated in this chapter.

There were also some differences in the LMCT region of the UV-Vis spectra after reoxidation by O_2 . For the MOR, MFI, and *BEA zeolites, the LMCT band showed an

obvious blue shift after reoxidation by the O₂ feed when compared to the dehydrated form. This result suggests that the majority of these Cu²⁺ species exist as isolated Cu²⁺ without bridging ligands. In the case of the CHA zeolites, a shoulder peak centered at 350–400 nm was observed in the UV-Vis spectra after reoxidation. This feature is assigned to Cu dimers on the zeolite with bridging extraframework oxo ligands^[45,65,80,91]. This result suggests that more dimeric Cu²⁺ exists on the CHA zeolites than on the other zeolites after reoxidation. In contrast, similar features were observed in the d–d transition region after reoxidation by O₂, regardless of the zeolite structure or Cu ion exchange level. The d–d transition was observed as a single broad band with a peak at 720–740 nm that was slightly blue shifted when compared to the dehydrated form. These results suggest that the effect of the zeolite structure or extraframework OH ligand (unique to Cu²⁺ on CHA zeolites) on the previously described coordination environment is partially suppressed by the coordination of residual NH₃ and that the Cu²⁺ species on all the zeolites are in similar conditions after the reoxidation reaction.

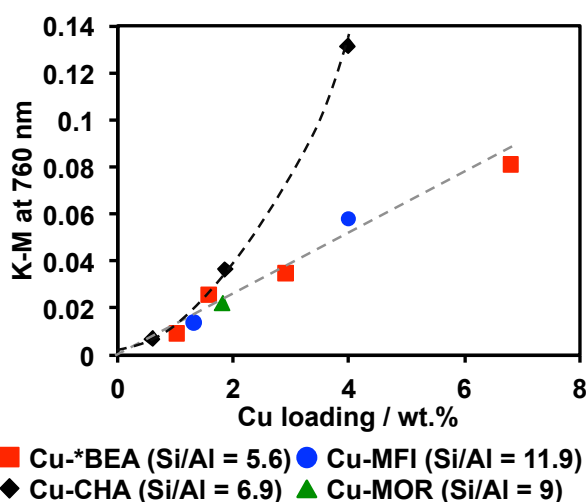


Figure 3.9. Relationship between Cu loading on zeolites and intensity at 760 nm (KM unit; d-d transition band of Cu²⁺) in the *in-situ* UV-Vis spectra of dehydrated forms. The gray dashed line shows the relationship on MOR, MFI, and *BEA zeolites and the black dashed line show the relationship on CHA zeolite.

The reduction and oxidation behaviors of the Cu ions on the zeolites were investigated by time-resolved measurements using the intensity at 760 nm (KM unit) as the indicator of Cu²⁺ concentration. Figure 3.9 shows the relationship between the Cu loading on zeolites and the intensity at 760 nm (KM unit) for the dehydrated forms. Good linear

relationships were observed, except for the CHA zeolites with higher Cu loadings, likely because the structural diversity of highly distorted Cu^{2+} ions with extraframework ligands^[76,77] on CHA zeolites is greater than that of the Cu^{2+} species on the other zeolites. The amount of Cu^{2+} on the zeolites after pretreatment was estimated using the transient reaction in Scheme B. The results were in good agreement with the Cu concentrations determined by ICP-AES measurements (Figure 3.10), and it is suggested that almost all Cu ions in the dehydrated form exist as Cu^{2+} .

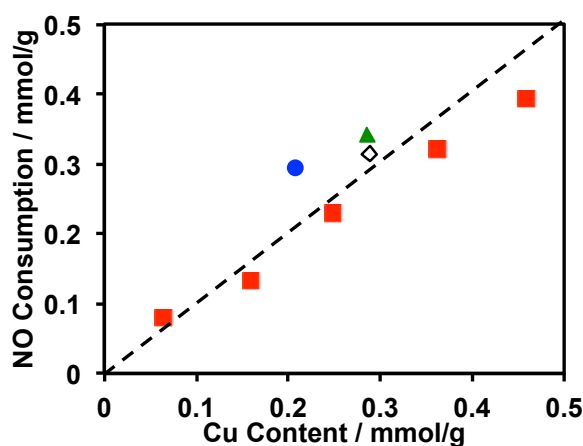


Figure 3.10. Relationship between the ICP-AES based Cu content of the Cu-zeolites and the amount of Cu^{2+} estimated by consumed amount of NO during the transient response at 473 K according to **Scheme B**.

Figure 3.11 shows the typical time-resolved profiles of the intensities at 760 nm (KM unit) for Cu-*BEA zeolite with a Cu^{2+} ion exchange level of 21% under feeds of (a) 500 ppm NH_3 + 500 ppm NO and (b) 5% O_2 . As shown in Figure 3.11a, the intensity at 760 nm (KM unit) decreased with the formation of N_2 under 500 ppm NH_3 + 500 ppm NO. This phenomenon shows that Cu^{2+} was reduced to Cu^+ with N_2 formation. As shown in Figure 3.11b, a rapid increase in the intensity at 760 nm (KM unit) was observed upon switching to the 5% O_2 feed, which is consistent with the reoxidation of Cu^+ to Cu^{2+} . The saturated intensity under O_2 was almost the same as that of the dehydrated form, and thus almost complete reoxidation occurs. It has been suggested by DFT calculations that Cu ions with an oxidation state of +2 form dimeric Cu complexes with bridging O_2 (such as side-on peroxo or bis(μ -oxo) structures) and surrounding ammonia ligands during the reoxidation cycle of NH_3 -SCR^[52,79]. A strong adsorption at 350 nm, a weak and broad adsorption around 650 nm,

and no adsorption at wavelengths longer than 700 nm were reported for biomimetic O₂-bridging dimeric Cu complexes with similar structures^[80–82]. Therefore, such O₂-bridging dimeric Cu intermediates formed during the reoxidation cycle are likely invisible in the time-resolved UV-Vis measurements at 760 nm, even when their oxidation state is divalent, and the majority of detected species are isolated Cu²⁺ and dimeric Cu²⁺ with extraframework bridging oxo ligands on zeolites. In other words, it is strongly suggested that the observed phenomenon in the time-resolved measurements under the O₂ flow in this chapter is the formation of Cu²⁺ on zeolites. This assumption does not indicate that the Cu⁺ to Cu²⁺ reoxidation process with O₂ does not proceed through the formation of O-bridging dimeric Cu intermediates, only that the formation of Cu²⁺ on zeolites after migration from dimeric Cu intermediates with bridging O₂ and surrounding amine ligands is observed during the time-resolved UV-Vis measurements.

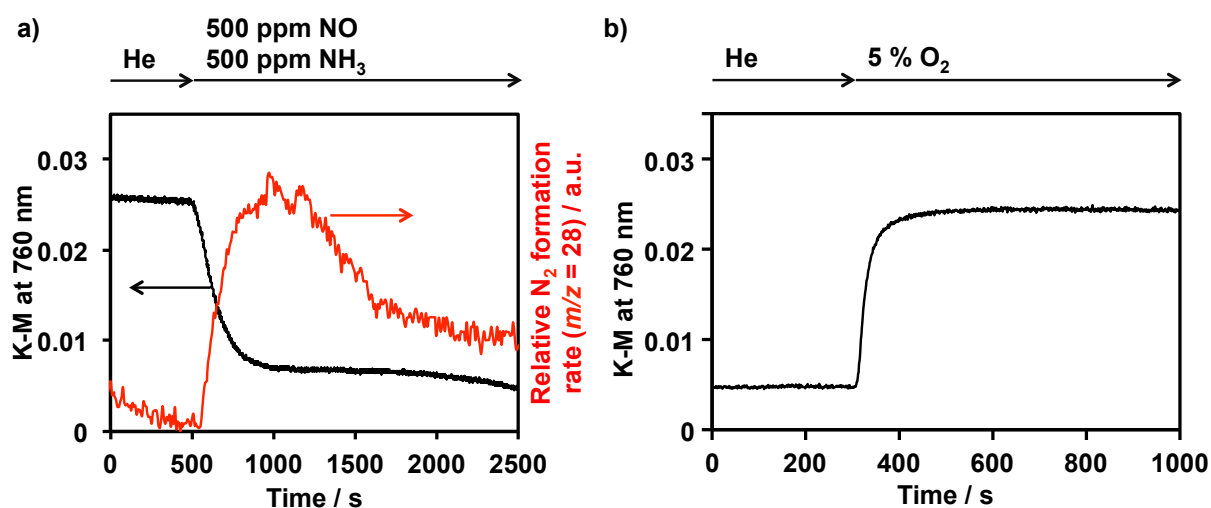


Figure 3.11. Time-resolved UV-Vis profiles for the KM at 760 nm (d-d transition band of Cu²⁺) and MS intensity of $m/z = 28$ (N₂) of Cu-*BEA (21 % Cu ion-exchange level) in the transition response switching to (a) 500 ppm NH₃ + 500 ppm NO flow and (b) 5 % O₂ flow at 473 K.

Figures 3.12–15 show the time-resolved profiles over the Cu-ion-exchanged MOR, MFI, *BEA, and CHA zeolites with Cu ion exchange levels of ~30%. Complete reoxidation was only observed only on the *BEA zeolites with low Cu ion exchange levels (<40%). Further, reduction by NO + NH₃ was not complete on *BEA zeolites, whereas the reduction process proceeded until the d–d transition band almost completely disappeared over the other

zeolites. These results suggest that the higher NH_3 -SCR rate over the *BEA zeolite than those over the other zeolites, as shown in Figure 3.5, is related to the reoxidation process rather than the reduction process.

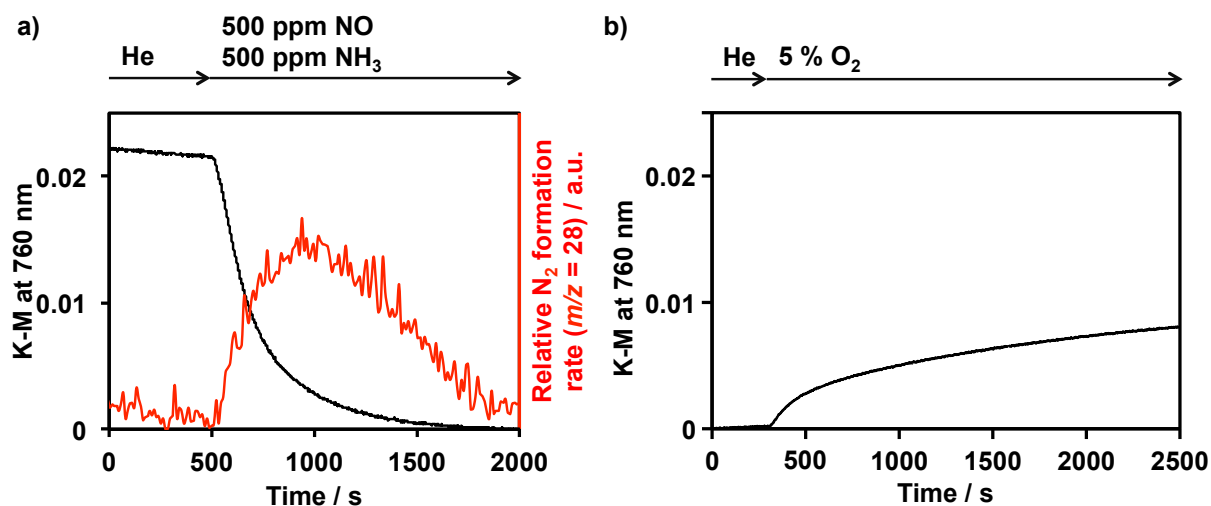


Figure 3.12. Time-resolved UV-Vis profiles for the KM at 760 nm (d-d transition band of Cu^{2+}) and MS intensity of $m/z = 28$ (N_2) of Cu-MOR (36 % Cu ion-exchange level) in the transition response switching to (a) 500 ppm NH_3 + 500 ppm NO flow and (b) 5 % O_2 flow at 473 K.

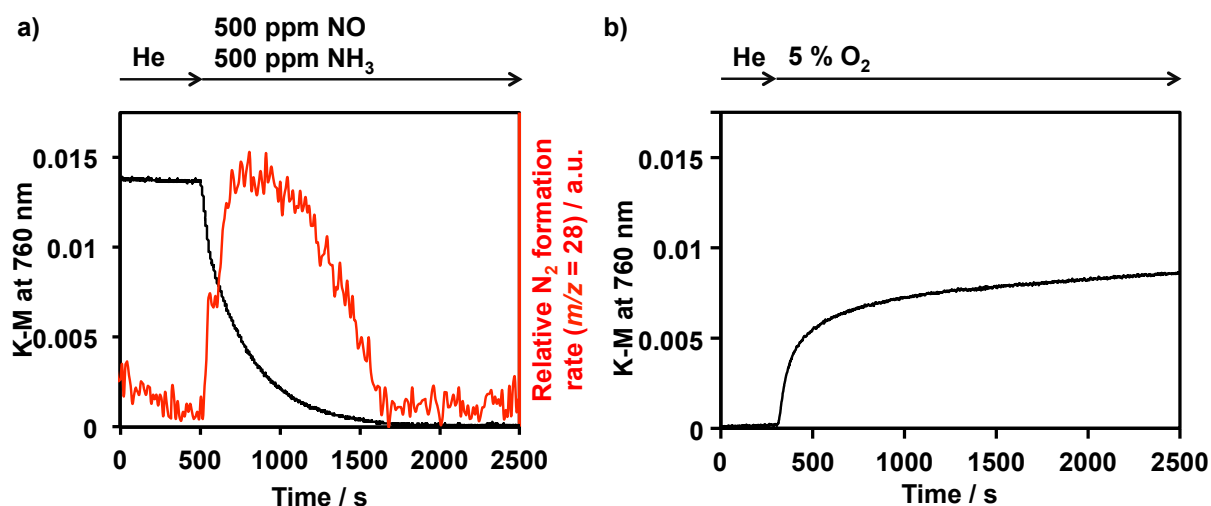


Figure 3.13. Time-resolved UV-Vis profiles for the KM at 760 nm (d-d transition band of Cu^{2+}) and MS intensity of $m/z = 28$ (N_2) of Cu-MFI (33 % Cu ion-exchange level) in the transition response switching to (a) 500 ppm NH_3 + 500 ppm NO flow and (b) 5 % O_2 flow at 473 K.

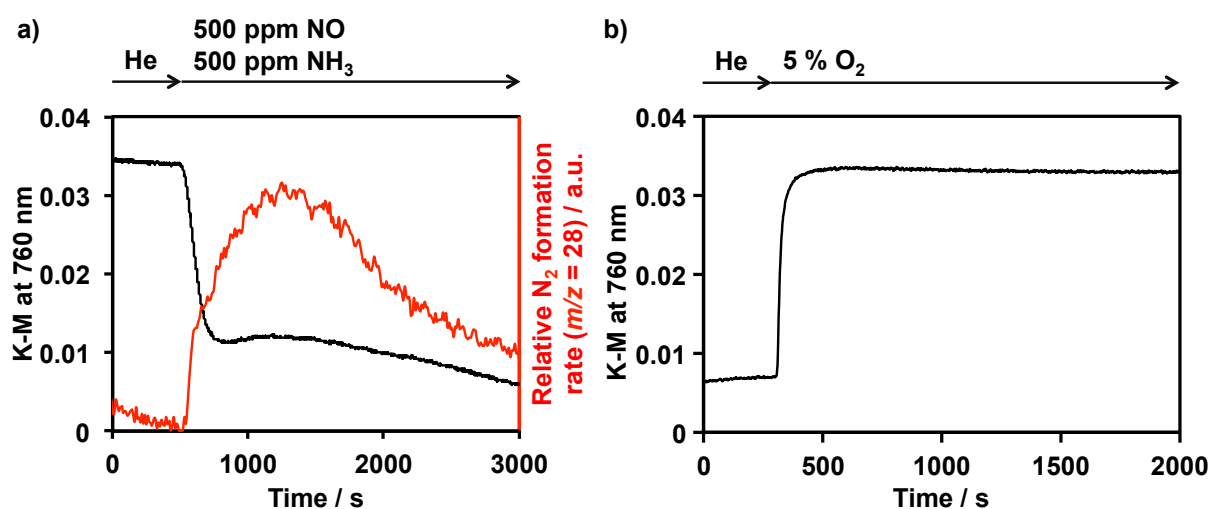


Figure 3.14. Time-resolved UV-Vis profiles for the KM at 760 nm (d-d transition band of Cu^{2+}) and MS intensity of $m/z = 28$ (N_2) of Cu-*BEA (39 % Cu ion-exchange level) in the transition response switching to (a) 500 ppm NH_3 + 500 ppm NO flow and (b) 5 % O_2 flow at 473 K.

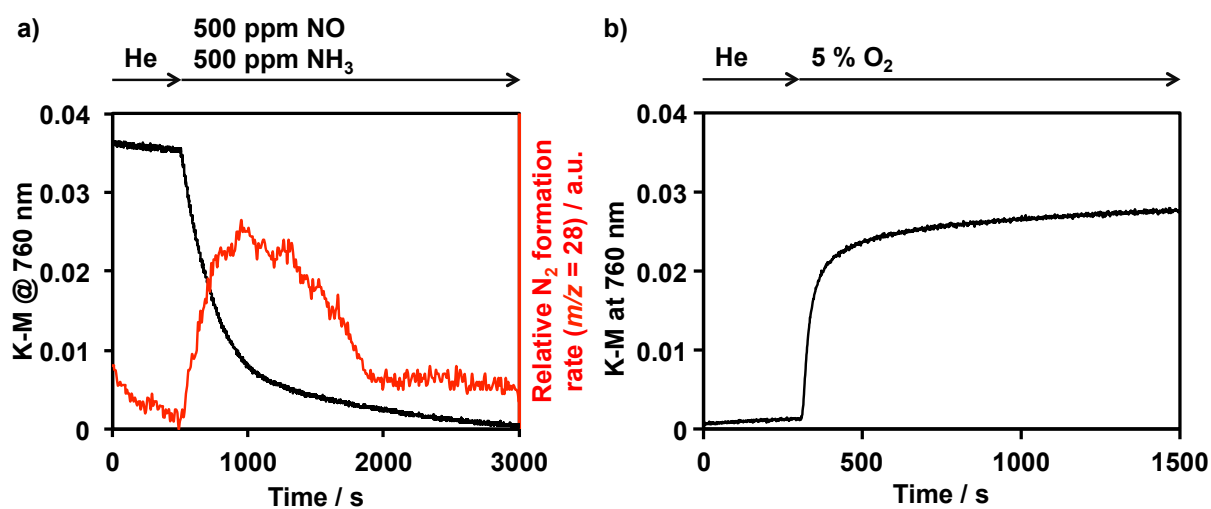


Figure 3.15. Time-resolved UV-Vis profiles for the KM at 760 nm (d-d transition band of Cu^{2+}) and MS intensity of $m/z = 28$ (N_2) of Cu-CHA (29 % Cu ion-exchange level) in the transition response switching to (a) 500 ppm NH_3 + 500 ppm NO flow and (b) 5 % O_2 flow at 473 K.

3.3.4. Relationship between the Cu oxidation rate under transient conditions and the NH_3 -SCR rate

The dynamic reduction–oxidation processes of Cu ions over zeolites related to the

steady-state reaction were investigated by analyzing the time-resolved UV-Vis profiles. As shown in the previous section, the intensity at 760 nm (KM unit) in the UV-Vis spectra of dehydrated Cu-zeolites had a good linear relationship with Cu loading, except for the CHA zeolites, and the d–d transition band after reoxidation by O₂ had similar features, regardless of the zeolite. Therefore, it is suggested that the observed intensity at 760 nm (KM unit) has a similar coefficient and can be used as an indicator of the concentration of Cu²⁺ on zeolites. Based on this assumption, the time derivative of the time-resolved data was calculated, which gave a profile with a sharp peak (Figure 3.16). The peak maxima in the derivative profiles are thought to be proportional to the reoxidation rates of Cu ions (d[Cu²⁺]/dt). Moreover, this reoxidation rate is thought to correspond to the formation rate of Cu²⁺, except for dimeric Cu complexes with bridging O₂ and surrounding ammonia ligands. Figure 3.17 shows the derivative profiles over the Cu-ion-exchanged MOR, MFI, *BEA, and CHA zeolites with Cu ion exchange levels of ~30%.

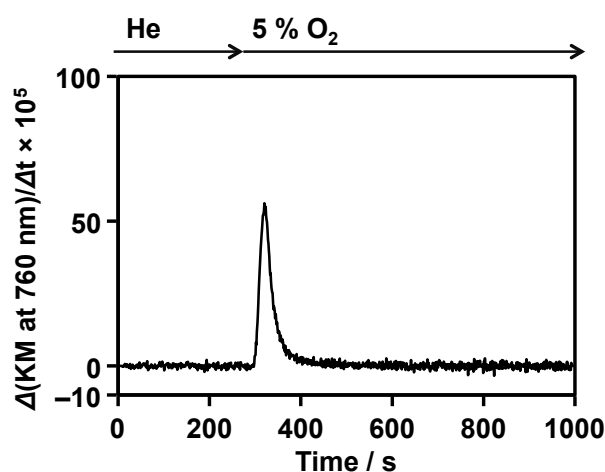


Figure 3.16. The time derivative of time-resolved UV-Vis profiles for the KM at 760 nm (d-d transition band of Cu²⁺) of Cu-*BEA (21 % Cu ion-exchange level) in the transition response switching to 5 % O₂ flow at 473 K.

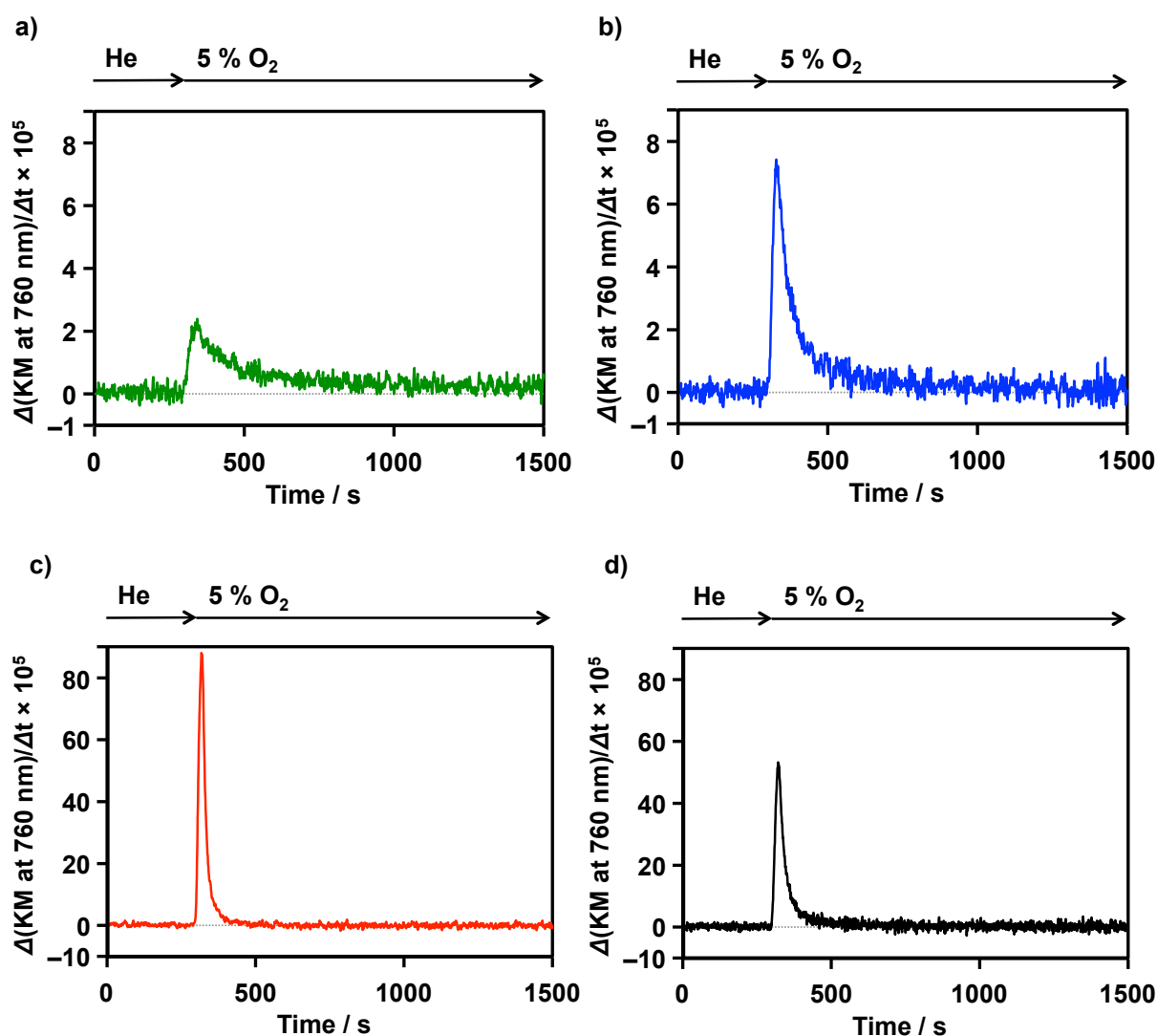


Figure 3.17. The time derivative of time-resolved UV-Vis profiles for the KM at 760 nm (d-d transition band of Cu^{2+}) of (a) Cu-MOR (36 % Cu ion-exchange level), (b) Cu-MFI (33 % Cu ion-exchange level), (c) Cu-*BEA (36 % Cu ion-exchange level), and (d) Cu-CHA (29 % Cu ion-exchange level) in the transition response switching to 5 % O_2 flow at 473 K.

The reoxidation rates of Cu ions were plotted as a function of the mean Cu density in micropores (Figure 3.18). As shown in Figure 3.18, the oxidation rates of Cu ions obtained from the time-resolved UV-Vis measurements were similar to the rates for steady-state NH_3 -SCR. The log-log plot of the NH_3 -SCR rates versus the reoxidation rates of Cu ions over all the zeolites (Figure 3.19.a) clearly shows a good linear relationship, regardless of the zeolite structure. Figure 3.19.b shows the plot for different zeolite topologies with similar Cu densities in micropores. The steady-state NH_3 -SCR rates and the reoxidation rates of Cu ions

calculated show the same sequence, which indicates that the calculation method established in this chapter can be used to assess the reoxidation rate of Cu ions in the working state accurately. Moreover, it is clearly shown that the differences in the steady-state NH₃-SCR rates over various zeolites shown in Figure 3.5 that were obtained using the designated reaction conditions originate from the common rate-determining reoxidation process of Cu ions. In summary, the reoxidation process of Cu ions, which is related to the formation of isolated Cu²⁺, is strongly affected by the zeolite structure, even when the ion-exchange capacity per micropore and Cu density in micropores are similar.

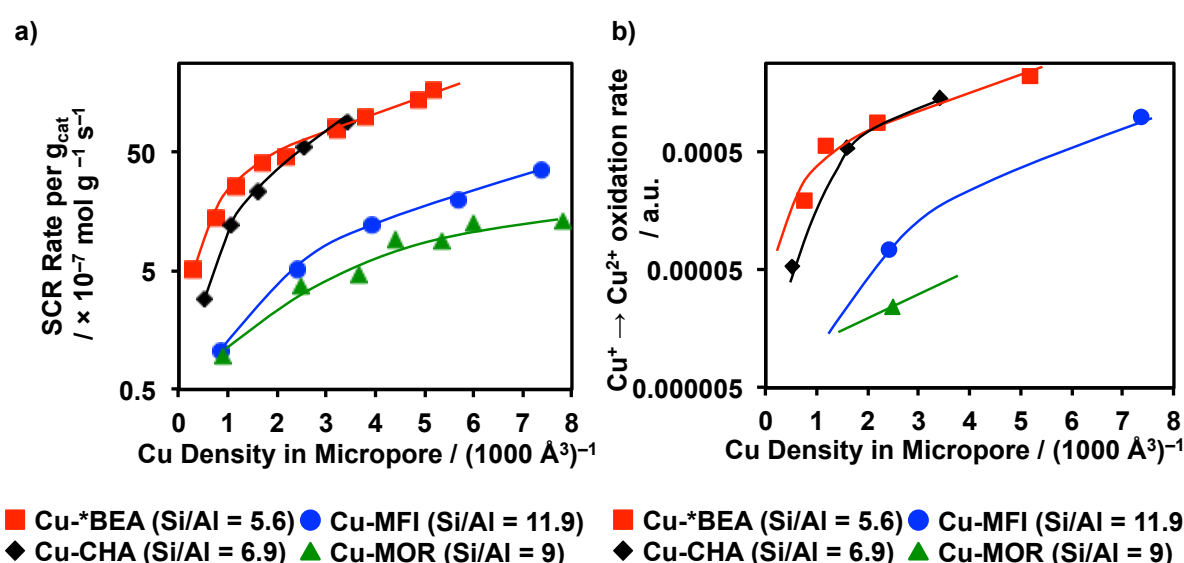


Figure 3.18. Correlation between the (a) standard NH₃-SCR rate per g_{cat} at 473 K or (b) Cu⁺ → Cu²⁺ oxidation rate at 473 K and Cu Density in Micropore over the MOR (▲), MFI (●), *BEA (■), and CHA(◆) zeolites.

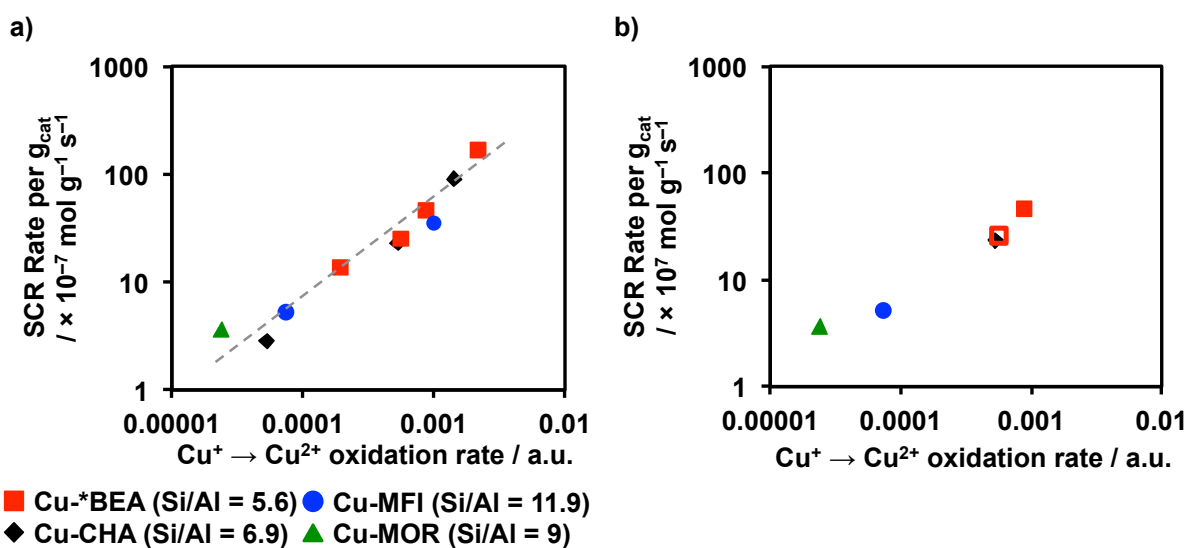


Figure 3.19. Correlation between the standard NH_3 -SCR rate per g_{cat} at 473 K and $Cu^+ \rightarrow Cu^{2+}$ oxidation rate at 473 K over the MOR (\blacktriangle), MFI (\bullet), *BEA (\blacksquare), and CHA (\blacklozenge) zeolites with (a) various mean Cu Density in Micropore and (b) similar mean Cu Density in Micropore. In the Fig. 12b, Cu Density in Micropore the CHA (\blacklozenge) zeolite is middle of the two *BEA (\blacksquare and \square) zeolite samples.

3.3.5. Distribution of Cu^{2+} species on zeolites

As suggested by the d-d transitions of Cu^{2+} in the UV-Vis spectra obtained using Scheme 1, the majority of Cu^{2+} species after reoxidation by O_2 are NH_3 -adsorbed Cu^{2+} ions that are not liberated from O_Z , even under NH_3 flow at 473 K. From this result, it can be assumed that the Cu^{2+} accommodation properties of zeolites are affected by the local structure and are related to the differences in the reoxidation properties of Cu ions over different zeolites.

The coordination environments of Cu^{2+} on the ion-exchange sites of zeolites with several topologies were investigated through NO probe IR measurements after O_2 treatment of the $\sim 30\%$ ion-exchanged zeolites^[83]. Figure 3.20 shows the IR spectra of NO adsorbed on the Cu-*BEA and Cu-CHA zeolites at room temperature (~ 25 °C) after evacuation and subsequent exposure to 15 kPa O_2 at 773 K. The corresponding IR spectra for the Cu-*MOR and Cu-MFI zeolites are shown in Figure 3.21. A broad band was observed at $1850\text{--}2000$ cm^{-1} , which is assignable to NO adsorbed on Cu^{2+} ^[83]. The characteristics of these adspecies were affected by the type of zeolite. On the *BEA, MFI, and MOR zeolites, a broad and asymmetric, but relatively simple adspecies band centred near 1900 cm^{-1} was observed. The

minor adspecies observed at higher wavenumbers ($>1950\text{ cm}^{-1}$) were more obvious on the *BEA zeolites. For the main adspecies around 1900 cm^{-1} , the band maximum for the *BEA zeolites was observed at slightly lower wavenumbers than those for the MFI and MOR zeolites, and better separation was observed for the *BEA zeolites than for the MFI and MOR zeolites. The asymmetric shape and the shift of the band maximum suggest that this band consists of several overlapping basic bands.

Dědeček *et al.*^[83] reported that a broad band was observed for NO adsorbed on Cu^{2+} over FAU, ERI, MOR, and MFI zeolites, which consisted of overlapping basic bands centred at 1921 (1909), 1912, 1906, and 1895 cm^{-1} . The same group established that the bands at 1921 (1909) and 1912 cm^{-1} are assignable to NO adsorbed on Cu^{2+} adjacent to two framework Al atoms, whereas the band at 1895 cm^{-1} is assignable to NO adsorbed on Cu^{2+} adjacent to a single framework Al atom. In addition, these species are assigned to NO adsorbed on square-pyramidal Cu^{2+} and square-planar Cu^{2+} , respectively. From this assignment, the results in the previous paragraph can be understood as follows: the broad band observed near 1900 cm^{-1} consists of overlapping bands at 1912 and 1895 cm^{-1} , and the contribution from the band at 1895 cm^{-1} is higher on *BEA zeolites than on MOR and MFI zeolites. In other words, it is suggested that a larger population of Cu^{2+} adjacent to a single framework Al atom and/or with square-planar coordination exists on *BEA zeolites than on MFI and MOR zeolites.

Compared to those on the other zeolites, the adspecies observed on the CHA zeolite were much more complex despite this zeolite having the simplest framework structure, which contains only crystallographically equivalent T sites. As a unique feature of NO adspecies on Cu^{2+} , bands at higher wavenumbers ($>1920\text{ cm}^{-1}$) were clearly observed. The complexity of the IR band for Cu^{2+} species on CHA zeolites is similar to the splitting of the d–d transition band for Cu^{2+} in the UV-Vis spectra of dehydrated CHA zeolites (Figure 3.7). The IR band consists of at least four overlapping bands at 1947, 1928, 1912, and 1895 cm^{-1} . In previous reports on CHA zeolites, the former two bands are assigned to NO adsorbed on bare $\text{Cu}^{2+}\text{-O}_Z$ species in 6 MR, whereas the latter two bands are assigned to NO adsorbed on $[\text{Cu}(\text{OH})]^+\text{-O}_Z$ species in 8 MR^[45].

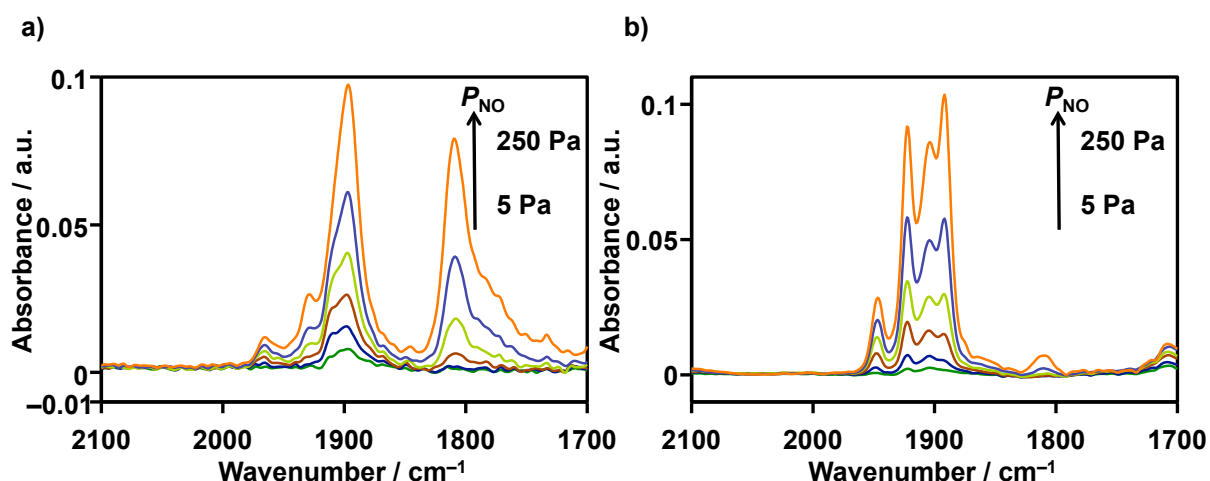


Figure 3.20. IR spectra of NO adsorbed on the (a) Cu-*BEA (39 % Cu ion-exchange level) and (b) Cu-CHA (29 % Cu ion-exchange level) zeolites at room temperature (ca. 25 °C) after 15 kPa O₂ treatment at 773 K.

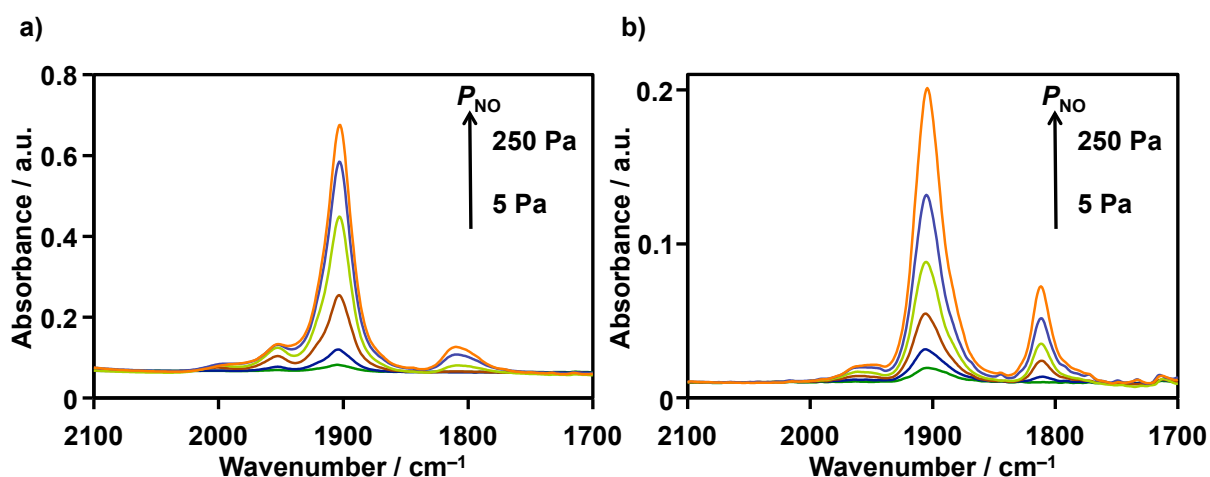


Figure 3.21. IR spectra of NO adsorbed on the (a) Cu-MOR (36 % Cu ion-exchange level) and (b) Cu-MFI (33 % Cu ion-exchange level) zeolites at room temperature (ca. 25 °C) after 15 kPa O₂ treatment at 773 K.

The distribution of different Cu²⁺ species on Cu-zeolites was investigated semiquantitatively by curve fitting the IR spectra for NO (250 Pa) adsorption (Figure 3.22). Using curve fitting, Dědeček *et al.* frequently obtained a basic band at 1912 cm⁻¹ as a basic band produced by the curve fittings^[83]. In this chapter, curve fitting instead gave a band at 1904 cm⁻¹. However, the current band at 1904 cm⁻¹ and that at 1912 cm⁻¹ in the previous report^[83] are thought to be the same, with the different positions caused by differences in the

algorithm employed for curve fitting. Therefore, the basic band at 1904 cm^{-1} in this chapter is assigned to NO adsorbed on Cu^{2+} adjacent to two framework Al atoms or/and with square-pyramidal coordination, and the band at 1895 cm^{-1} is assigned to NO adsorbed on Cu^{2+} adjacent to a single framework Al atom or/and with square-planar coordination, as the previous report^[83].

As shown in Figure 3.22, the distribution between the bands at 1904 and 1895 cm^{-1} (blue and purple lines, respectively) varied depending on the zeolite topology. In the IR spectra for NO adsorbed on Cu^{2+} of the *BEA and CHA zeolites, which exhibit high reoxidation rates and NH_3 -SCR rates, there is a large contribution from the band at 1895 cm^{-1} , whereas in those of the MFI and MOR zeolites, which exhibit low reoxidation rates and NH_3 -SCR rates, there is a small contribution from this band. Moreover, the contribution of this band was larger for MFI zeolite than for MOR zeolite. These results suggest that the zeolites that are favourable for accommodation of the Cu^{2+} species adjacent to a single framework Al atom or/and with square-planar coordination are suitable to achieve high NH_3 -SCR rates.

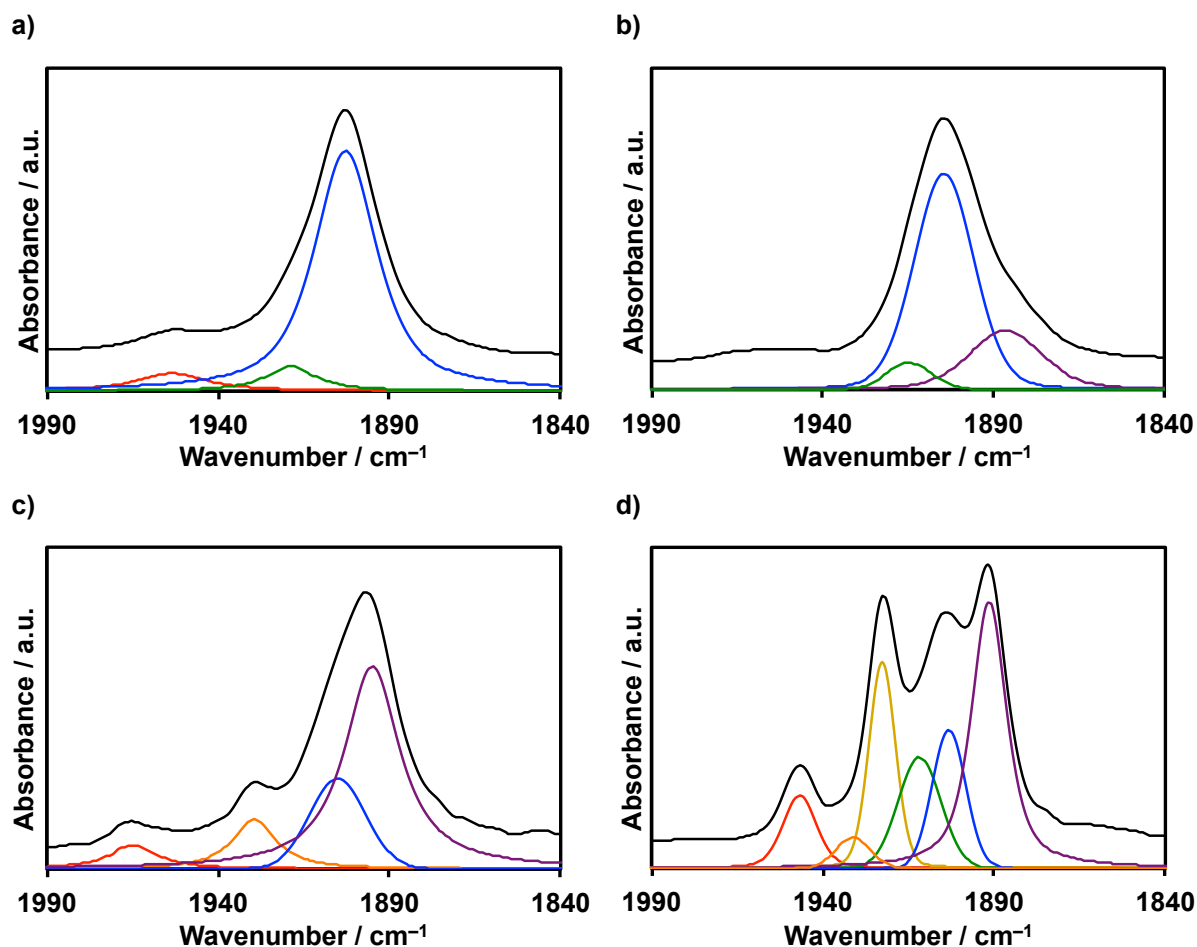


Figure 3.22. The curve-fitting of IR spectra of NO (250 Pa) adsorbed on the (a) Cu-MOR (36 % Cu ion-exchange level), (c) Cu-MFI (33 % Cu ion-exchange level), (c) Cu-*BEA (39 % Cu ion-exchange level), and (d) Cu-CHA (29 % Cu ion-exchange level) zeolites at room temperature (ca. 25 °C) after 15 kPa O₂ treatment at 773 K. Red, orange, yellow, green, blue, and purple line shows the basic band at 1965–1950, 1930, 1920, 1912, 1904, and 1895 cm⁻¹, respectively.

Table 3.1. Area ratio of observed adspecies, Area ratio between the band at 1904 cm⁻¹ and those at 1895 cm⁻¹, and the position of peak maximums of d-d transition bands observed in UV-Vis spectra over zeolites with different topologies.

Zeolite	Peak / cm ⁻¹	Area ratio / %	$\frac{A(1895\text{ cm}^{-1})}{A(1904\text{ cm}^{-1})}$	d-d transition band in UV-Vis spectra
MOR (Si/Al = 9)	1953	7.66	0	777
	1919	7.74		
	1903	84.6		
MFI (Si/Al = 12)	1915	6.09	0.36	753
	1904	69.1		775
	1886	24.8		
*BEA (Si/Al = 5.6)	1965	6.56	3.29	745
	1929	11.9		
	1905	19.0		
	1895	62.5		
CHA (Si/Al = 6.9)	1947	8.95	2.69	762
	1931	3.33		
	1923	18.6		
	1912	15.0		
	1903	14.7		
	1891	39.4		

Table 3.1 shows the area ratio of each species and the area ratio between the bands at 1904 and 1895 cm⁻¹ ($A(1895\text{ cm}^{-1})/A(1904\text{ cm}^{-1})$) for each zeolite. Moreover, the peak maxima of the d-d transition bands observed in the UV-Vis spectra of the dehydrated forms are also shown. The increase in $A(1895\text{ cm}^{-1})/A(1904\text{ cm}^{-1})$ shows the same trend as the shift of the d-d transition band to lower wavelengths. Both phenomena indicate the increase in the fraction of Cu²⁺ with square-planar coordination structure. The agreement between the assignments for the d-d transition of Cu²⁺ in the UV-Vis spectra (Section 3.3.3) and for NO adsorbed on Cu²⁺ in the IR spectra shows that the discussions on coordination environments for Cu²⁺ species based on these two techniques complement each other for determining the coordination environments for Cu²⁺ species.

3.3.6. Structure and distribution of ion-exchange sites on zeolites

The coordination environments for Cu^{2+} described in the previous section can be affected by the local zeolite structure. It has been suggested that *BEA, MFI, and MOR zeolites have three types of structurally similar ion-exchange sites for divalent cations, called α , β , and γ ^[84]. CHA zeolites have ion-exchange sites called σ , ω , and τ ^[85]. However, owing to the distribution in the zeolite framework, limited sites are located on the micropore surfaces. The σ site in CHA zeolites is similar to the β site in other zeolites, as both sites involve a planar 6 MR. In contrast, the τ site is located in an 8 MR. These sites face the surface of the cage in CHA zeolites^[85]. In contrast, all the sites in MFI zeolites face the micropores^[86]. However, in *BEA zeolites, only the β site faces the micropores^[87,88], whereas for MOR zeolites, only the α site faces the main 12 MR main micropores^[89].

DFT calculations have suggested that a divalent transition metal cation at the α site exhibits square-pyramidal coordination in a planar 5 MR^[88,90], whereas that at the β or σ site acquires square-planar coordination in a planar 6 MR^[85,88]. Based on these assignments and the current results, it is suggested that zeolites with β or σ sites facing the micropores, such as *BEA or CHA zeolites, tend to facilitate $\text{Cu}^+ \rightarrow \text{Cu}^{2+}$ oxidation through O-bridging dimeric Cu intermediates owing to the formation of square-planar Cu^{2+} on the zeolites. In contrast, it is difficult to accommodate isolated Cu^{2+} formed in the reoxidation process in zeolites with α sites facing the micropores, such as MFI or MOR zeolites.

As shown in Figure 3.19, the NH_3 -SCR rate and the reoxidation rate over each zeolite have different dependencies on the mean Cu density in micropores. The reaction rates over the *BEA zeolites with low Cu densities in the micropores were much higher than those over any other zeolite, and the rate increased with the increase in Cu density. The reaction rates over the CHA zeolites were almost in proportion to the Cu density. However, the reaction rates over the MFI zeolites were small and increased with the increase in Cu density, similar to those over the *BEA zeolites. The reaction rates over the MOR zeolites were small and remained almost constant as the Cu density increased. The suggested origins of these trends are as follows.

In the case of the MOR zeolites, only the α sites, which provide a minor contribution to the reoxidation process, face the main 12 MR channel, whereas the β sites are located at the intersection between two 8 MR. These structural features result in a small reoxidation rate of Cu^+ that is independent of the Cu density, even though the straight 12 MR channel system can be assumed to be beneficial for the diffusion of mobile Cu^+ -ammonia

complexes in the micropores and the formation of O-bridging dimeric Cu intermediates (a more detailed discussion of the dimensions of the channel system can be found in the Appendix).

In the case of the MFI zeolites, the β sites are located at the intersection between the straight and sinusoidal channels. As this site is in a highly curved position, the accommodation of isolated Cu^{2+} is difficult. Furthermore, for the MFI zeolites, the α sites in the straight channel and the γ sites in the sinusoidal channel face the micropores, but their contributions to the reoxidation process seem to be much smaller than that of the β sites. Thus, facilitating O-bridging dimeric Cu intermediate formation by increasing the Cu density in micropores does not effectively increase the oxidation rate.

In the case of the CHA zeolites, the distance between the nearest σ sites is long. Therefore, at low Cu densities in the micropores, obtaining an isolated Cu^{2+} from the O-bridging dimeric Cu intermediates is difficult. However, the CHA zeolite can accommodate not only bare Cu^{2+} on the σ sites (6 MR) but also the $[\text{Cu}^{2+}-\text{OH}]^+$ complex on the τ sites (8 MR), and it has been observed that the σ sites are first occupied by bare Cu^{2+} and then the $[\text{Cu}^{2+}-\text{OH}]^+$ complex as the Cu loading increases.⁵⁶ Therefore, almost all the O_z bound to Al atoms can accommodate Cu^{2+} at higher Cu densities in the micropores. For this reason, facilitating the formation of O-bridging dimeric Cu intermediates by increasing the Cu density in micropores directly increase the reoxidation rate (= formation rate of Cu^{2+} on the zeolite); therefore, the reaction rate is sensitive to the Cu density in the micropore. This explanation is consistent with the strong dimeric Cu^{2+} features observed in the UV-Vis spectra of the CHA zeolites after reoxidation by O_2 .

The *BEA zeolites have a twisted neighboring arrangement of β sites in the micropores. This structural feature is assumed to be favourable for accommodating isolated Cu^{2+} from the O-bridging dimeric Cu intermediates at low Cu densities in the micropores. This explanation is supported by the rapid formation of isolated Cu^{2+} (d-d transition at ~740 nm and LMCT without strong adsorption at 350 nm) under O_2 flow observed in the time-resolved UV-Vis measurements of the Cu-*BEA catalysts, even at low Cu densities in the micropores. However, the *BEA zeolites have a large proportion of 5 MR on the surface of the micropore channels, and it is known that 5 MR in zeolites cannot contain two Al atoms^[91]. Moreover, for *BEA zeolites with compositions similar to that used in this chapter, it has been reported that 50%–65% of Al atoms are in an unpaired sequence, which is unfavorable for charge balancing bare divalent cations^[88]. Instead, the charge of bare divalent

cations is mostly balanced by the AlSiSiAl sequences of 6 MR in *BEA zeolites with compositions similar to that used in this chapter^[88]. These findings suggest that facilitating the formation of mobile O-bridging intermediates by increasing the Cu density in the micropores for the *BEA zeolites does not effectively increase the reoxidation rate at higher Cu densities in micropores because the Al atoms in β sites, which are favorable for accommodating isolated Cu^{2+} , are limited.

3.4. Conclusions

The catalytic activities of Cu-zeolites with different topologies for low-temperature NH₃-SCR were investigated. The effects of the Cu density on the reaction rate for NH₃-SCR at 473 K over zeolites with MOR, MFI, *BEA, and CHA topologies were compared. The formation of dimeric Cu intermediates in the micropore of different zeolites, which are thought to be involved in the rate-determining step, was assessed based on the effect of the Cu density in micropores on the reaction rates. The MOR zeolites showed a low NH₃-SCR rate per Cu, irrespective of the Cu density in micropores. The *BEA zeolites showed an extremely high reaction rate per Cu at low Cu densities in micropores, whereas the rate with the CHA zeolites increased drastically with increase in the Cu density in micropores.

For each zeolite, the rate for the reoxidation cycle, as calculated based on time-resolved UV-Vis measurements, showed a similar dependence on the Cu density in micropores as the NH₃-SCR rate. Moreover, the calculated reoxidation rates were almost proportional to the overall reaction rates, indicating that the reoxidation dynamics were quantitatively measured. The zeolite topology had a large effect on the reoxidation dynamics from Cu⁺ to Cu²⁺ during the NH₃-SCR, even though this reaction has been thought to proceed via the redox of Cu ions liberated from the zeolite framework. Based on *operando* UV-Vis spectra combined with a quantitative analysis of the consumed reactants during the same transient measurements, it was suggested that the majority of Cu²⁺ is coordinated to NH₃ but still interacts with the zeolite framework oxygen, even under NH₃ flow. Thus, it is assumed that the effect of zeolite topology on the reoxidation cycle is due to their ability to accommodate divalent ions. An investigation of the coordination environment of Cu²⁺ in each zeolite using NO probe IR measurements revealed that the distribution between pyramidal and planar Cu²⁺ states was largely affected by the type of zeolite. It was suggested that the local structure and the distribution of ion-exchange sites for divalent ions predominately determine the distribution of the Cu²⁺ structures, which are responsible for the effects of different zeolites on the reoxidation cycle during NH₃-SCR. These results indicate that zeolite topology can potentially be exploited to develop Cu-zeolite catalysts that have both high reaction rates for NH₃-SCR and low Cu volumetric densities.

References

- [1] C. Görsmann, *Johnson Matthey Technol. Rev.* **2015**, *59*, 139.
- [2] T. Seiyama, T. Arakawa, T. Matsuda, Y. Takita, N. Yamazoe, *J. Catal.* **1977**, *48*, 1.
- [3] W. B. Williamson, J. H. Lunsford, *J. Phys. Chem.* **1976**, *80*, 2664.
- [4] M. Iwamoto, S. Yokoo, K. Sakai, S. Kagawa, *J. Chem. Soc., Faraday. Trans. 1* **1981**, *77*, 1629.
- [5] M. Iwamoto, H. Furukawa, S. Kagawa, *Stud. Surf. Sci. Catal.* **1986**, *28*, 943.
- [6] Y. Li, W. K. Hall, *J. Catal.* **1991**, *129*, 202.
- [7] M. Iwamoto, H. Yahiro, K. Tanda, N. Mizuno, Y. Mine, S. Kagawa, *J. Phys. Chem.* **1991**, *95*, 3727.
- [8] M. Iwamoto, H. Yahiro, Y. Yu-u, S. Shundo, N. Mizuno, *Shokubai* **1990**, *32*, 430.
- [9] W. Held, A. Konig, T. Richter, L. Puppe, *SAE Transaction*, **1990**, *99*, Section 4, 209.
- [10] J. G. M. Brandin, L. A. H. Andersson, C.U.I. Odenbrand, *Catal. Today* **1989**, *4*, 187.
- [11] E. Y. Choi, I.-S. Nam, Y. G. Kim, J. S. Chung, J. S. Lee, M. Nomura, *J. Mol. Catal.* **1991**, *69*, 247.
- [12] T. Komatsu, M. Nunokawa, I. S. Moon, T. Takahara, S. Nanba, T. Yashima, *J. Catal.* **1994**, *148*, 427.
- [13] S. Brandenberger, O. Kröcher, A. Tissler, R. Althoff, *Catal. Rev.-Sci. Eng.* **2008**, *50*, 492.
- [14] C. H. F. Peden, *J. Catal.* **2019**, *373*, 384.
- [15] I. Bull, W.-M. Xue, P. Burk, R.S. Boorse, W.M. Jaglowski, G.S. Koermer, A. Moini, J. A. Patchett, J. C. Dettling, M. T. Caudle, *US Patent* **2009**, *7*, 610, 662.
- [16] J. H. Kwak, R. G. Tonkyn, D. H. Kim, J. Szanyi, C. H. F. Peden, *J. Catal.* **2010**, *275*, 187.
- [17] J. H. Kwak, D. Tran, S. D. Burton, J. Szanyi, J. H. Lee, C. H. F. Peden, *J. Catal.* **2012**, *287*, 203.
- [18] M. Moliner, C. Franch, E. Palomares, M. Grillb, A. Corma, *Chem. Commun.* **2012**, *48*, 8264.
- [19] N. Martin, C. R. Boruntea, M. Moliner, A. Corma, *Chem. Commun.* **2015**, *51*, 11030.
- [20] J. D. Albarracin-Caballero, I. Khurana, J. R. Di Iorio, A. J. Shih, J. E. Schmidt, M. Dusselier, M. E. Davis, A. Yezerets, J. T. Miller, F. H. Ribeiro, R. Gounder, *React. Chem. Eng.* **2017**, *2*, 168.
- [21] D. Jo, T. Ryu, G. T. Park, P. S. Kim, C. H. Kim, I.-S. Nam, S. B. Hong, *ACS Catal.* **2016**,

6, 2443.

[22] J. Kim, S. J. Cho, D. H. Kim, *ACS Catal.* **2017**, *7*, 6070.

[23] J. H. Lee, Y. J. Kim, T. Ryu, P. S. Kim, C. H. Kim, S. B. Hong, *Appl. Catal. B* **2017**, *200*, 428.

[24] Y. Shan, X. Shi, J. Du, Y. Yu, H. He, *Catal. Sci. Technol.* **2019**, *9*, 106.

[25] S. V. Priya, T. Ohnishi, Y. Shimada, Y. Kubota, T. Masuda, Y. Nakasaka, M. Matsukata, K. Itabashi, T. Okubo, T. Sano, N. Tsunoji, T. Yokoi, M. Ogura, *Bull. Chem. Soc. Jpn.* **2018**, *91*, 355.

[26] N. Nakazawa, S. Inagaki, Y. Kubota, *Adv. Porous Mater.* **2016**, *4*, 219.

[27] A. Chokkalingam, W. Chaikittisilp, K. Iyoki, S. H. Keoh, Y. Yanaba, T. Yoshikawa, T. Kusamoto, T. Okubo, T. Wakihara, *RSC Adv.* **2019**, *9*, 16790.

[28] J. Zhu, Z. Liu, L. Xu, T. Ohnishi, Y. Yanaba, M. Ogura, T. Wakihara, T. Okubo, *J. Catal.* **2020**, *391*, 346.

[29] L. Xu, C. Shi, Z. Zhang, H. Gies, F.-S. Xiao, D. De Vos, T. Yokoi, X. Bao, M. Feyen, S. Maurer, B. Yilmaz, U. Müller, W. Zhang, *Microporous Mesoporous Mater.* **2014**, *200*, 304.

[30] Y. Wang, T. Nishitoba, Y. Wang, X. Meng, F.-S. Xiao, W. Zhang, B. Marler, H. Gies, D. De Vos, U. Kolb, M. Feyen, R. McGuire, A.-N. Parvulescu, U. Müller, and T. Yokoi, *Ind. Eng. Chem. Res.* **2020**, *59*, 7375.

[31] Z. Liu, T. Wakihara, K. Oshima, D. Nishioka, Y. Hotta, S. P. Elangovan, Y. Yanaba, T. Yoshikawa, W. Chaikittisilp, T. Matsuo, T. Takewaki, Tatsuya Okubo, *Angew. Chem. Int. Ed.* **2015**, *54*, 5683.

[32] R. Ransom, R. Moulton, D. F. Shantz, *J. Catal.* **2020**, *382*, 339.

[33] T. Sonoda, T. Maruo, Y. Yamasaki, N. Tsunoji, Y. Takamitsu, M. Sadakane, T. Sano, *J. Mater. Chem. A* **2015**, *3*, 857.

[34] Y. Kakiuchi, Y. Yamasaki, N. Tsunoji, Y. Takamitsu, M. Sadakane, T. Sano, *Chem. Lett.* **2016**, *45*, 122.

[35] E. Mitani, Y. Yamasaki, N. Tsunoji, M. Sadakane, T. Sano, *Microporous Mesoporous Mater.* **2018**, *267*, 192.

[36] Y. Kakiuchi, T. Tanigawa, N. Tsunoji, Y. Takamitsu, M. Sadakane, T. Sano, *Appl. Catal. A* **2019**, *575*, 357.

[37] F. Gao, Y. Wang, N. M. Washton, M. Kollaf, J. Szanyi, C. H. F. Peden, *ACS Catal.* **2015**, *5*, 6780.

[38] T. Usui, Z. Liu, S. Ibe, J. Zhu, C. Anand, H. Igarashi, N. Onaya, Y. Sasaki, Y. Shiramata,

- T. Kusamoto, T. Wakihara, *ACS Catal.* **2018**, *8*, 9165.
- [39] Z. Zhao, R. Yu, C. Shi, H. Gies, F.-S. Xiao, D. De Vos, T. Yokoi, X. Bao, U. Kolb, R. McGuire, A.-N. Parvulescu, S. Maurer, U. Müller, W. Zhang, *Catal. Sci. Technol.* **2019**, *9*, 241.
- [40] Y. Cui, Y. Wang, D. Mei, E. D. Walter, N. M. Washton, J. D. Holladay, Y. Wang, J. Szanyi, C. H. F. Peden, F. Gao, *J. Catal.* **2019**, *378*, 363.
- [41] Y. Cui, Y. Wang, E. D. Walter, J. Szanyi, Y. Wang, F. Gao, *Catal. Today* **2020**, *339*, 233.
- [42] M. A. Newton, A. J. Knorpp, V. L. Sushkevich, D. Palagin, J. A. van Bokhoven, *Chem. Soc. Rev.* **2020**, *49*, 1449.
- [43] D. W. Fickel, R. F. Lobo, *J. Phys. Chem. C* **2010**, *114*, 1633.
- [44] S. T. Korhonen, D. W. Fickel, R. F. Lobo, B. M. Weckhuysen, A. M. Beale, *Chem. Commun.* **2011**, *47*, 800.
- [45] R. Zhang, J.-S. McEwen, M. Kollar, F. Gao, Y. Wang, J. Szanyi, C. H. F. Peden, *ACS Catal.* **2014**, *4*, 4093.
- [46] V. F. Kispersky, A. J. Kropf, F. H. Ribeiro, J. T. Miller, *Phys. Chem. Chem. Phys.* **2012**, *14*, 2229.
- [47] F. Gao, E. D. Walter, M. Kollar, Y. Wang, J. Szanyi, C. H. F. Peden, *J. Catal.* **2014**, *319*, 1.
- [48] C. Paolucci, A. A. Verma, S. A. Bates, V. F. Kispersky, J. T. Miller, R. Gounder, W. N. Delgass, F. H. Ribeiro, W. F. Schneider, *Angew. Chem. Int. Ed.* **2014**, *53*, 11828.
- [49] T. V. W. Janssens, H. Falsig, L. F. Lundegaard, P. N. R. Vennestrøm, S. B. Rasmussen, P. G. Moses, F. Giordanino, E. Borfecchia, K. A. Lomachenko, C. Lamberti, S. Bordiga, A. Godiksen, S. Mossin, P. Beato, *ACS Catal.* **2015**, *5*, 2832.
- [50] C. Paolucci, A. A. Parekh, I. Khurana, J. R. Di Iorio, H. Li, J. D. A. Caballero, A. J. Shih, T. Anggara, W. N. Delgass, J. T. Miller, F. H. Ribeiro, R. Gounder, W. F. Schneider, *J. Am. Chem. Soc.* **2016**, *138*, 6028.
- [51] F. Gao, D. Mei, Y. Wang, J. Szanyi, C. H. F. Peden, *J. Am. Chem. Soc.* **2017**, *139*, 4935.
- [52] C. Paolucci, I. Khurana, A. A. Parekh, S. Li, A. J. Shih, H. Li, J. R. Di Iorio, J. D. Albarracin-Caballero, A. Yezerets, J. T. Miller, W. N. Delgass, F. H. Ribeiro, W. F. Schneider, R. Gounder, *Science* **2017**, *357*, 898.
- [53] J. Luo, D. Wang, A. Kumar, J. Li, K. Kamasamudram, N. Currier, A. Yezerets, *Catal. Today* **2016**, *267*, 3.

- [54] C. B. Jones, I. Khurana, S. H. Krishna, A. J. Shih, W. Nicholas Delgass, J. T. Miller, F. H. Ribeiro, W. F. Schneider, R. Gounder, *J. Catal.* **2020**, *389*, 140.
- [55] C. Paolucci, J. R. Di Iorio, W. F. Schneider, R. Gounder, *Acc. Chem. Res.* **2020**, *53*, 1881.
- [56] A. Martini, E. Borfecchia, K. A. Lomachenko, I. A. Pankin, C. Negri, G. Berlier, P. Beato, H. Falsig, S. Bordiga, C. Lamberti, *Chem. Sci.* **2017**, *8*, 6836.
- [57] J. Song, Y. Wang, E. D. Walter, N. M. Washton, D. Mei, L. Kovarik, M. H. Engelhard, S. Proding, Y. Wang, C. H. F. Peden, F. Gao, *ACS Catal.* **2017**, *7*, 8214.
- [58] M. De Prins, E. Verheyen, A. Hoffmann, G. Vanbutsele, S. Pulinthanathu Sree, S. Kerkhofs, L. Van Tendeloo, F.-W. Schütze, J. Martens, *J. Catal.* **2020**, *390*, 224.
- [59] M. H. Groothaert, J. A. Bokhoven, A. A. Battiston, B. M. Weckhuysen, R. A. Schoonheydt, *J. Am. Chem. Soc.* **2003**, *125*, 7629.
- [60] M. H. Groothaert, P. J. Smeets, B. F. Sels, P. A. Jacobs, R. A. Schoonheydt, *J. Am. Chem. Soc.* **2005**, *127*, 1394.
- [61] P. Vanelderen, B. E. R. Snyder, M.-L. Tsai, R. G. Hadt, J. Vancauwenbergh, O. Coussens, R. A. Schoonheydt, B. F. Sels, E. I. Solomon, *J. Am. Chem. Soc.* **2015**, *137*, 6383.
- [62] J. S. Woertink, P. J. Smeets, M. H. Groothaert, M. A. Vance, B. F. Sels, R. A. Schoonheydt, E. I. Solomon, *Proc. Natl. Acad. Sci. USA* **2009**, *106*, 18908.
- [63] S. H. Krishna, C. B. Jones, J. T. Miller, F. H. Ribeiro, R. Gounder, *J. Phys. Chem. Lett.* **2020**, *11*, 5029.
- [64] C. Liu, H. Kubota, T. Amada, K. Kon, T. Toyao, Z. Maeno, K. Ueda, J. Ohyama, A. Satsuma, T. Tanigawa, N. Tsunoji, T. Sano, K. Shimizu, *ChemCatChem* **2020**, *12*, 3050.
- [65] A. Satsuma, J. Shibata, A. Wada, Y. Shinozaki and T. Hattori, *Stud. Surf. Sci. Catal.* **2003**, *145*, 235.
- [66] F. Gao, C. H. F. Peden, *Catalysts* **2018**, *8*, 140.
- [67] F. Giordanino, P. N. R. Vennestrom, L. F. Lundegaard, F. N. Stappen, S. Mossin, P. Beato, S. Bordiga, C. Lamberti, *Dalton Trans.* **2013**, *42*, 12741.
- [68] R. A. Schoonheydt, *Catal. Rev.-Sci. Eng.* **1993**, *35*, 129.
- [69] J. Bjerrum, C. J. Ballhausen, C. K. Jørgensen, *Acta. Chem. Scand.* **1954**, *8*, 1275.
- [70] L. N. Trevani, J. C. Roberts, Peter R. Tremaine, *J. Sol. Chem.* **2001**, *30*, 585.
- [71] A. Delabie, K. Pierloot, M. H. Groothaert, B. M. Weckhuysen, R. A. Schoonheydt, *Microporous Mesoporous Mater.* **2000**, *37*, 209.
- [72] K. A. Lomachenko, E. Borfecchia, C. Negri, G. Berlier, C. Lamberti, P. Beato, H. Falsig,

- S. Bordiga, *J. Am. Chem. Soc.* **2016**, *138*, 12025.
- [73] A. Delabie, K. Pierloot, M. H. Groothaert, R. A. Schoonheydt, L. G. Vanquickenborne, *Eur. J. Inorg. Chem.* **2002**, 515.
- [74] A. B. P. Lever, *Inorganic Electronic Spectroscopy (Second Edition)*, Elsevier, Amsterdam, **1984**, Chap. 6, 376.
- [75] J. Dědeček, B. Wichterlová, *J. Phys. Chem. B* **1997**, *101*, 10233.
- [76] H. Li, C. Paolucci, I. Khurana, L. N. Wilcox, F. Göttl, J. D. Albarracin-Caballero, A. J. Shih, F. H. Ribeiro, R. Gounder, W. F. Schneider, *Chem. Sci.* **2019**, *10*, 2373.
- [77] A. Godiksen, F. N. Stappen, P. N. R. Vennestrøm, F. Giordanino, S. B. Rasmussen, L. F. Lundegaard, S. Mossin, *J. Phys. Chem. C* **2014**, *118*, 23126.
- [78] M. H. Groothaert, K. Lievens, H. Leeman, B. M. Weckhuysen, R. A. Schoonheydt, *J. Catal.* **2003**, *220*, 500.
- [79] C. Liu, H. Kubota, T. Toyao, Z. Maeno, K. Shimizu, *Catal. Sci. Technol.* **2020**, *10*, 3586.
- [80] L. M. Mirica, X. Ottenwaelder, T. Daniel P. Stack, *Chem. Rev.* **2004**, *104*, 1013.
- [81] X. Ottenwaelder, D. Jackson Rudd, M. C. Corbett, K. O. Hodgson, B. Hedman, T. Daniel P. Stack, *J. Am. Chem. Soc.* **2006**, *128*, 9268.
- [82] B. T. Op't Holt, M. A. Vance, L. M. Mirica, D. E. Heppner, T. Daniel P. Stack, E. I. Solomon, *J. Am. Chem. Soc.* **2009**, *131*, 6421.
- [83] J. Dědeček, Z. Sobalík, Z. Tvarůžková, D. Kaucký, B. Wichterlová, *J. Phys. Chem.* **1995**, *99*, 16327.
- [84] B. Wichterlová, Z. Sobalík, J. Dědeček, *Appl. Catal. B* **2003**, *41*, 97.
- [85] K. Mlekodaj, J. Dedecek, V. Pashkova, E. Tabor, P. Klein, M. Urbanova, R. Karcz, P. Sazama, S. R. Whittleton, H. M. Thomas, A. V. Fishchuk, S. Sklenak, *J. Phys. Chem. C* **2019**, *123*, 7968.
- [86] J. Dědeček, D. Kaucký, B. Wichterlová, *Microporous Mesoporous Mater.* **2000**, *35-36*, 483.
- [87] J. Dědeček, L. Čapek, D. Kaucký, Z. Sobalík, B. Wichterlová, *J. Catal.* **2002**, *211*, 198.
- [88] P. Sazama, E. Tabor, P. Klein, B. Wichterlova, S. Sklenak, L. Mokrzycki, V. Pashkkova, M. Ogura, J. Dedecek, *J. Catal.* **2016**, *333*, 102.
- [89] J. Dědeček, B. Wichterlová, *J. Phys. Chem. B* **1999**, *103*, 1462.
- [90] A. Delabie, K. Pierloot, M. H. Groothaert, B. M. Weckhuysen, R. A. Schoonheydt, *Phys. Chem. Chem. Phys.* **2002**, *4*, 134.
- [91] T. Takaishi, M. Kato, K. Itabashi, *Zeolites*, **1995**, *15*, 21.

Chapter 4

Dependence of reaction rates for NH₃-SCR over Cu-Zeolites with several topologies on O₂

4.1. Introduction

Selective catalytic reduction of NO_x using NH₃ as a reducing agent (NH₃-SCR) is one of the most effective ways to remove NO_x from exhausts with O₂-rich compositions. A lot of catalysts for the reaction have been developed, such as V-based mixed oxide, Fe-zeolites, and Cu-zeolites^[1]. Among the catalysts so far, Cu-zeolites exhibit a high reaction rate at a low NO₂ concentration (standard SCR) in a low temperature region (below 550 K)^[1]. Therefore, the current central trend of the study on the catalysts for NH₃-SCR is based on Cu-zeolites. Since the development of Cu/SSZ-13 zeolite catalyst with CHA topology, which exhibits a high reaction rate in wide temperature region, high selectivity into N₂, and a high durability under hydrothermal conditions^[2], a wide variety of zeolites were tested toward the application of NH₃-SCR³.

In the catalytic activity tests of NH₃-SCR, it is often the case that the O₂ concentration in the reaction feed is fixed at a certain value^[3,4], and the effect of O₂ pressure on the reaction rate has attracted little attention. The current application of NH₃-SCR is mainly the removal of NO_x emitted from diesel engine. The emission contains an excess amount of O₂ (typically 2–17 %)^[5]. A portion of the O₂ contained in the exhaust is steadily consumed over other catalysts for exhaust purification processes (*e.g.*, diesel oxidation catalyst; DOC and diesel particulate filter; DPF)^[6]. The DOC catalyst plays a role in oxidative removal of unburned hydrocarbon (HC) and carbon monoxide (CO) using O₂. Particulate matter (PM) is trapped on the DPF and eliminated by catalytic combustion using O₂ and NO_x. In the exhaust purification system of diesel engine, such DOC and DPF units are generally mounted at the upstream of the SCR catalyst. The state-of-the-art SCR system of diesel engines tends to be integrated to DPF to make the whole system compact^[7]. Moreover, the application of exhaust gas recirculation (EGR) system, which introduces a part of exhaust into engine cylinder to make the temperature of combustion decrease, resulting in the decrease of thermal NO_x, is in progress for the combustion process^[8]. These purification technologies will make the temperature of exhaust and the concentration of O₂ lower than they are.

On the other hand, a recent fundamental research^[9] has shown that the reaction rate for NH₃-SCR over Cu-SSZ-13 zeolite catalyst is greatly influenced by the O₂ pressure in a low O₂ pressure region (concentration below 15 %) at 473 K, where the overall rate of this reaction is largely affected by the oxidation of Cu ion on zeolites by O₂^[10]. It is shown in the literature^[9] that the apparent first-order SCR rate constant increases with increasing Cu volumetric density. However, the significant rate drop at the O₂ partial pressure below 15 kPa

is a common behaviour of Cu-SSZ-13 zeolite regardless of its composition. Considering the recent trends on the composition of emission from practical diesel engines and the behavior of Cu-SSZ-13 zeolite catalyst described above, it is desired to obtain a rational principle to widen the active window for exhaust composition at low reaction temperatures (~ 473 K) to pass future regulations^[11].

In this chapter, a comparative study is conducted regarding NH_3 -SCR reaction rate dependence on the O_2 pressure at 473 K over Cu ion-exchanged MOR, MFI, CHA and *BEA zeolites from the viewpoint of “Cu density in micropores” to understand the effect of zeolite topology on the dependence.

4.2. Experimental

Preparation of the catalysts used in this chapter was described in chapter 2. The reaction rates were measured by using the same equipment and condition as used in chapter 3. The reaction rate was calculated by determining the amount of NO converted to N₂ per second, which was divided by the amount of Cu in the catalyst. The O₂ concentration was kept at 5 % during the pretreatment at 873 K, followed by cooling the temperature to 473 K. Then, the O₂ concentration was altered from 1 to 15 %, and more than 10 min was needed to reach steady-state NO conversion at each targeted O₂ concentration. Formed NO₂ was transformed to NO by a catalyser unit attached to a chemical luminescence NO_x analyser (HORIBA VA-3000); therefore, the NO conversion detected by the analyser was regarded as the NO_x conversion and the effect of background NO₂ was eliminated.

4.3. Results and Discussion

4.3.1. Dependence of O₂ pressure on NH₃-SCR rates per Cu over a reference Cu-SSZ-13 catalyst

First of all, the catalytic activity of a reference Cu-SSZ-13 catalyst (C905 shown in Chapter 2) with a similar composition to state-of-the-art commercial catalyst for NH₃-SCR was measured. It is reported that the composition of the catalyst, Si/Al and Cu/Al ratios ~9.5 and 0.3, respectively, corresponding 3.1 wt.% Cu^[12], which is higher than any catalyst used in the report^[9] on dependence of NH₃-SCR rates on O₂ pressure.

Figure 4.1 shows the temperature dependence of the catalytic activity. This catalyst exhibited the activity for a steady-state standard NH₃-SCR reaction. Both the NO and NH₃ conversions increased from 423 to 573 K, and the NO conversion decreased over 673 K with almost complete consumption of NH₃. It has been suggested that NH₃ oxidation by O₂ occurs as a side reaction over 573 K and the selectivity for NH₃ in NH₃-SCR decreases^[13], which explains the phenomena observed at high reaction temperatures in Figure 4.1. In the low-temperature region around 473 K, the NH₃ and NO conversions were similar, and it means that the NH₃ selectivity during NH₃-SCR was almost 100%.

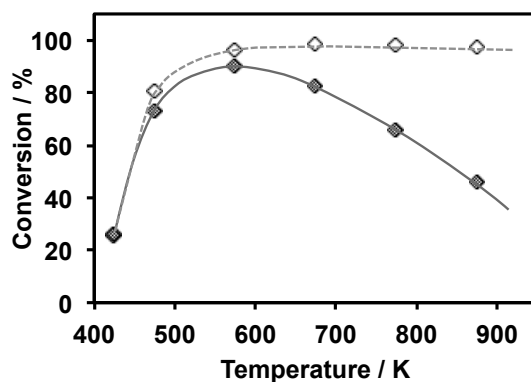


Figure 4.1. The temperature dependence of the catalytic activity for the reference Cu-SSZ-13 zeolite catalyst with the composition similar to the commercial catalyst.

Figure 4.2.a shows the rate dependence on O₂ pressure for NH₃-SCR per Cu ((mole NO to N₂)/(mole Cu) s⁻¹) by a kinetic measurement at 473 K over the reference Cu-SSZ-13 catalyst. Similar to the previous report by Jones *et al.*,^[9] a Langmuirian dependence was observed. The reaction order with respect to O₂ for NH₃-SCR per Cu was determined according to the following power law model equation^[4a].

$$(\text{NH}_3\text{-SCR rate per Cu}) = A_0 \times \exp(-E_{\text{app}}/RT) \times (P_{\text{O}_2})^\alpha$$

The α in this equation expresses the reaction order for O_2 . Figure 4.2a was re-plotted to log-log axes (Figure 4.2b) to know the slope corresponding to α according to the following equation (an explanation for the previous equation obtained by an equivalent transformation).

$$\ln(\text{NH}_3\text{-SCR rate per Cu}) = \ln(A_0) - E_{\text{app}}/RT + \alpha \times \ln(P_{\text{O}_2})$$

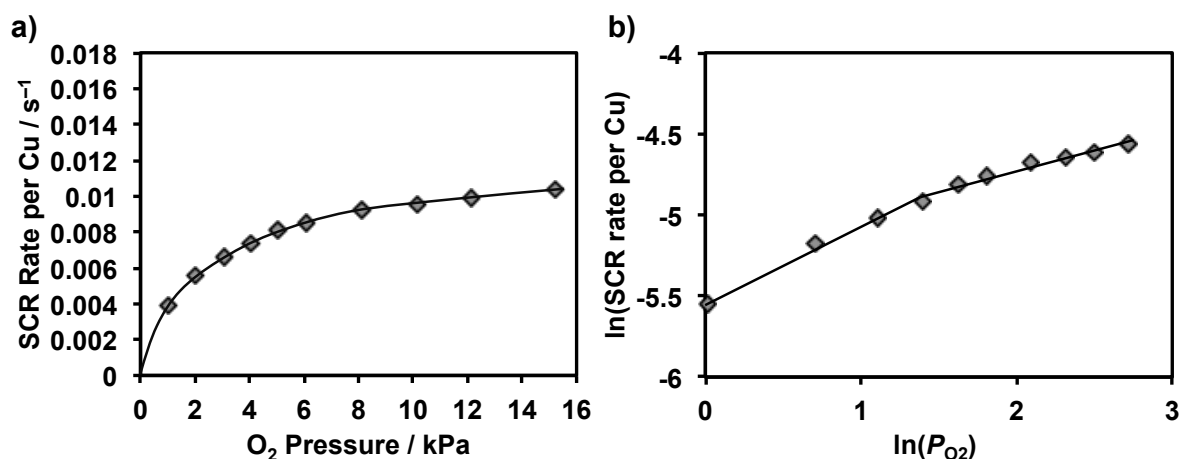


Figure 4.2. a) The dependence of $\text{NH}_3\text{-SCR}$ rate per Cu at 473 K on O_2 pressure and b) the log-log plot for the calculation of apparent O_2 order over the reference Cu-SSZ-13 catalyst.

As shown in Figure 4.2b, the log-log plot did not follow a linear relationship. It is observed that the slope of the plot decreased with increase in O_2 partial pressure in the reaction flow. This result shows that the reaction order for O_2 decreases with increase in O_2 partial pressure.

This phenomenon can be explained by the suggested redox mechanism between Cu^+ and Cu^{2+} in the micropore of zeolites. The reduction of Cu^{2+} to Cu^+ is thought to proceed by $\text{NH}_3 + \text{NO}$ co-reductants^[14], and the oxidation of Cu^+ to Cu^{2+} is thought to proceed by O_2 oxidant^[15]. It has been observed by several *operando* analyses that both Cu^+ and Cu^{2+} exist under a steady-state $\text{NH}_3\text{-SCR}$ condition^[16], although the ratio between two oxidation states depends both on the composition of Cu-zeolites and the reaction conditions. This fact indicates that the reaction rate is not solely limited by the rate for the Cu^{2+} reduction step (reduction half-cycle) nor Cu^+ oxidation step (oxidation half-cycle)^[10]. In other words, the

reduction and oxidation half-cycles are kinetically relevant under the conditions below 523 K and at 5–20 kPa O₂ pressure over Cu-SSZ-13 zeolite^[10].

From the description above, the phenomenon observed in Figure 4.2b can be understood as follows; the reaction is mainly dominated by the oxidation half-cycle under a low O₂ partial pressure reaction condition because the supply of oxidant is relatively insufficiency, and the oxidation half-cycle rate is improved with increasing the O₂ partial pressure. The reaction order for O₂ could be calculated in the low P_{O_2} region (≤ 4 kPa) and high P_{O_2} region ($5 \leq P_{O_2} \leq 15$ kPa). The results are shown in Table 4.1. The reaction order for O₂ decreased with increasing O₂ pressure, but did not reach to zero-order in the O₂ pressure region in this chapter. It is indicated from the results that the effect of oxidation half-cycle on the whole reaction rate remains in all P_{O_2} region in this chapter, and the effect becomes stronger in a lower O₂ pressure region below 5 kPa than in the higher O₂ pressure region over this Cu-SSZ-13 catalyst. The apparent activation energy (E_{app}) for the reaction the around 473 K calculated from the Arrhenius plots (Figure 4.3) was not changed obviously (Table 4.2) in the O₂ pressure region between 1 and 15 %. The magnitude for the E_{app} was typical for the NH₃-SCR over Cu-zeolite catalysts^[4]. Therefore, it is confirmed that the rate-determining step itself is not changed by altering the reaction condition.

Table 4.1. The reaction order for O₂ at 473 K over several P_{O_2} region.

O ₂ partial pressure region / kPa	Reaction order for O ₂
1–4	0.46
10–15 %	0.14

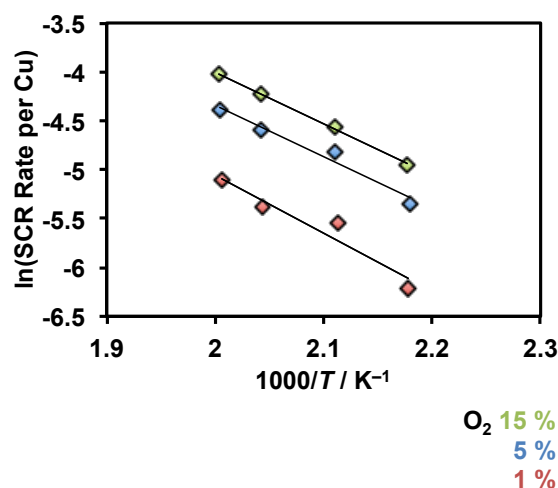


Figure 4.3. The Arrhenius plots around 473 K under several O₂ pressure reaction condition over the reference Cu-SSSZ-13 catalyst.

Table 4.2. The apparent activation energy around 473 K under several O₂ pressure reaction condition over the reference Cu-SSSZ-13 catalyst.

O ₂ partial pressure / kPa	E_{app} / kJ mol ⁻¹
1	49
5	44
15	44

4.3.2. The dependence of O₂ pressure on NH₃-SCR rates per Cu over Cu-zeolite catalysts with several topologies

The same measurements were conducted over the Cu-zeolite catalysts with MOR, MFI, *BEA, and CHA topologies that have similar cation density in micropores of zeolites and several Cu density in micropores. The selection of the samples were conducted to obtain the enough information on the three-dimensionally behavior over each topology of the NH₃-SCR rate per Cu as function of the O₂ partial pressure and Cu density in micropores. On each topology, the Cu loading with ~ 3 wt.% was also measured to show the difference during the same Cu content.

As shown in Figures 4.4, the Langmuirian dependence of reaction rates on O₂ pressure until saturation was observed only on the CHA and *BEA zeolites with the highest Cu density in micropores. On the other zeolites, reaction rates showed a monotonic increase along with the O₂ pressure increase. However, the magnitudes of the increase in the reaction

rate were drastically affected by zeolite topologies and Cu density in micropores.

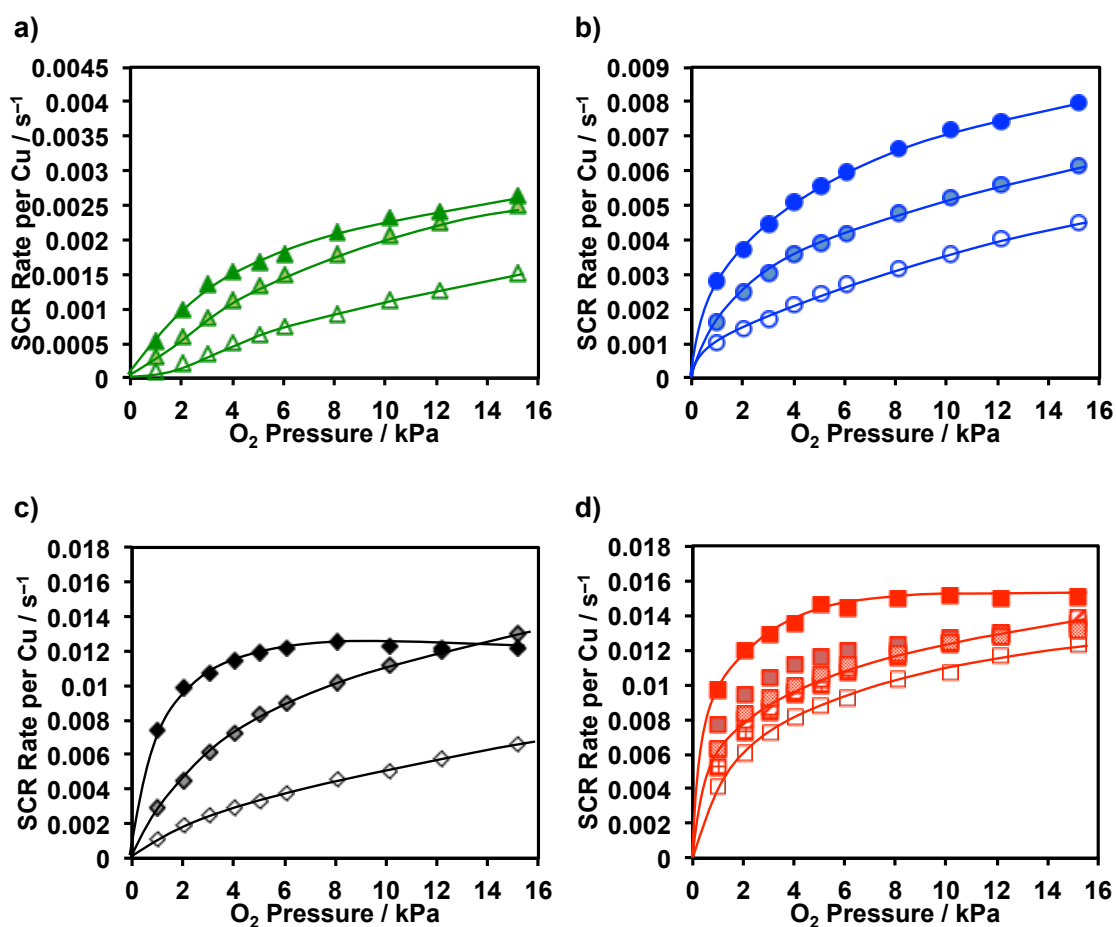


Figure 4.4. The dependence of NH₃-SCR rate per Cu at 473 K on O₂ pressure over a) MOR, b) MFI, c) CHA, and d) *BEA zeolite catalyst with several Cu density in micropores.

The Cu-MOR zeolite exhibited the lowest NH₃-SCR rate per Cu over all O₂ pressure region (Figure 4.4a). Note that the scale of Y axis in Figure 4.4a is quarterly large as that in Figure 4.2a. A little increase was observed in both magnitudes and slopes of NH₃-SCR rate per Cu along with increasing Cu density in micropores. However, the rate was far smaller than that of the reference Cu-SSZ-13 zeolite catalyst, even with the higher Cu density.

The Cu-MFI zeolite exhibited a higher NH₃-SCR rate per Cu over all O₂ pressure region than Cu-MOR zeolite (Figure 4.4b). The scale of Y axis in Figure 4.4b is as large as a half of that in Figure 4.2a. In the case of the MFI zeolite, the increase was also observed in both magnitudes and slopes of NH₃-SCR rate per Cu with increasing Cu density in micropores. The reaction rate and its increase over Cu-MFI zeolite was larger than over

Cu-MOR zeolite. However, the reaction rate over Cu-MFI zeolite was smaller than over the reference Cu-SSZ-13 zeolite catalyst regardless of Cu density in micropores. Even the Cu-MFI zeolite with Cu density in micropores at $7.4 (1000 \text{ \AA}^3)^{-1}$ (approximately 3 times as large as the reference Cu-SSZ-13 zeolite) did not represent an exception.

In the case of Cu-CHA zeolite, the increase behaviour in NH_3 -SCR rate per Cu along with O_2 pressure was largely affected by the Cu density in micropores (Figure 4.4c). The catalyst with a low Cu density in micropores showed relatively steady increase in NH_3 -SCR rate per Cu along with O_2 pressure. On the other hand, the catalyst showed the rapid increase in NH_3 -SCR rate per Cu in low O_2 pressure region, and the rate became constant in the higher O_2 pressure region ($> 6 \text{ kPa}$). Note that the slight decrease in NH_3 -SCR rate per Cu of the Cu-CHA zeolite with the largest Cu density in micropores over 8 kPa O_2 pressure region is mainly caused by the increase in the formation of N_2O . Interestingly, the zeolites with Cu density in micropores at 1.6 and $3.4 (1000 \text{ \AA}^3)^{-1}$ exhibited almost the same NH_3 -SCR rate per Cu when O_2 pressure was at 15 kPa . This result suggests that they would reach the zero-order dependence on O_2 pressure, which means that the oxidation half-cycle does not determine the overall rate in the O_2 pressure region regardless of Cu density in micropores.

Among the Cu-zeolite catalysts, Cu-*BEA zeolite exhibited relatively low dependence of NH_3 -SCR rate per Cu on O_2 pressure (Figure 4.4d). Moreover, the effect of Cu density in micropores of the catalyst was small on the behavior of the rate along with O_2 pressure. In other words, the Cu-*BEA zeolite catalyst exhibited a high NH_3 -SCR rate per Cu even in low Cu density in micropores and low O_2 pressure region. Surprisingly, even the Cu-*BEA zeolite catalyst with Cu density in micropores at $0.76 (1000 \text{ \AA}^3)^{-1}$ exhibited a higher NH_3 -SCR rate per Cu than the reference Cu-SSZ-13 catalyst with Cu density in micropores at $2.7 (1000 \text{ \AA}^3)^{-1}$.

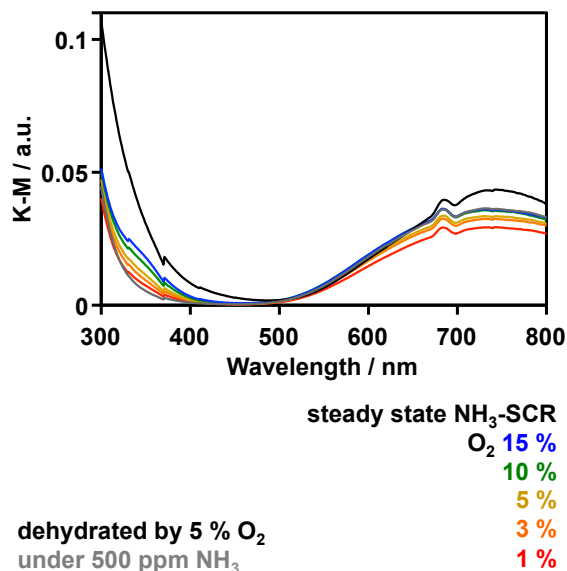


Figure 4.5. The diffuse reflectance UV-Vis spectra of Cu-*BEA zeolite catalyst under steady-state NH₃-SCR gas mixture flow with several O₂ concentration at 473 K.

Figure 4.5 shows the diffuse reflectance UV-Vis spectra of Cu-*BEA zeolite catalyst with Cu density in micropores at $1.7 \text{ (1000 \text{ \AA}^3)^{-1}}$ under steady-state NH₃-SCR gas mixture flow with several O₂ concentration at 473 K. The LMCT band below 350 nm and d-d transition band centered at $\sim 730 \text{ nm}$ was observed. Recently, a large fraction of LMCT band at 350 nm was observed in the diffuse reflectance UV-Vis spectra of Cu-AEI zeolites during steady-state NH₃-SCR below 473 K^[17]. The band was assigned to the $(\mu\text{-}\eta^2\text{:}\eta^2\text{-peroxo})$ dicopper(II) complex, which is suggested to be the important intermediate forming during the oxidation half-cycle by using time dependent density functional theory (TD-DFT) calculation applying B3LYP hybrid functional^[17]. In the case of the diffuse reflectance UV-Vis spectra of Cu-*BEA zeolite, the intensity of the band was small and increased slightly with increase of O₂ pressure of the reaction gas. This result suggests that such the intermediate for the oxidation half-cycle also forms over the Cu-*BEA zeolite and the formation efficiency increases with increase in O₂ pressure, however, they consumed rapidly and detection efficiency in the time scale of UV-Vis measurement is small. In the $(\mu\text{-}\eta^2\text{:}\eta^2\text{-peroxo})$ dicopper(II) complex with amine ligands with N/Cu ratio of 2, it is reported that the d-d transition band is not observed in wavenumber region longer than 700 nm^[18]. According to the discussion in Chapter 3, the d-d transition band centered at $\sim 730 \text{ nm}$ can be assigned to the Cu²⁺ with main ligand of O₂ and adsorbed small number of NH₃ (less than 3). Figure 4.5 shows the diffuse reflectance UV-Vis spectra of same zeolite after dehydration by 5 % O₂

flow and during 500 ppm NH₃ flow at 473 K. The blue-shift of the d-d transition band by NH₃ adsorption was not observed obviously. It was same during steady-state NH₃-SCR gas feed at 473 K. These results suggest that the main observed Cu²⁺ species during steady-state NH₃-SCR at 473 K was not the Cu²⁺ dimer species with bridging O ligand and surrounding amine ligands, but the isolated Cu²⁺ with O_Z and adsorbed small number of NH₃ ligands. The intensity of the d-d transition band was hardly affected by O₂ concentration of the NH₃-SCR gas mixture. It was reported that the intensity of the d-d transition band for Cu²⁺ decreases in low O₂ concentration condition of the NH₃-SCR gas mixture during the same measurement over Cu-SSZ-13 zeolite with Cu/Al = 0.30 and Si/Al = 15, and it is suggested that it was caused by slow oxidation half-cycle in low O₂ concentration condition^[18]. Compared to the result in the previous report^[18], the effect of O₂ concentration on the d-d transition band intensity for Cu²⁺ on the Cu-*BEA zeolite was small. Therefore, it is suggested by the measurement that the high NH₃-SCR rate per Cu over Cu-*BEA catalysts over wide range of O₂ pressure condition, which is observed in Figure 4.4.d, is mainly generated by the high formation efficiency for the isolated Cu²⁺ mainly surrounded by O_Z, which is the final product of oxidation half-cycle and can work as the initial state of the reduction half-cycle, even in low O₂ pressure condition during the steady-state reaction. In other words, it is suggested that the population of the Cu ion that can work as the active center for both reduction and oxidation redox cycle is effectively generated on the *BEA zeolite and this is the origin of the high reaction rate in both low Cu density in micropores and O₂ pressure.

4.3.3. The behavior of low pressure apparent O₂ order for NH₃-SCR rates per Cu over Cu-zeolite catalysts with several topologies along with Cu density in micropores

The reaction order for O₂ was calculated in a similar manner as the reference Cu-SSZ-13 catalyst in a low O₂ pressure region (≤ 5 kPa). The results were displayed as a function of Cu density in micropores (Figure 4.6). As shown in Figure 4.6, the reaction order for O₂ decreased with increase in the Cu density in micropores for all the zeolites investigated in this study. This result was consistent with the previous report on Cu-SSZ-13 zeolites with several Cu densities^[16] and can be understood by the increase in the rate for the oxidation half-cycle with increasing Cu density in micropores. When the reaction order for O₂ was compared among the Cu-zeolites with a similar Cu density in micropores, the tendency was observed that Cu-zeolite with a high reaction rate showed a low reaction order for O₂. This result means that the effect of O₂ pressure on the reaction rate is negligible over a catalyst

with a high reaction rate such as Cu-CHA with high Cu density in micropores or Cu-*BEA.

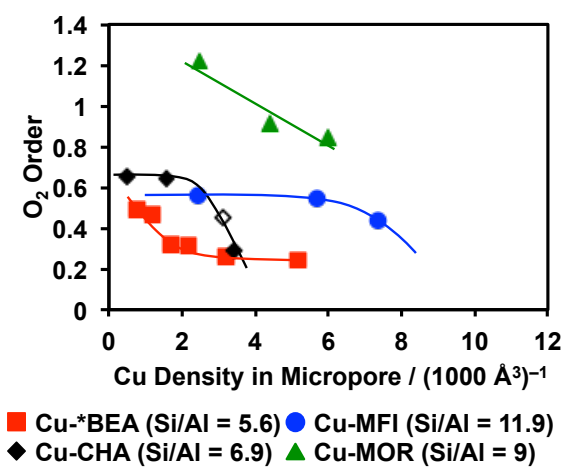


Figure 4.6. The relationship between apparent reaction order for O₂ in the O₂ pressure region (≤ 5 kPa) and the Cu density in micropores.

4.4. Conclusions

Dependence of NH₃-SCR rate on O₂ partial pressure was investigated at 473 K over Cu ion-exchanged MOR, MFI, CHA and *BEA zeolites with several “Cu density in micropores”. The reaction rate with respect to O₂ was largely affected by the zeolite topology. Among the zeolites investigated here, Cu-*BEA zeolite catalyst exhibited a higher reaction rate regardless of the Cu density in micropores (or Cu loading) than a Cu-SSZ-13 reference catalyst in the whole range of Cu content tested in this study. The Cu-*BEA zeolite has a promising potential as the effective catalyst for NH₃-SCR in a wide range of O₂ partial pressure.

References

- [1] C. Görsmann, *Johnson Matthey Technol. Rev.* **2015**, *59*, 139.
- [2] J. H. Kwak, R. G. Tonkyn, D. H. Kim, J. Szanyi, C. H. F. Peden, *J. Catal.* **2010**, *275*, 187.
- [3] (a) M. Moliner, C. Franch, E. Palomares, M. Grillb, A. Corma, *Chem. Commun.* **2012**, *48*, 8264; (b) D. Jo, T. Ryu, G. T. Park, P. S. Kim, C. H. Kim, I.-S. Nam, S. B. Hong, *ACS Catal.* **2016**, *6*, 2443; (c) S. V. Priya, T. Ohnishi, Y. Shimada, Y. Kubota, T. Masuda, Y. Nakasaka, M. Matsukata, K. Itabashi, T. Okubo, T. Sano, N. Tsunoji, T. Yokoi, M. Ogura, *Bull. Chem. Soc. Jpn.* **2018**, *91*, 355; (d) J. Zhu, Z. Liu, L. Xu, T. Ohnishi, Y. Yanaba, M. Ogura, T. Wakihara, T. Okubo, *J. Catal.* **2020**, *391*, 346.
- [4] (a) F. Gao, E. D. Walter, E. M. Karp, J. Luo, R. G. Tonkyn, J. H. Kwak, J. Szanyi, C. H. F. Peden, *J. Catal.* **2013**, *300*, 20; (b) S. A. Bates, A. A. Verma, C. Paolucci, A. A. Parekh, T. Anggara, A. Yezerets, W. F. Schneider, J. T. Miller, W. N. Delgass, F. H. Ribeiro, *J. Catal.* **2014**, *312*, 87.
- [5] İ. A. Reşitoğ, K. Altinişik, A. Keskin, *Clean. Techn. Environ. Policy* **2015**, *17*, 15.
- [6] B. K. Yun, M. Y. Kim, *Appl. Therm. Eng.* 2013, **50**, 152.
- [7] G. Cavataio, J. R. Warner, J. W. Girard, J. Ura, D. Dobson, C. K. Lambert, *SAE Int. J. Fuels Lubr.*, **2009**, *2*, 342.
- [8] M. Zheng, G. T. Reader, J. G. Hawley, *Energy Convers. Manag.* **2004**, *45*, 883.
- [9] C. B. Jones, I. Khurana, S. H. Krishna, A. J. Shih, W. N. Delgass, J. T. Miller, F. H. Ribeiro, W. F. Schneider, R. Gounder, *J. Catal.* **2020**, *389*, 140.
- [10] C. Paolucci, J. R. Di Iorio, W. F. Schneider, R. Gounder, *Acc. Chem. Res.* **2020**, *53*, 1881.
- [11] C. H. F. Peden, *J. Catal.*, 2019, **373**, 384.
- [12] J. Luo, F. Gao, K. Kamasamudram, N. Currier, C. H. F. Peden, A. Yezerets, *J. Catal.* **2017**, *348*, 291.
- [13] F. Gao, C. H. F. Peden, *Catalysts* **2018**, *8*, 140.
- [14] C. Paolucci, A. A. Parekh, I. Khurana, J. R. Di Iorio, H. Li, J. D. A. Caballero, A. J. Shih, T. Anggara, W. N. Delgass, J. T. Miller, F. H. Ribeiro, R. Gounder, W. F. Schneider, *J. Am. Chem. Soc.* **2016**, *138*, 6028.
- [15] C. Paolucci, I. Khurana, A. A. Parekh, S. Li, A. J. Shih, H. Li, J. R. D. Iorio, J. D. Albarracin-Caballero, A. Yezerets, J. T. Miller, W. N. Delgass, F. H. Ribeiro, W. F. Schneider, R. Gounder, *Science* **2017**, *357*, 898.
- [16] C. Liu, H. Kubota, T. Amada, K. Kon, T. Toyao, Z. Maeno, K. Ueda, J. Ohyama, A.

- Satsuma, T. Tanigawa, N. Tsunoji, T. Sano, K. Shimizu, *ChemCatChem* **2020**, *12*, 3050.
- [17] A. Oda, H. Shionoya, Y. Hotta, T. Takewaki, K. Sawabe, A. Satsuma, *ACS Catal.* **2020**, *10*, 12333.
- [18] B. T. O. Holt, M. A. Vance, L. M. Mirica, D. E. Heppner, T. Daniel P. Stack, E. I. Solomon, *J. Am. Chem. Soc.* **2009**, *131*, 6421.

Chapter 5

**Investigation on the formation of active site
for NO direct decomposition
over Cu-Zeolites with several topologies**

5.1. Introduction

Copper species loaded onto zeolites show uniquely high catalytic activity and selectivity for several reactions, including redox cycle reactions such as partial oxidation of methane to methanol^[1], selective catalytic reduction with ammonia (NH₃-SCR)^[2,3], and direct decomposition of NO^[4]. Therefore, the properties of copper species on zeolites (*i.e.*, local structure, redox property, and interaction with several molecular) have generated great interest. Recently, since the discovery of Cu-CHA zeolite catalysts for NH₃-SCR^[5] and the application of them into the methane partial oxidation to methanol^[6], extensive studies on the structure and reactivity of Cu active sites on Cu-CHA zeolites have been performed^[7-9]. Moreover, these results have been combined with catalytic test results to improve the catalytic process, particularly in the methane partial oxidation to methanol^[10]. The combination of catalytic activity tests and Cu active site investigation has successfully led to improvements in the catalytic performance, not only on Cu-CHA, but also on other Cu-zeolites with higher structural complexity than Cu-CHA, such as Cu-MOR^[11].

In contrast to the progress in the performance of Cu-zeolites for NH₃-SCR and methane partial oxidation to methanol processes, recent catalytic improvements for direct decomposition of NO have been much smaller. The direct decomposition of NO into N₂ and O₂ ($2 \text{ NO} \rightarrow \text{N}_2 + \text{O}_2$) does not require any additional reducing agent and proceeds through the simplest system. Therefore, this process is the most desirable route for NO removal. Several metal oxides have been reported as catalysts for direct decomposition of NO^[12,13]. Among the reported catalysts, Cu ion-exchanged zeolites (Cu-zeolites), and in particular, excessively ion-exchanged ($\text{Cu}^{2+}/\text{Al} > 0.5$) MFI zeolite (Cu-MFI), have been demonstrated to show uniquely high catalytic activity for the NO direct decomposition^[4,14,15]. However, the small reaction rate, poor hydrothermal stability of parent MFI zeolites, and inhibition of the reaction by O₂, H₂O, and SO₂ are known to be their drawbacks. Therefore, improvement of Cu-MFI catalysts is desired for practical applications. To indicate the methods for designing catalysts with improved activity, the properties of Cu-MFI should be understood. In particular, the structure and nature of the active sites related to the reaction have attracted great interest, and several analyses have been conducted through combined characterization techniques. It is well known that the catalytic activity of Cu-MFI catalysts for the NO direct decomposition increases with the increase in the Cu ion-exchange level, fitted with an S-shape curve^[15]. Moreover, the relationship between catalytic activity and the Cu ion-exchange level is affected by the structure of the parent zeolites^[16]. Therefore, it is suggested that the active

sites are composed of Cu ion exchanged on zeolites, with a specific framework structure.

Much discussion on the active Cu sites on the zeolites for the NO direct decomposition has been taken place based on a variety of techniques, such as temperature programmed desorption (TPD) [17–20], IR spectroscopy using probe molecules [18,21–30], photoluminescence [24–27,29,31–34], UV-Vis-NIR [19,28,29,33,35], ESR [22,24,25,30,33,36], and XAFS [20,26,28,30,37,38], including *in-situ* measurements. In the discussion on characterization of the active Cu sites on the zeolites, several structures have been suggested. From the results, Cu⁺ formed by the reduction of Cu²⁺ at the ion-exchange sites on zeolites through the high-temperature pretreatment in the inert gas feed or high-vacuum (auto-reduction) [15,22] have been suggested as catalytic centre for the NO direct decomposition. Moreover, two conflicting major explanations have been offered for the origin of the relationship between the activities of Cu-MFI catalysts for the NO direct decomposition and the ion-exchange level.

1. MFI zeolite has several ion-exchangeable sites. The Cu ion on the easily exchangeable site (occupied at the lower ion-exchange level) exhibits less activity, and the Cu ion on the less exchangeable site (occupied at the higher ion-exchange level) has a higher activity. Wichterlova et al. conducted photoluminescence measurements of Cu⁺ on Cu-MFI and observed two emission bands at 480 and 540 nm [32]. They assigned the former band to the Cu ions adjacent to two Al atoms in the zeolite framework and the latter band to the Cu ions adjacent to one Al atom in the zeolite framework. They observed a proportional relationship between the emission band at 540 nm and the catalytic activity in the direct decomposition of NO [28,32]. They assumed that the reason for the observation is that the Cu ions adjacent to one Al framework atom have a high reducibility to Cu⁺ and play the role of catalytic center. This explanation agrees with the fact that the catalytic activity per Cu ion is large for zeolites with higher Si/Al ratio [16].

2. The active site for the NO direct decomposition is two or more adjacent Cu ions on the ion-exchange sites of the MFI zeolite, which can form easily at the higher ion-exchange levels. Groothaert *et al.* conducted *in-situ* XAFS and diffuse reflectance UV-Vis-NIR measurements of Cu-MFI zeolites with several ion-exchange levels, and from the analysis of the obtained data sets, they suggested the existence of bis(μ -oxo)dicopper core on the Cu-MFI zeolites, with a higher ion-exchange level in the NO direct decomposition and of catalytic cycles involving the species [35].

However, the above information from the characterization of active Cu sites on the zeolites does not necessarily support the development of the Cu-zeolite catalysts superior to

Cu-MFI, because it is not clear what the unique property is that causes the MFI zeolites to serve as good catalytic supports for the NO direct decomposition. It can be assumed that MFI zeolites have some property suitable to accommodate the active sites for the NO direct decomposition. However, the study that characterized the active sites for the NO direct decomposition focused only on MFI zeolites, or the studies comparing MFI zeolite with other zeolites have not extensively discussed the results of catalytic activity tests^[17-35]. As a result, the origin of the high catalytic activity of Cu-MFI compared to the other major zeolites (*e.g.*, FAU, MOR, and *BEA)^[6,39] is not well understood.

One way to explore the Cu-zeolite catalysts better than Cu-MFI is to compare different zeolites in the role of catalytic support. A high catalytic activity of Cu-MFI for the NO direct decomposition was found, compared to Cu-FAU and Cu-MOR zeolites^[16]. In the literature described above demonstrated that the catalytic activity per Cu ion has a linear correlation with the Si/Al ratio^[16]. More recently, only two other series of reports^[40-42] have used that Cu-zeolites, other than MFI zeolite, have been used for the direct decomposition of NO, to the best of the author's knowledge.

One study shows the dependence of different Cu/Al/Si ratios and counter cations of the parent zeolite (H^+ , Na^+ , NH_4^+) on catalytic activity of Cu-*BEA zeolites^[40]. This study reported that turnover frequency (TOF) values of Cu ion on Cu-*BEA zeolite in the NO direct decomposition are high and comparable to those of Cu ions on Cu-MFI zeolites. The other studies tested Cu-MEL^[41], Cu-MTW^[41], and mesoporous Cu-MFI and Cu-MEL^[42] zeolites, demonstrating TOF values of Cu ions on Cu-MEL and Cu-MTW zeolites are approximately twice to that of them on Cu-MFI zeolite.

In contrast to the study on the NO direct decomposition, there are some examples in the catalysts for other reactions using Cu-zeolite systems, in which better catalysts than the Cu-MFI have been successfully developed. In recent years, studies on Cu-zeolite catalysts have mainly focused on application as catalysts for NH_3 -SCR and methane partial oxidation to methanol. These studies have revealed that there are zeolites that serve as catalyst supports more optimally than conventional MFI zeolite. In particular, the discovery of Cu-CHA catalysts for NH_3 -SCR^[5], which possesses higher activity, selectivity, and hydrothermal stability than Cu-*BEA and Cu-MFI zeolites possess, has induced an extensive study on this catalyst^[7-9]. Moreover, Cu-zeolite catalysts using other newly synthesized zeolites, such as AEI^[43,44], high-silica LTA and UFI^[45], and KFI^[46] zeolites are reported. The group the author is belonging to has also reported that recently synthesized Cu-zeolite catalysts showed an

excellent catalytic activity and high hydrothermal stability^[47].

This chapter aims to conduct the comparative study on the formation of Cu species active for the NO direct decomposition over Cu-zeolites with similar “cation density in micropores”. It has been reported that all of the adopted zeolites have local structures of ion-exchange sites similar to the MFI zeolite^[48,49]. In the recent theoretical study, it was suggested that the N–N formation step additional to the O₂ desorption step, which is often considered as the rate-determining step for the reaction, is the pathway with high activation energy for the reaction over Cu-MFI zeolites^[50]. This suggestion presents a possibility that the requirement for the Cu species active for the NO direct decomposition over Cu-zeolites involves both N–N formation activity and O₂ desorption ability. Moreover, considering the old O₂-TPD study on Cu-FAU zeolite^[51] and recent studies for methane partial oxidation over Cu-zeolites^[10,52,53], formation of the stable dimer species with bridging oxo species can be assumed over Cu species on zeolites over 423 K during steady-state NO direct decomposition. In other words, there is a concern that the existence of Cu species with N–N formation activity but without O₂ desorption ability, which would be observed in the spectroscopic studies on Cu⁺ species formed by pretreatments in high temperature and inert conditions, is overlooked in the results from the catalytic test using the steady-state reaction condition. Therefore, a pulse reaction test for the NO direct decomposition was adopted to evaluate the N–N formation activity of Cu species formed by pretreatments in high temperature and inert conditions, which would be observed in spectroscopic techniques in this work.

It was shown that the catalytic activities of Cu-*BEA zeolites for the NO direct decomposition are comparable to those of Cu-MFI and Cu-MOR zeolites. However, Cu-MFI and Cu-MOR zeolites have higher efficiency in active site formation than Cu-*BEA zeolite. The NO probe IR measurements revealed that the Cu⁺ formation ratio to the exchanged Cu ion on Cu-MOR is superior to that on other Cu-zeolites, however, Cu⁺ formed on Cu-MFI zeolites are more suitable to accommodate dinitrosyl adspecies than those on Cu-*BEA and Cu-MOR zeolites, despite the similar local structures of the ion-exchange sites. These results suggest that Cu⁺ on Cu-MFI zeolite are in a more open coordination environment than on the other Cu-zeolites. Because of this, high efficiency in active site formation would be observed on Cu-MFI zeolite in spite of the coexistence of large amount of Cu²⁺.

5.2. Experimental

5.2.1. Reaction test for NO direct decomposition

Reaction tests for NO direct decomposition were carried out using a home-made pulse reactor directly connected to GC-TCD, with a molecular sieve 5A column (3 mm i.d.). A mixture of the Cu-zeolites (0.050 g) and SiC (100 mesh, 0.150 g, Wako Chemical Co.) were placed in quartz tubes (4 mm i.d.) and pretreated at 773 K for 2 h under a helium stream of $25 \text{ cm}^3 \cdot \text{min}^{-1}$. NO mixture gas (5.5 cm^3 , 2.09 vol.% balanced in He) was injected as a single pulse to the catalysts under a helium stream of $25 \text{ cm}^3 \cdot \text{min}^{-1}$ at 773 K. The activities of Cu-zeolites for NO direct decomposition were evaluated by the conversion of NO into N_2 . The quantitative assessment for formed N_2 was conducted by the same procedure as the reaction tests for NO direct decomposition except for the amount of Cu-zeolites (0.030 g) and pulse number of NO introduction.

5.2.2. *In situ* IR measurements

Fourier Transform Infrared (FT-IR) spectra were recorded at a resolution of 4 cm^{-1} by a spectrometer (JASCO FT-IR 4600), equipped with a triglycine sulfate detector. The 40 mg samples were pressed into thin self-supporting wafers with 20 mm diameter and placed into an IR cell, attached to a closed gas-circulation system and CaF_2 windows. Prior to the adsorption experiments, samples were pretreated at 773 K under high vacuum for 1 h. The spectra between the pretreatment and NO adsorption experiment at room temperature were used as background. The NO adsorption spectra were recorded after NO dosage at increasing pressure from 5 to 2000 Pa at room temperature. The IR spectra obtained by the subtraction of the background spectra from the NO adsorption spectra were shown, unless otherwise noted. The deconvolution of the IR spectra into the bands was carried out employing Voigt distribution in the JASCO Spectra Manager Suite.

5.3. Results and Discussion

5.3.1. Correlation between ion-exchange level of Cu-zeolites and activity for NO direct decomposition

The activities of Cu-zeolites for NO direct decomposition were evaluated by the conversion of NO into N₂ using the first pulse of NO (2.09 vol.%, He balance, 5.5 cm³) introduced into a pulse reactor directly connected to a GC-TCD. In most cases, O₂ was not detected. It is known that within the initial period of the reaction, O₂ formation in the direct decomposition of NO over Cu-zeolite catalysts was not detected by GC measurement^[4,54]. Moreover, it is also reported that NO₂ forms as a result of the side reaction between residual NO and formed O₂^[4,54], and the detection of NO₂ is difficult in the GC measurements with the molecular sieve 5A column. Those studies show that N₂ formation is not affected by the amount of O₂ formed.

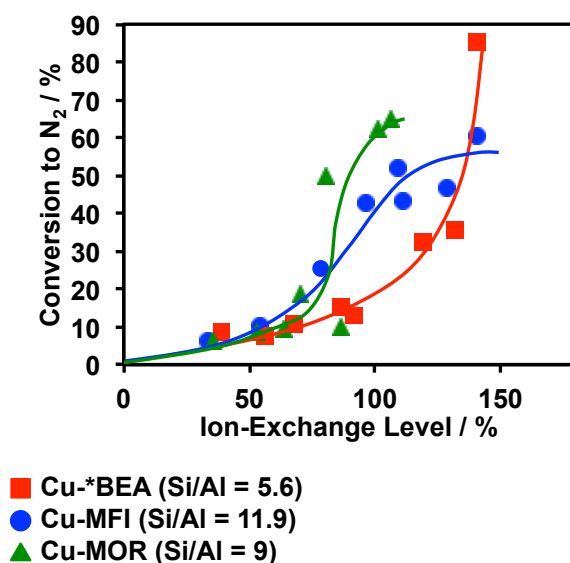


Figure 5.1. Correlation between the Cu ion-exchange level and the conversion of NO into N₂ in the direct decomposition of NO at 773 K over Cu-zeolites with different framework structure.

Over all zeolites, conversion of NO into N₂ increased along with Cu ion-exchange level, fitted with an S-shaped curve, as shown in Figure 5.1. Cu-MOR and Cu-*BEA exhibited N₂ formation activities for NO direct decomposition comparable to Cu-MFI at 773

K in initial reaction conditions. However, the ion-exchange level where the N₂ formation activity rapidly increased was different for each zeolite. For the Cu-MFI and Cu-MOR zeolites, the point of catalytic activity enhancement was observed at the 80% ion-exchange level. For the Cu-*BEA zeolite, the point of N₂ formation activity enhancement was observed around the 130% ion-exchange level. The rapid increase in N₂ formation activity at low ion-exchange levels suggests that the active site effectively forms on the zeolite. Therefore, the active site would form more effectively on MFI and MOR zeolites than on *BEA zeolite. The rate per Cu was calculated by the following equation:

$$\text{Rate per Cu / s}^{-1} = (\text{amount of N}_2 \text{ formed per second})/(\text{amount of Cu})$$

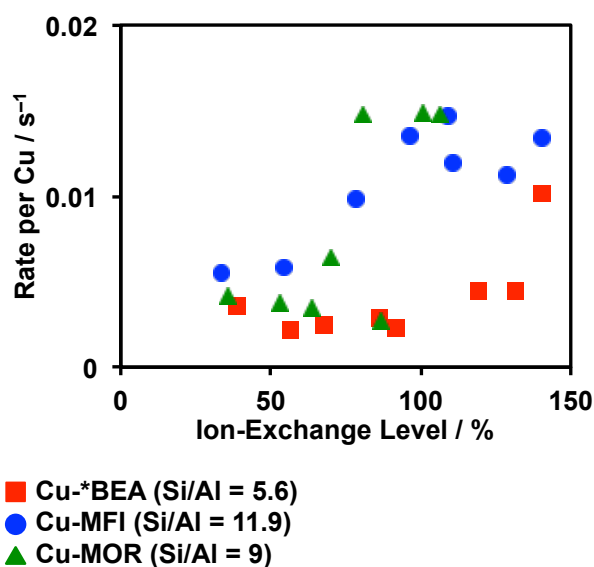


Figure 5.2. Correlation between the Cu ion-exchange level and the rate per Cu for the direct decomposition of NO at 773 K over Cu-zeolites with different topologies.

Over all zeolites, the rate per Cu also increased along with Cu ion-exchange level, as shown in Figure 5.2. This Cu ion-exchange level dependence of rate per Cu shows that the N₂ formation activity increase behaviour of the Cu-zeolites shown in Figure 5.1 is not only because of the Cu contents increase.

Figure 5.3 shows the result of quantitative assessment of formed N₂ over the M9 MOR zeolite at 773 K. The N₂ formation amount decreased with the pulse number of NO introduction and settled into a certain conversion into N₂. The sum amount of formed N₂ was larger than N₂/Cu ratio of 1.2, and O₂ formation was not observed. These results show that the

NO direct decomposition over the MOR zeolite is the partial catalytic process and meaning of the results shown in Figure 5.1 is the assessment of initial activity of Cu-zeolites that directly reflect the nature of Cu species formed by ion-exchange and the following pretreatment in He flow at 773 K.

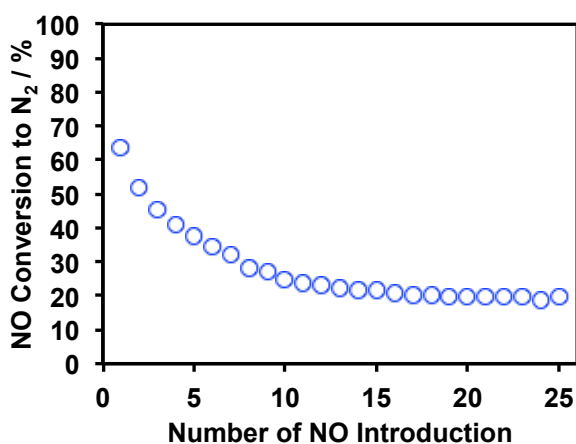


Figure 5.3. Result of a quantitative assessment for NO direct decomposition at 773 K over the M9 zeolite by using the pulse reactor.

It is well known that the activity of the Cu-MFI zeolite catalyst for NO direct decomposition has an S-shaped dependence on the copper ion-exchange level^[15]. However, this behaviour has not been reported for any other zeolite, to the best of the author's knowledge. For Cu-MFI zeolites, this phenomenon has been explained by either existence of several ion-exchange sites or formation of multinuclear Cu sites, as mentioned in the introduction. However, these explanations have only been discussed in reference to Cu-MFI zeolites, and it is not clear whether or not these features are unique to Cu-MFI zeolites due to the lack of comparative studies. To understand how the differences in catalytic properties are related to the differences in zeolite frameworks, the characteristics of Cu-zeolites need to be compared.

5.3.2. NO probe IR measurement

Several reports indicate that the activity for direct decomposition of NO per Cu ion increases with the increase in the framework Si/Al ratio of ion-exchanged zeolites^[16,32]. Iwamoto *et al.* suggested that pressure swing adsorption measurements indicate that this phenomenon is related to the adsorbability of NO because the NO adsorbable amount per Cu

ion increases with the framework Si/Al ratio, regardless of the zeolite structure^[55]. Wichterlova *et al.* suggested that this phenomenon is related to the increase in Cu ion balanced by one framework Al based on the photoluminescence measurements^[32]. However, there has been no report on the description of activity difference for NO direct decomposition among several Cu-zeolites, to the best of the author's knowledge. To investigate the key feature of zeolites related to active site formation, NO probe IR measurements were employed. The active site for NO direct decomposition over Cu-zeolites is suggested to be the Cu⁺ generated by the reduction of Cu²⁺.^[15] Reduction of Cu²⁺ to Cu⁺ at the ion-exchange sites on zeolites occurs through the high-temperature pretreatment in the inert gas feed or high-vacuum (auto-reduction).^[15,22] It would be possible to estimate the Cu²⁺/Cu⁺ ratio based on NO probe IR measurements because NO is adsorbable on both Cu²⁺ and Cu⁺.^[56] Moreover, it is possible to estimate the ratio among several different Cu²⁺ sites and be compared among several Cu-zeolites with different Si/Al ratio^[14,15].

Figure 5.4 shows the IR spectra of NO adsorbed on selected Cu-zeolites (Z4, Z9, B12, M9 samples). Assignments of the peaks are shown in Table 5.1.^[21,25,57-59] As the main NO adspecies, the bands at 1900, 1827, 1813, and 1734 cm⁻¹ were observed. They are assigned to Cu²⁺-NO, the symmetric mode of Cu⁺-(NO)₂, Cu⁺-NO, and the asymmetric mode of Cu⁺-(NO)₂, respectively. The band at 1900 cm⁻¹, assigned to Cu²⁺-NO, was observed as the overlapping of two bands at 1912 cm⁻¹ and 1895 cm⁻¹, which was more significant on the B12 sample than on other samples. They are assigned by Wichterlova *et al.* to NO adsorbed onto Cu²⁺, balanced by two framework Al of zeolite, and that by one framework Al of zeolite, respectively^[25]. Over all samples, no clear peak shift of IR band was observed on any framework structure. This result suggests that the framework structure effect on the electron transfer between exchanged Cu ion on the zeolites and adsorbed NO is not large. However, the ratio of the each peak area to the sums is different. The peak area ratio were calculated by deconvolution of the IR spectra, and the ratio of each NO adspecies were estimated.

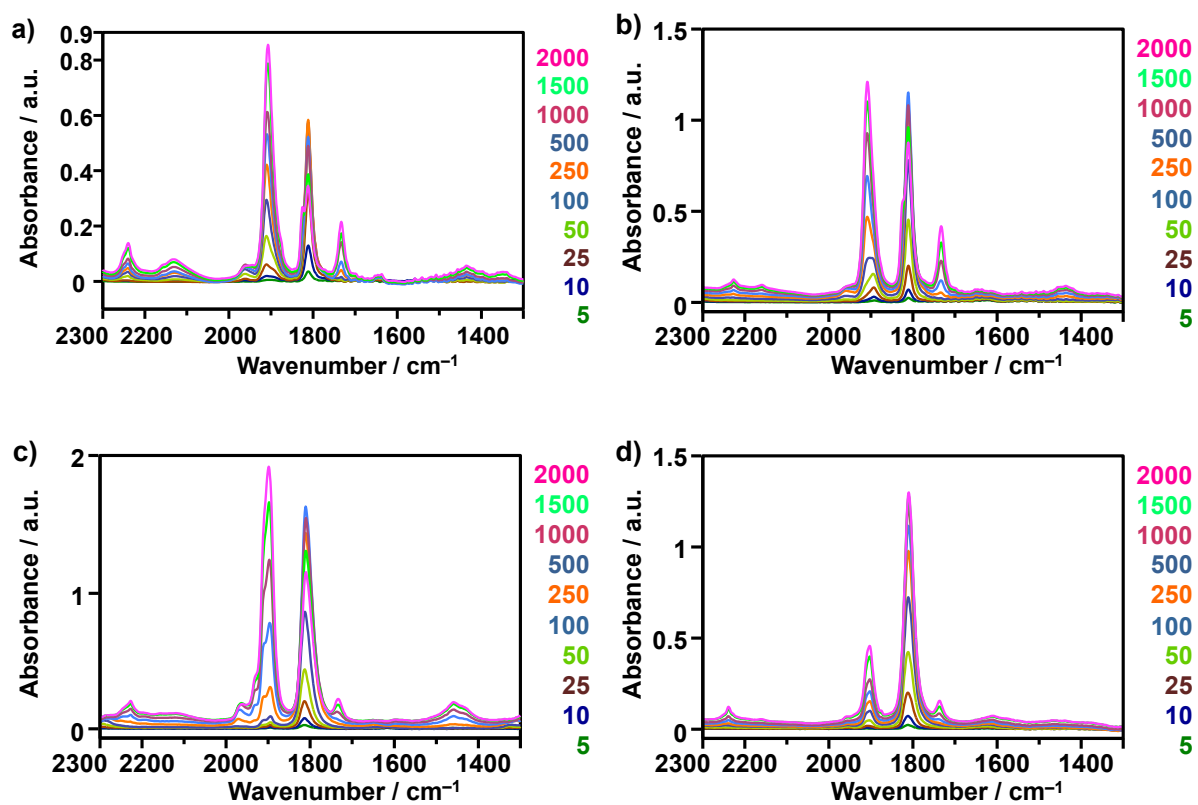


Figure 5.4. NO adsorbed FT-IR spectra of a) Z4, b) Z9, c) B12, and d) M9 sample with introduction pressure from 5 to 2000 Pa.

Table 5.1. Assignments of the peaks observed on IR spectra of NO_x species absorbed on Cu-Zeolites.

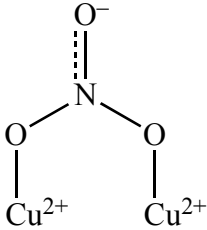
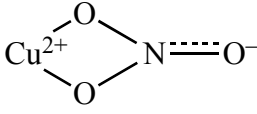
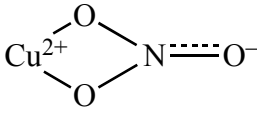
Wavenumber / cm ⁻¹	Assignment	Ref.
2128	Cu ⁺ -NO ⁺	33a
1912	(AlO ₄) ₂ ²⁻ -Cu ²⁺ -NO	13e
1895	(AlO ₄) ⁻ -Cu ²⁺ -NO	13e
1827	Cu ⁺ -(NO) ₂ (syn)	13a
1813	Cu ⁺ -NO	13a
1734	Cu ⁺ -(NO) ₂ (asyn)	13a
1630	Cu ²⁺ -NO ₂	33b
1621		33c
1598	Cu ²⁺ -NO ₂	33b
1571		33c
1517		33c
1300	NO ₃ ⁻	-

Figure 5.5 shows the changes of peak area ratio along with the NO pressure. Each peak area ratio of each peak was calculated by the following equation:

Peak Area Ratio($x \text{ cm}^{-1}$)

$$= \frac{A(x \text{ cm}^{-1})}{A(1900 \text{ cm}^{-1}) + A(1813 \text{ cm}^{-1}) + A(1827 \text{ cm}^{-1}) + A(1734 \text{ cm}^{-1})} \times 100$$

IR band at 1900, 1813, and 1734 cm⁻¹ were chosen as representatives of Cu²⁺-NO, Cu⁺-NO, and Cu⁺-(NO)₂ adspecies, respectively. In the deconvolution of the IR spectra, the bands at 1813 and 1827 cm⁻¹ were difficult to separate in some spectra because of too low intensity of

the band at 1827 cm^{-1} . As shown in Figure 5.5, the increase in the ratio of the band at 1900 cm^{-1} and the band at 1734 cm^{-1} , and a decrease in the band at 1813 cm^{-1} was observed along with the increase in NO adsorption pressure. The observed transition of the band area transition with NO adsorption pressure was characteristic for each sample. For the MOR sample (M9 : filled green triangle marker), over the entire NO adsorption pressure region, the band at 1813 cm^{-1} , assigned to $\text{Cu}^+\text{-NO}$, was observed as the main signal. The increase in the band at 1900 cm^{-1} , which is assigned to $\text{Cu}^{2+}\text{-NO}$, with increase in NO adsorption pressure was small. Especially at $P_{\text{NO}} = 2000\text{ Pa}$, the peak area ratio of the band at 1900 cm^{-1} was smaller than that of any other samples. This result suggests that, on the MOR zeolite used in this research, the Cu ion at the position accessible to the adsorbents is easily reducible to Cu^+ . For the *BEA sample (B12 : filled red square marker), in the low NO adsorption pressure region (below $\sim 500\text{ Pa}$), the $\text{Cu}^+\text{-NO}$ adspecies is observed as the main signal. The occupancy of the signal on the B12 sample is similar to that for the M9 sample in this region. On the other hand, in the high NO adsorption pressure region (above $\sim 500\text{ Pa}$), a significant increase in the $\text{Cu}^{2+}\text{-NO}$ adspecies was observed. This result suggests two possibilities. The first one is that, on the *BEA zeolite used in this research, the Cu ion at the sites easily accessible to the adsorbent is easily reducible to Cu^+ , while those at the other sites are not as reducible. The other one is that Cu^+ on the *BEA zeolite used in this research is easily oxidized to Cu^{2+} in an NO atmosphere. In either case, because P_{NO} was about 2000 Pa in the reaction condition for the catalytic tests, therefore, the $\text{Cu}^+/\text{Cu}^{2+}$ ratio of B12 in the reaction condition would be smaller than that of M9. This would affect the small efficiency of active site formation on the *BEA zeolite. Finally, for the MFI samples (Z9 and Z4 : filled blue circle marker and hollow blue marker, respectively), the ratio of the band at 1900 cm^{-1} , assigned to $\text{Cu}^{2+}\text{-NO}$, was larger than that for M9 and B12 over almost the entire NO adsorption pressure region. This means that, among the Cu ions accessible for the adsorbents, the ratio of Cu^{2+} not easily reducible to Cu^+ is larger on the MFI zeolites than those on MOR and *BEA zeolites. However, as is shown in Figure 5.5c, the formation of $\text{Cu}^+\text{-(NO)}_2$ adspecies was more significant on the MFI zeolites than on the MOR and *BEA zeolites. Above results and discussions suggest that the ratio of Cu^+ formed by auto-reduction to total exchanged Cu ion was larger on MOR zeolite than on MFI and *BEA zeolites. However, the Cu^+ on MFI zeolite is more favourable to accommodate the dinitrosyl adspecies than that on MOR and *BEA zeolites. It can be assumed that adsorption site with a low coordination atom density is favourable to accommodate the dinitrosyl adspecies. Therefore, the key factor in the

greater effectiveness of the active site formation on MFI and MOR zeolites than on *BEA zeolite is the ratio to the total exchanged Cu ions and coordination environment of the Cu^+ ion on the zeolites, formed by the ion-exchange and following high temperature pretreatment in an inert atmosphere, respectively.

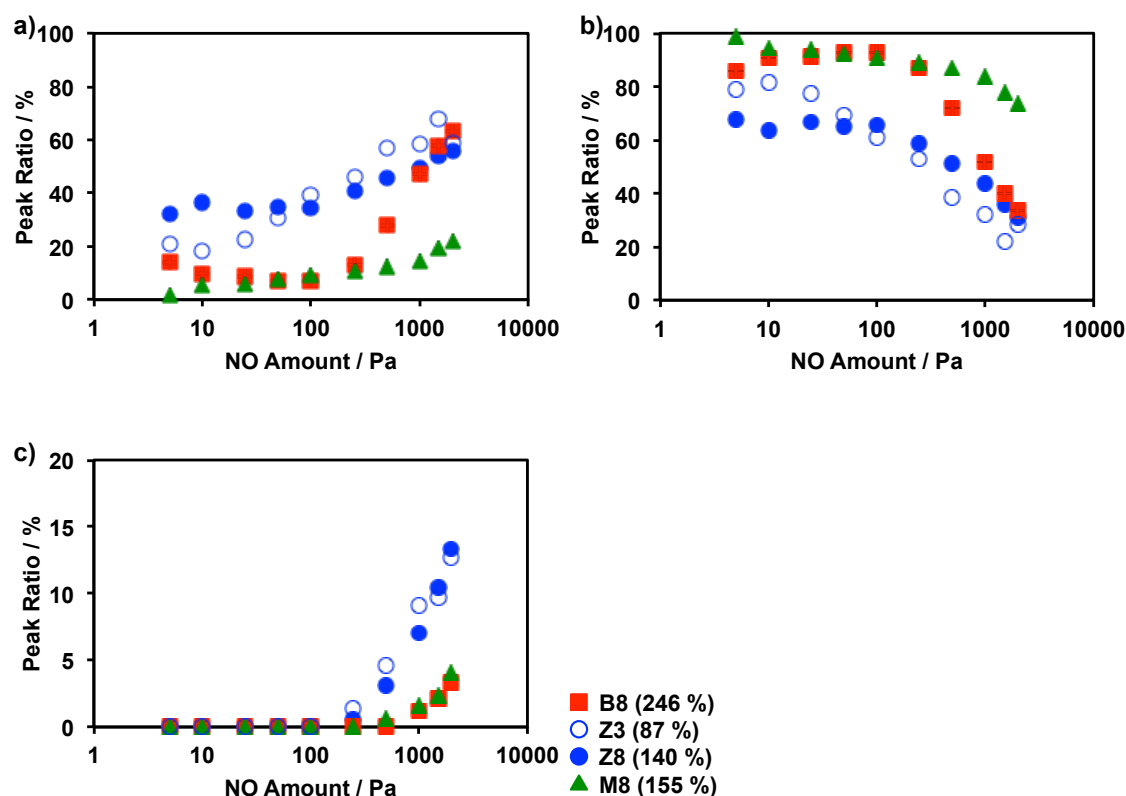


Figure 5.5. The peak area ratio of the band observed at a) 1900 cm^{-1} ($= \text{Cu}^{2+}\text{-NO}$), b) 1813 cm^{-1} ($= \text{Cu}^+\text{-NO}$), c) 1734 cm^{-1} ($= \text{Cu}^+\text{-(NO)}_2$, asymmetric) of the on the spectra.

5.3.3. Origin of framework effects on active site formation

It can be assumed that the coordination environment surrounding the exchanged ion on zeolites is affected by the local structure of the ion-exchange sites on zeolite frameworks, as determined by the structure of the zeolite frameworks. It is known that MFI, MOR, and *BEA zeolite have three types of multivalent ion-exchange sites called α , β , and γ (Figure 5.6)^[49,50]. Although these sites are in different framework structures, their local structure is similar to each other. However, their distribution in the zeolite channel system differs, depending on the zeolite framework structure. In MFI zeolite, all ion-exchange sites are on the surface of the 10 MR micropore channels. MFI zeolite has a straight channel, a sinusoidal

channel, and the intersection of these channels. The α site is on the straight channel, the β site is on the intersection, and the γ site faces both the straight channel and sinusoidal channel (Figure 5.6a and 5.6b). MOR zeolite has parallel 12 MR straight channel and deformed 8 MR straight channel. It also has 8 MR channel, interconnecting the former two channels. The α site is on the 12 MR channel, the β site is on the intersection of the two 8 MR channels, and the γ site is on the 8 MR channel interconnecting the 12 MR straight channel and deformed 8 MR straight channel (Figure 5.6c). *BEA zeolite has the crossing straight 12 MR channels along the x axis and y axis. On the *BEA zeolite, only the β site faces the 12 MR, and other sites are inside the walls where reactants are difficult to diffuse into (Figure 5.6d). Thus, it is assumed that only Cu ions exchanged on the β site could function as active sites for catalytic reaction. The location of multivalent ion-exchange sites is summarized in Table 5.2. It is assumed that the difference in the coordination environment of the Cu ion would be affected by the distribution of the multivalent ion-exchange sites in the zeolite frameworks.

Based on the density functional theory (DFT) calculations, Nachtigall *et al.* reported that in MFI zeolites with Al at the channel intersection, Cu^+ could coordinate only with the oxygen atoms of the AlO_4 tetrahedron^[60]. Their discussion primarily focused on the assignments of reported photoluminescence spectra of Cu^+ on Cu-MFI zeolites. Considering the comparative NO probe IR measurements presented in this chapter, the ion-exchange sites of MFI zeolites would be more favourable for formation of such Cu^+ in a highly open coordination environment than other zeolites.

In summary, the results presented in this chapter on the N_2 formation activity in NO direct decomposition by pulse reactor, together with previous studies, suggest that the well-known high catalytic activity of Cu-MFI, compared with other Cu-zeolites, for NO direct decomposition is originated by the open coordination environment of the exchanged Cu ion, and is affected by the distribution of ion-exchange sites in the zeolite frameworks.

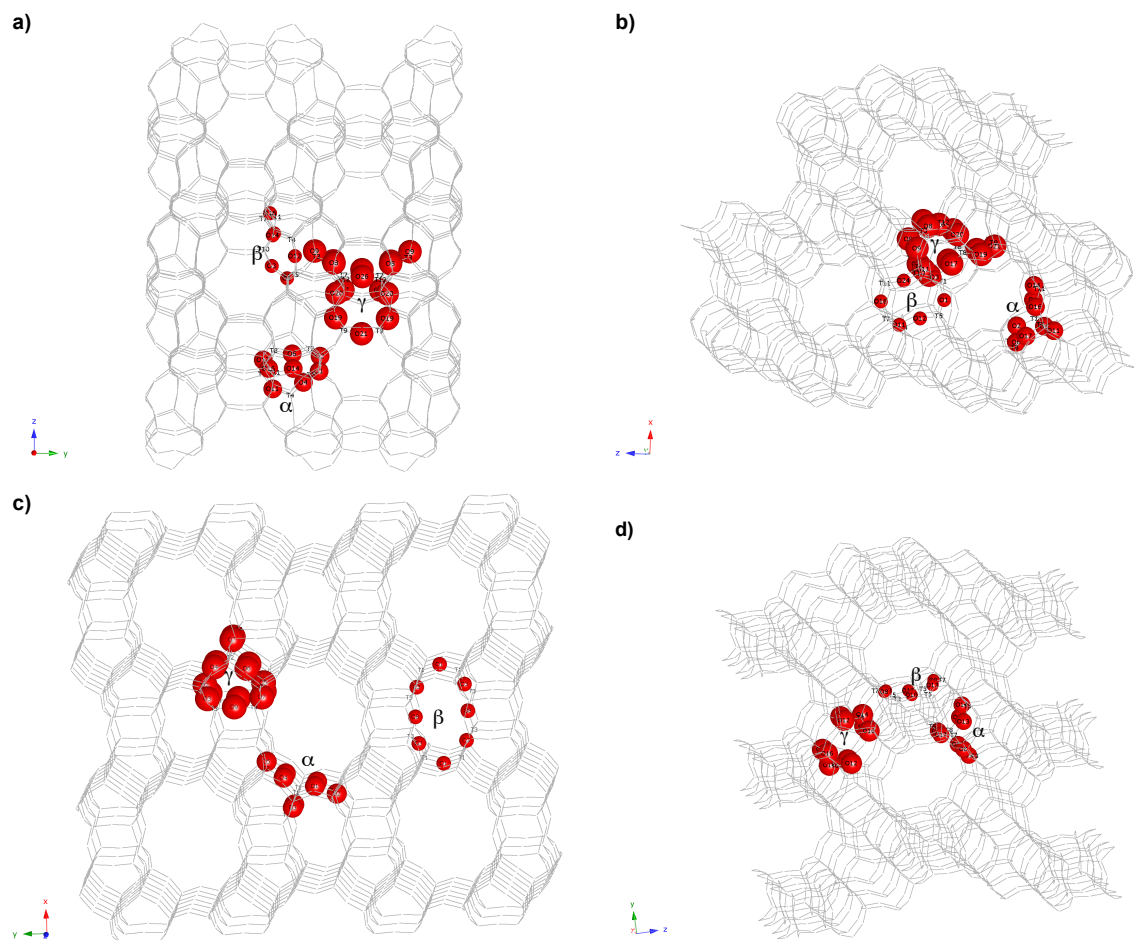


Figure 5.6. Multivalent ion exchange sites on micropore of a) MFI from x axis view (along the sinusoidal channel), b) MFI from y axis view (along the straight channel), c) MOR from z axis view, and d) *BEA zeolite from y axis view. The red spheres are framework oxygen atoms belonging to the ion-exchange sites.

Table 5.2. Facing channel of the multivalent ion-exchange site in the channel system of zeolite topologies.

Topology	α	β	γ
MFI	Straight 10 MR	Intersection (10 MR \times 10 MR)	Both Straight and Sinusoidal 10 MR
MOR	12 MR	Intersection (8 MR \times 8 MR)	8 MR
*BEA	12 MR	6 MR	6 MR

5.4. Conclusions

In this chapter, it was shown by the NO direct decomposition at 773 K that not only Cu-MFI zeolites, but also Cu-*BEA and Cu-MOR zeolites exhibited high N₂ formation activity at the initial stage of reaction. The N₂ formation activity on Cu-*BEA was comparable to those on Cu-MFI and Cu-MOR zeolites. Moreover, for all zeolites, the N₂ formation activity in the NO direct decomposition increased along with increase in the Cu ion-exchange level, and fitted an S-shaped curve, similar to the previously reported one for Cu-MFI. However, the ion-exchange level where the sharp N₂ formation activity increased was different for each zeolite. The observed ion-exchange level of Cu-zeolites where the sharp N₂ formation activity increase was in the following order: MOR \approx MFI < *BEA. The sharp increase in N₂ formation activity at small ion-exchange levels means that the active site effectively forms on the zeolite. Therefore, the active site would form more efficiently on MFI and MOR zeolites than on *BEA zeolite. The results of NO probe IR measurements revealed that the Cu⁺ formation ratio to the exchanged Cu ion on Cu-MOR is superior to those on other Cu-zeolites, however, Cu⁺ formed on Cu-MFI is more suitable to accommodate dinitrosyl adspecies than those on Cu-*BEA and Cu-MOR, despite the similar local structures of the ion-exchange sites. The result described above suggests that there is a large amount of Cu²⁺ not easily reducible to Cu⁺ on Cu-MFI, while Cu⁺ formed on Cu-MFI are in a more open coordination environment than on other zeolites, leading to the high efficiency of active site formation. The interpretation of these results by being combined with the discussion in previous reports suggest that the difference in the oxidation state distribution (Cu⁺/Cu²⁺ ratio) and coordination environment can be affected by the distribution of the ion-exchange sites in the zeolite frameworks. The results presented in this chapter including both the activity tests for the NO direct decomposition by a pulse reactor and spectroscopic study on the Cu species of several Cu-zeolites, which is thought to be evaluating the character of Cu species in similar conditions, highlighting new insights into the origin of the well-known higher catalytic activity of Cu-MFI for the NO direct decomposition than those of other Cu-zeolites. This knowledge should help the modification of Cu-zeolite catalysts for the NO direct decomposition.

References

- [1] M. H. Groothaert, P. J. Smeets, B. F. Sels, P. A. Jacobs, R. A. Schoonheydt, *J. Am. Chem. Soc.* **2005**, *127*, 1394.
- [2] T. Seiyama, T. Arakawa, T. Matsuda, Y. Takita, N. Yamazoe, *J. Catal.* **1977**, *48*, 1.
- [3] T. Komatsu, M. Nunokawa, I. S. Moon, T. Takahara, S. Nanba, T. Yashima, *J. Catal.* **1994**, *148*, 427.
- [4] M. Iwamoto, S. Yokoo, K. Sakai, S. Kagawa, *J. Chem. Soc., Faraday. Trans. 1* **1981**, *77*, 1629.
- [5] J. H. Kwak, R. G. Tonkyn, D. H. Kim, J. Szanyi, C. H. F. Peden, *J. Catal.* **2010**, *275*, 187.
- [6] M. J. Wulfers, S. Teketel, B. Ipek, R. F. Lobo, *Chem. Commun.* **2015**, *51*, 4447.
- [7] A. M. Beale, F. Gao, I. Lezcano-Gonzalez, C. H. F. Peden, J. Szanyi, *Chem. Soc. Rev.* **2015**, *44*, 7371.
- [8] F. Gao, C. H. F. Peden, *Catalysts* **2018**, *8*, 140.
- [9] E. Borfecchia, P. Beato, S. Svelle, U. Olsbye, C. Lamberti, S. Bordiga, *Chem. Soc. Rev.* **2018**, *47*, 8097.
- [10] D. K. Pappas, E. Borfecchia, M. Dyballa, I. A. Pankin, K. A. Lomachenko, A. Martini, M. Signorile, S. Teketel, B. Arstad, G. Berlier, C. Lamberti, S. Bordiga, U. Olsbye, K. P. Lillerud, S. Svelle, P. Beato, *J. Am. Chem. Soc.* **2017**, *139*, 14961.
- [11] D. K. Pappas, A. Martini, M. Dyballa, K. Kvande, S. Teketel, K. A. Lomachenko, R. Baran, P. Glatzel, B. Arstad, G. Berlier, C. Lamberti, S. Bordiga, U. Olsbye, S. Svelle, P. Beato, E. Borfecchia, *J. Am. Chem. Soc.* **2018**, *140*, 15270.
- [12] M. Haneda, H. Hamada, *C. R. Chimie* **2016**, *19*, 1254.
- [13] Q. Sun, Z. Wang, D. Wang, Z. Hong, M. Zhou, X. Li, *Catal. Sci. Technol.* **2018**, *8*, 4563.
- [14] M. Iwamoto, H. Furukawa, Y. Mine, F. Uemura, S. Mikuriya, S. Kagawa, *J. Chem. Soc., Chem. Commun.* **1986**, 1272.
- [15] M. Iwamoto, H. Yahiro, K. Tanda, N. Mizuno, Y. Mine, S. Kagawa, *J. Phys. Chem.* **1991**, *95*, 3727.
- [16] M. Iwamoto, H. Furukawa, S. Kagawa, *Stud. Surf. Sci. Catal.* **1986**, *28*, 943.
- [17] Y. L. John, N. Armor, *Appl. Catal.*, 1991, *76*, L1.
- [18] Z. Wang, A. V. Sklyarov, G. W. Keulks, *Catal. Today* **1997**, *33*, 291.
- [19] Y. Teraoka, C. Tai, H. Ogawa, H. Furukawa, S. Kagawa, *Appl. Catal. A* **2000**, *200*, 167.
- [20] P. D. Costa, B. Moden, G. D. Meitzner, D. K. Leeza, E. Iglesia, *Phys. Chem. Chem. Phys.* **2002**, *4*, 4590.

- [21] M. Iwamoto, H. Yahiro, N. Mizuno, W.-X. Zhang, Y. Mine, H. Furukawa, S. Kagawa, *J. Phys. Chem.* **1992**, *96*, 9360.
- [22] E. Giamello, D. Murphy, G. Magnacca, C. Morterra, Y. Shioya, T. Nomura, M. Anpo, *J. Catal.* **1992**, *136*, 510.
- [23] J. Valyon, W. K. Hall, *J. Phys. Chem.* **1993**, *97*, 1204.
- [24] M. Anpo, Y. Shioya, H. Yamashita, E. Giamello, C. Morterra, M. Che, H. H. Patterson, S. Webber, S. Ouellette, M. A. Fox, *J. Phys. Chem.* **1994**, *98*, 5744.
- [25] J. Dědeček, Z. Sobalík, Z. Tvarůžková, D. Kaucký, B. Wichterlová, *J. Phys. Chem.* **1995**, *99*, 16327.
- [26] H. Yamashita, M. Matsuoka, K. Tsuji, Y. Shioya, M. Anpo, M. Che, *J. Phys. Chem.* **1996**, *100*, 397.
- [27] C. Lamberti, S. Bordiga, M. Salvalaggio, G. Spoto, A. Zecchina, F. Geobaldo, G. Vlaic, M. Bellatreccia, *J. Phys. Chem. B* **1997**, *101*, 344.
- [28] B. Wichterlová, J. Dědeček, Z. Sobalík, A. Vondrová, K. Klier, *J. Catal.* **1997**, *169*, 194.
- [29] B. Wichterlová, Z. Sobalík, J. Dědeček, *Catal. Today* **1997**, *38*, 199.
- [30] G. T. Palomino, P. Fisticaro, S. Bordiga, A. Zecchina, E. Giamello, C. Lamberti, *J. Phys. Chem. B* **2000**, *104*, 4064.
- [31] J. Dědeček, B. Wichterlová, *J. Phys. Chem.* **1994**, *98*, 5721.
- [32] B. Wichterlová, J. Dědeček, A. Vondrová, *J. Phys. Chem.* **1995**, *99*, 1065.
- [33] J. Dědeček, B. Wichterlová, *J. Phys. Chem. B* **1997**, *101*, 10233.
- [34] J. Dědeček, B. Wichterlová, *Phys. Chem. Chem. Phys.* **1999**, *1*, 629.
- [35] M. H. Groothaert, J. A. Bokhoven, A. A. Battiston, B. M. Weckhuysen, R. A. Schoonheydt, *J. Am. Chem. Soc.* **2003**, *125*, 7629.
- [36] S. C. Larsen, A. Aylor, A. T. Bell, J. A. Reimer, *J. Phys. Chem.* **1994**, *98*, 11533.
- [37] H. Hamada, N. Matsubayashi, H. Shimada, Y. Kintaichi, T. Ito, A. Nishijima, *Catal. Lett.* **1990**, *5*, 189.
- [38] D.-J. Liu, H. J. Robota, *Catal. Lett.* **1993**, *21*, 291.
- [39] Y. Li, W. K. Hall, *J. Catal.* **1991**, *129*, 202.
- [40] J. Dědeček, O. Bortnovsky, A. Vondrová, B. Wichterlová, *J. Catal.* **2001**, *200*, 160.
- [41] M. Y. Kustova, A. Kustov, S. E. Christiansen, K. T. Leth, S. B. Rasmussen, C. H. Christensen, *Catal. Commun.* **2006**, *7*, 705.
- [42] M. Y. Kustova, S. B. Rasmussen, A. L. Kustov, C. H. Christensen, *Appl. Catal. B* **2006**, *67*, 60.

- [43] Moliner, M. Franch, C. Palomares, E. Grillb, M. Corma, A. *Chem. Commun.* **2012**, *48*, 8264.
- [44] N. Martín, C. R. Boruntea, M. Moliner, A. Corma, *Chem. Commun.* **2015**, *51*, 11030.
- [45] D. Jo, T. Ryu, G. T. Park, P. S. Kim, C. H. Kim, I.-S. Nam, S. B. Hong, *ACS Catal.* **2016**, *6*, 2443.
- [46] J. Kim, S. J. Cho, D. H. Kim, *ACS Catal.* **2017**, *7*, 6070.
- [47] S. V. Priya, T. Ohnishi, Y. Shimada, Y. Kubota, T. Masuda, Y. Nakasaka, M. Matsukata, K. Itabashi, T. Okubo, T. Sano, N. Tsunoji, T. Yokoi, M. Ogura, *Bull. Chem. Soc. Jpn.* **2018**, *91*, 355.
- [48] B. Wichterlová, Z. Sobalík, J. Dědeček, *Appl. Catal. B* **2003**, *41*, 97.
- [49] P. Sazama, E. Tabor, P. Klein, B. Wichterlova, S. Sklenak, L. Mokrzycki, V. Pashkkova, M. Ogura, J. Dedecek, *J. Catal.* **2016**, *333*, 102.
- [50] P. K. Sajith, Y. Shiota, K. Yoshizawa, *ACS Catal.* **2014**, *4*, 2075.
- [51] M. Iwamoto, K. Maruyama, N. Yamazoe, T. Seiyama, *J. Phys. Chem.* **1977**, *81*, 622.
- [52] P. Vanelderen, B. E. R. Snyder, M.-L. Tsai, R. G. Hadt, J. Vancauwenbergh, O. Coussens, R. A. Schoonheydt, B. F. Sels, E. I. Solomon, *J. Am. Chem. Soc.* **2015**, *137*, 6383.
- [53] B. Ipek, M. J. Wulfers, H. Kim, F. Göttl, I. Hermans, J. P. Smith, K. S. Booksh, C. M. Brown, R. F. Lobo, *ACS Catal.* **2017**, *7*, 4291.
- [54] Y. Li, W. K. Hall, *J. Phys. Chem.* **1990**, *94*, 6145.
- [55] W.-X. Zhang, H. Yahiro, N. Mizuno, J. Izumi, M. Iwamoto, *Langmuir* **1993**, *9*, 2337.
- [56] F. Giordanino, P. N. R. Vennestrøm, L. F. Lundegaard, F. N. Stappen, S. Mossin, P. Beato, S. Bordiga, C. Lamberti, *Dalton. Trans.* **2013**, *42*, 12741.
- [57] M. Tortorelli, K. Chakarova, L. Lisi, K. Hadjiivanov, *J. Catal.* **2014**, *309*, 376.
- [58] T. Cheung, S. K. Bhargava, M. Hobday, K. Foger, *J. Catal.* **1996**, *158*, 301.
- [59] A. J. S. Mascarenhas, H. O. Pastore, *Langmuir* **2002**, *18*, 6875.
- [60] P. Nachtigall, D. Nachtigallova, J. Sauer, *J. Phys. Chem. B* **2000**, *104*, 1738.

Chapter 6

General conclusions and future perspectives

6.1. General Conclusions

In Chapter 2, toward the comparative study among the Cu-zeolites with several topologies, a descriptor for zeolites “cation density in micropores” was determined. The representative zeolite on each topology was selected with considering this parameter. The selected zeolites were subjected to the sodium to copper ion-exchange with the same procedure except for the concentration of Cu salt to achieve the stoichiometry controlled Cu ion-exchange until the excessive region. As a result, relatively well stoichiometry controlled sodium to copper ion-exchange was successfully achieved over all representative zeolites with similar “cation density in micropores”. Moreover, not only MFI zeolite, but also MOR and *BEA zeolites, could be successfully ion-exchanged until the excessive region, which are thought to be particularly suitable for NO direct decomposition.

In Chapter 3, the catalytic activities of Cu-zeolites with different topologies for NH₃-SCR at 473 K were investigated. As a result, it was revealed that the behavior of reaction rate for NH₃-SCR at 473 K along with the mean volumetric density of Cu ion in micropores was largely affected by the zeolites. The *in situ* UV-Vis measurement during the reaction gas mixtures suggested that the Cu²⁺ have interaction to O_Z ligands even under NH₃ flow at 473 K. The author proposed a calculation methodology to evaluate the rate for reduction-oxidation cycle based on time-resolved UV-Vis measurement and it was revealed that calculated rate for Cu⁺ → Cu²⁺ oxidation by O₂ flow have a good agreement with the rate for NH₃-SCR regardless of Cu density and zeolite topologies. This result strongly suggested that the observed phenomenon on reaction rate for NH₃-SCR at 473 K was mainly dominated by the oxidation steps. Considering these facts, a role of the local structure and distribution of ion-exchange sites for multivalent cation on the surface of zeolite micropores in the formation of Cu²⁺ during the reaction was suggested.

In Chapter 4, the dependence of NH₃-SCR rates on the O₂ pressure at 473 K was investigated. It was revealed that the dependence of rates on O₂ pressure was similar to the dependence on Cu density in micropores over the zeolites with same topology. Among the zeolites investigated here, the Cu-*BEA zeolite catalysts exhibited higher reaction rates regardless of the Cu density in micropores or Cu loading than a Cu-SSZ-13 reference catalyst whose composition is similar to the state-of-the-art commercial catalyst. In summary, a promising possibility was shown that the Cu-*BEA zeolite, which were revealed to exhibit high reaction rate even when the low Cu density in micropores in the Chapter 3, would work as effective catalyst even under low O₂ pressure reaction condition.

The results obtained by both chapters provide a three-dimensional behavior of reaction rate for NH₃-SCR at 473 K affected by oxidation half-cycle, which is thought to proceed among the several Cu cation and an O₂ molecular over zeolites with several topologies (Figure 6.1).

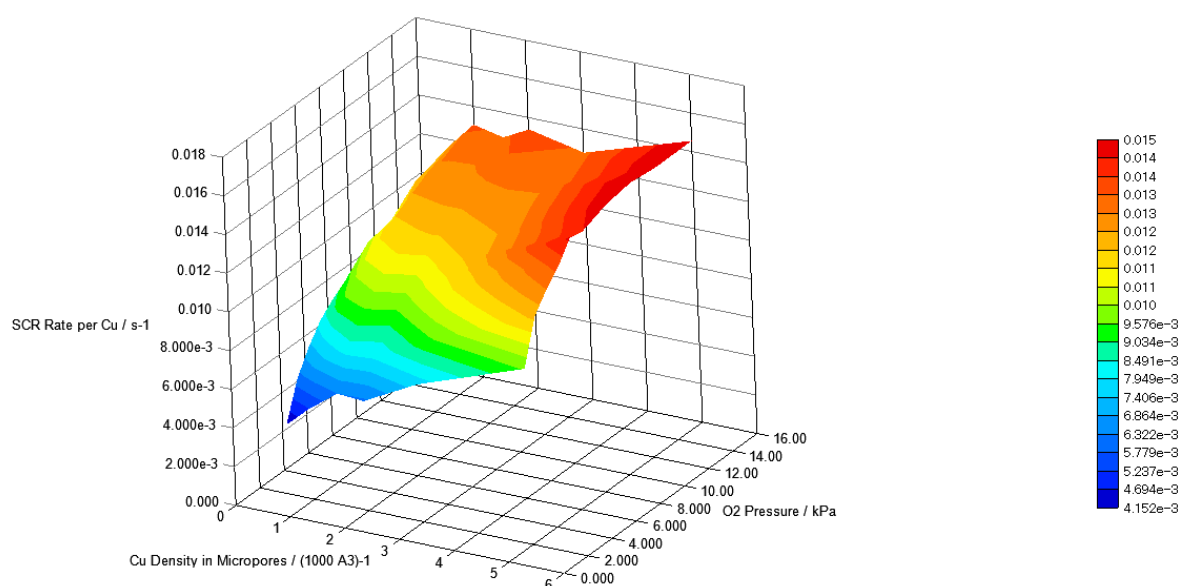


Figure 6.1. Graphical summary of the highlighted results for *BEA zeolite in Chapters 3 and 4.

In Chapter 5, NO direct decomposition at 773 K by using a pulse reactor over the Cu-zeolites was conducted. It was revealed that the efficiency for Cu species with N₂ formation activity follow the following order: MOR ≈ MFI > *BEA. This order was reverse to that for NH₃-SCR shown in chapter 3. NO probe IR measurement revealed that the population of Cu⁺ itself, and Cu⁺ in highly open coordination environment that is favorable for the formation of Cu⁺-(NO)₂ adspecies, are largely affected by the zeolite topologies. Considering the character of Cu species observed in both measurements, it was suggested that the formation efficiency for Cu species with N₂ formation activity have some relationship to both the Cu⁺/Cu²⁺ ratio and the coordination environments of Cu⁺. It was suggested that the description for the results can be obtained by the local structure and distribution of ion-exchange sites for multivalent cation on the surface of zeolite micropores.

The highlighted results in chapters 3 and 5 are summarized in Figure 6.2.

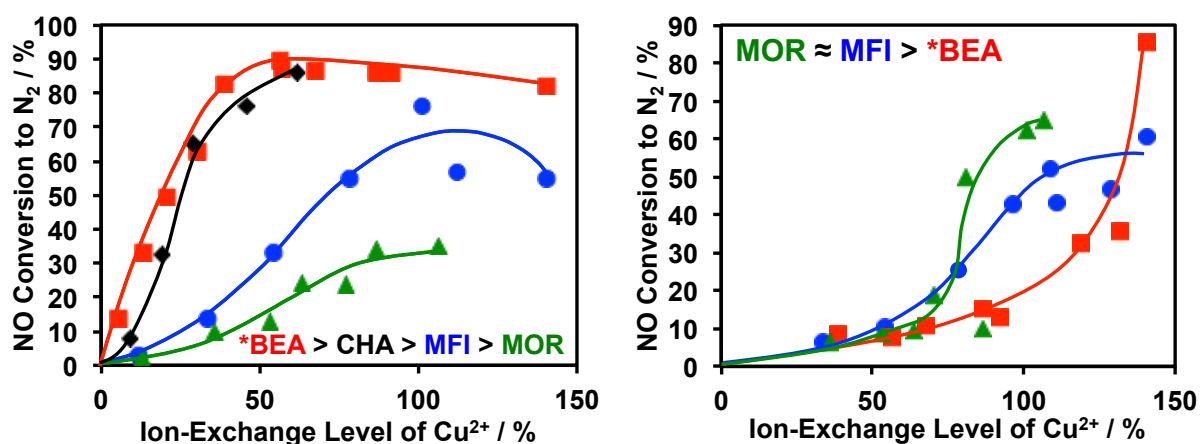
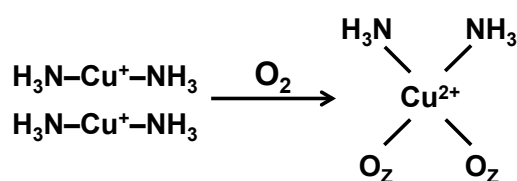


Figure 6.2. Graphical summary of the highlighted results in chapter 3 and 5.

By using the spectroscopic study on the structure and distribution of Cu species on each zeolite that forms by pretreatments similar to those prior to the reactions, it was suggested that the Cu species related to the high activity for each reaction and their role in the reactions were as shown in Figure 6.3.

NH₃-SCR

Square-planar Cu²⁺-O₂



NO direct decomposition

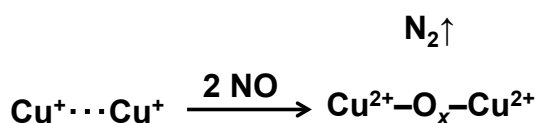
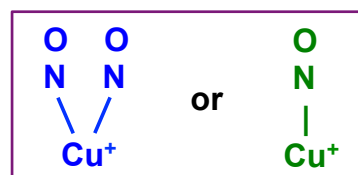


Figure 6.3. The suggested Cu species on zeolites related to the high activity for each reaction and their role in the reactions.

The structural features of zeolites that can be expected to play some role in the accommodation of the active Cu species described above were considered. It has been suggested that the multivalent cation like Cu is accommodated by ion-exchange sites on which several framework Al atoms can populate and the structures have been classed as

shown in Figure 6.4.

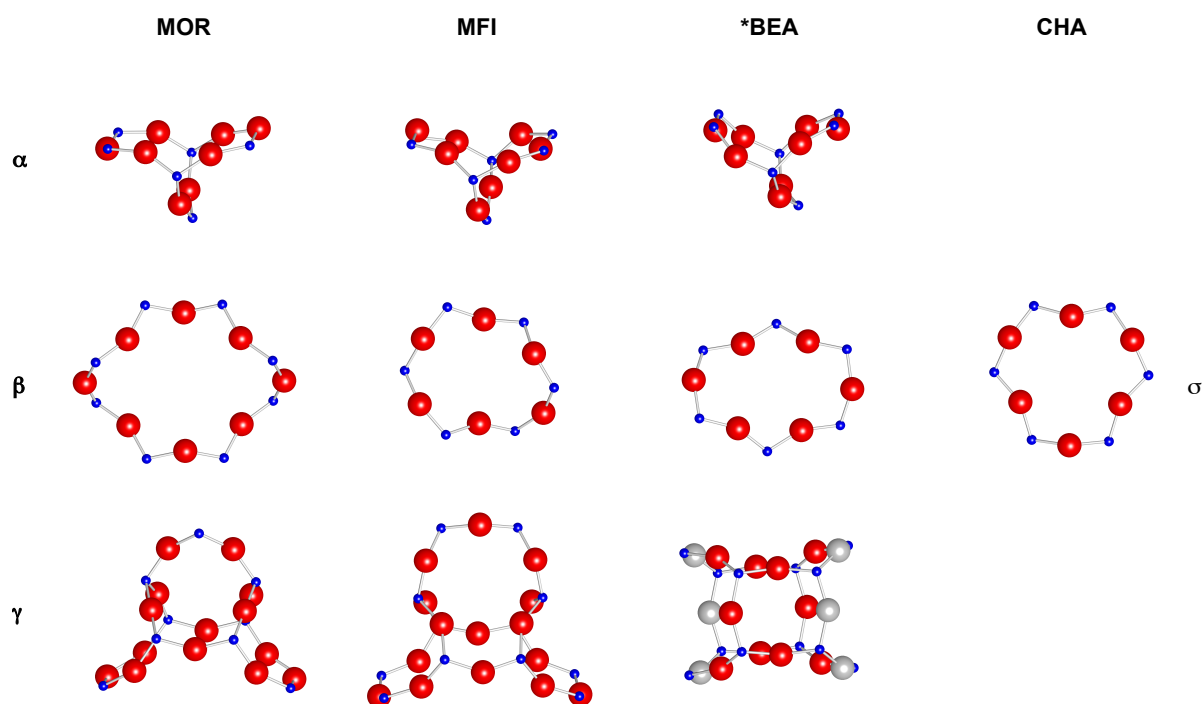


Figure 6.4. The ion-exchange sites for multivalent cation with several framework Al atoms.

By considering the distribution of ion-exchange sites in the main micropores of each zeolites, the structural features of zeolites playing a role in the accommodation of the active Cu species for targeted reactions were suggested as Figure 6.5.

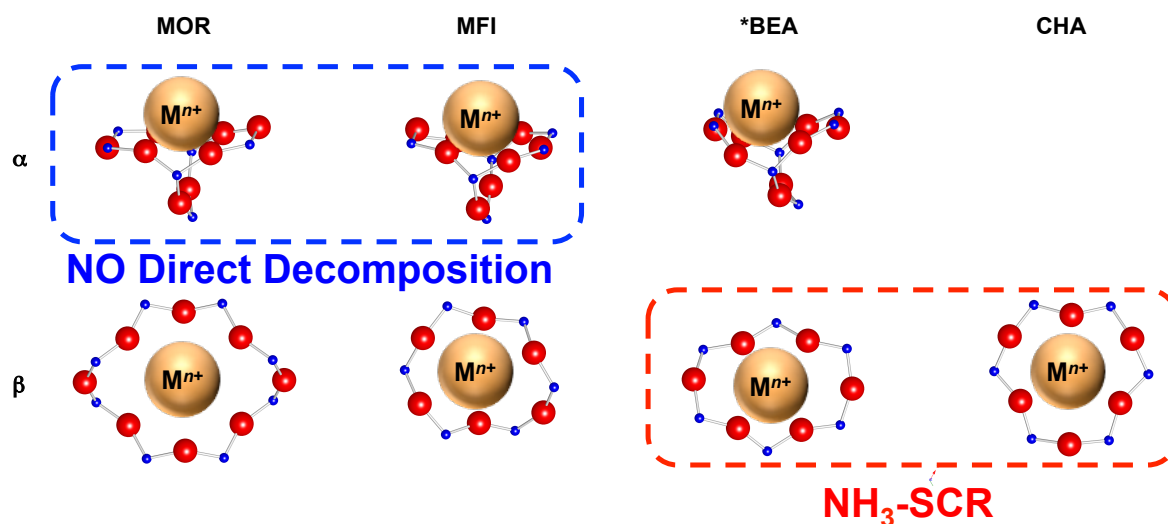


Figure 6.5. Graphical description for the suggested structural feature of zeolites in the accommodation of the active Cu species for targeted reactions.

Both α and β (+ σ on CHA zeolite) sites are constructed by a ring with more than 6 T atoms. However, the α site contains a bridging T atom inside the channel wall but the β (+ σ on CHA zeolite) site doesn't contain. Considering the result of ^{29}Si MAS NMR with minority of $\text{Q}^4(2\text{Al})$ species (presented in Chapter 2), the distribution of Al atoms in these sites can be expected like Figure 6.6.

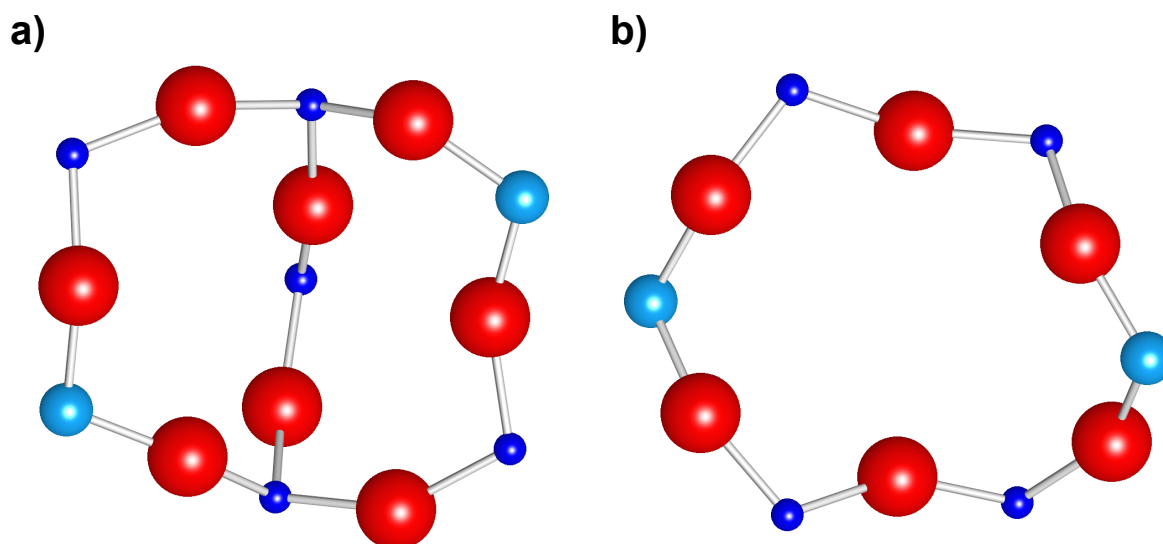
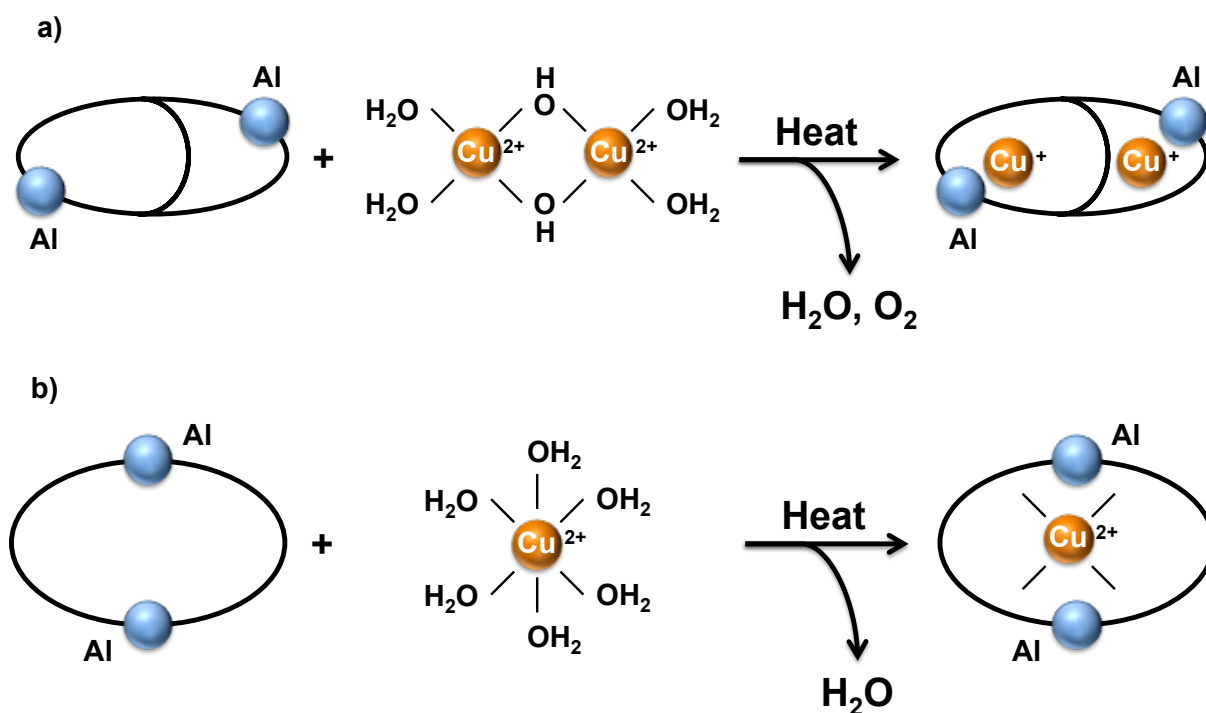


Figure 6.6. Expected Al distribution on a) α and b) β or σ sites on zeolites. Blue, light blue, and red sphere shows the Si, Al, and O atoms, respectively.

The great applicability of zeolites into the $\text{NH}_3\text{-SCR}$ and limited application of zeolites for NO direct decomposition are explained well by suggestion described above, because a variety of zeolites with structural fraction of β or σ sites on the surface of micropore are found in the database (<http://www.iza-structure.org/databases/>), while only a limited type of zeolites with structural fraction of α sites on the surface of micropore are found. Finally, their role in the accommodation of the active Cu species shown in Figure 6.3 can be suggested as Scheme 6.1.



Scheme 6.1. The suggested formation scheme for the Cu active sites shown in Figure 6.3 over a) α and b) β or σ sites on zeolites.

6.2. Future Perspectives

The conception of “cation density in micropores” for zeolites would present not only a rational method to conduct the comparative study among several zeolites with considering the reaction mechanisms, but also a rough expectation of limitation in maximum Al content intrinsic for zeolite topologies.

The methodology for the analysis of redox property of Cu species that was introduced in Chapter 3 would be expanded as a versatile way to understand the redox feature of the active metal species on heterogeneous catalysts during the reactions. The author believes that the addition of the spectroscopies other than UV-Vis or the methods for kinetic

analysis such as inert tracer introduction, high-speed switching and isotopic labeling, would efficiently extract the dynamic information of heterogeneous catalysts (*e.g.*, coordination environments for active metals, intermediates with importance and diffusion of participants) and they would lead to the quantum development in mechanic studies.

The author believes that the results presented in this thesis would work as a compass to the Cu-zeolite catalyst exploration using informatics based on the structural database of experimental and virtual zeolites. Additionally, the author hopes them to be the designed synthesis of zeolites with controlling the pore structure and arrangement of active sites. Through the attempts described above, the catalysts for cleaning air that can truly work regardless of reaction condition would be developed and the improvement in validity of emission would be achieved. Moreover, the control of dynamic properties for base metals including Cu would be achieved by zeolites and it would lead to the replacement of catalytic processes using precious metals.

Appendix

A1. Effect of Zeolite Topology on Reaction Rate for NH₃-SCR at 473 K – MOR and CHA Zeolites with a Similar Si/Al Ratio

Figure A1 shows the reaction rate per Cu for NH₃-SCR at 473 K over the Cu ion-exchanged MOR and CHA zeolites with similar Si/Al ratio plotted as functions of the Cu loading for each zeolite. As shown in the Figure A1, there are obvious differences on the reaction rate per Cu over whole Cu content region and the behavior along with Cu loading. The reaction rates per Cu over MOR zeolites were low compared to the CHA zeolite over whole Cu loading region. Moreover, the reaction rates per Cu over MOR zeolite were irrespectively to the Cu loading while those over CHA zeolites were almost in proportion to the Cu loading.

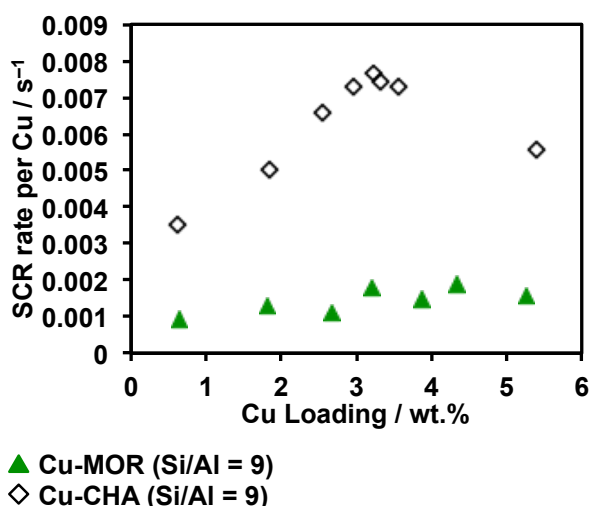


Figure A1. Correlation between the standard NH₃-SCR rate per Cu at 473 K and Cu loading over the MOR (▲) and CHA(◇) zeolites with Si/Al = 9.

Figure A2 shows the NH₃-TPD profiles of the NH₄-formed parent zeolites. The peak observed in higher temperature region is a peak for NH₃ desorption from the acid sites of zeolites. The NH₃ desorption peak in high temperature region means that the adsorbent have strong acidity. Thus, the result shown in Figure A2 means that both CHA and MOR zeolites have stronger acidity than *BEA or MFI zeolites.

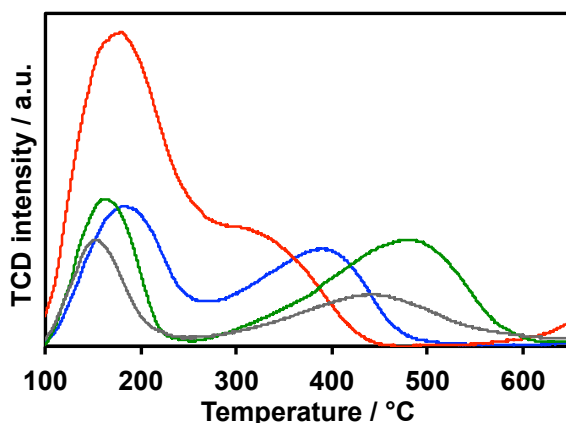


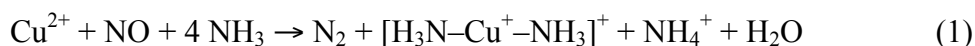
Figure A2. NH₃-TPD profiles of NH₄-formed parent zeolites. Gray, green, blue, and red lines show the profiles of CHA (Si/Al = 9), MOR (Si/Al = 9), MFI (Si/Al = 11.9), and *BEA (Si/Al = 5.6) zeolites, respectively.

The difference in the behavior of reaction rate per Cu along with Cu loading over CHA and MOR zeolites can be explained by mobility of Cu⁺ coordinated by NH₃ ligands, or the amount of Cu ion that can be reducible by NO + NH₃, according to the following mechanism for NH₃-SCR around 473 K. It is suggested that NH₃-SCR over Cu-CHA zeolites proceeds through the redox between Cu⁺ and Cu²⁺. Reduction of Cu²⁺ proceeds by reaction with NO + NH₃ and oxidation of Cu⁺ mainly by O₂. The formed Cu⁺ during NH₃-SCR is thought to be mobile in the zeolite micropore coordinated by NH₃, and the oxidation undergoes through O-bridged dimetric intermediates^[A1-3]. In the case of CHA zeolites, it has been suggested that the average distance among Cu ions decreases and the rate-determining Cu⁺ → Cu²⁺ oxidation step are promoted with the increase of the Cu ion space density^[A2,A3]. The trend of the reaction rate per Cu for the CHA zeolites in this work shows good agreement to the above description.

It has been reported in the comparative study among the CHA, AEI, and RTH zeolites^[A4] that the reaction rate over RTH zeolite is smaller than those over two other zeolites. This phenomenon is explained by the existence of a constrained and asymmetric 8 MR window (0.56 nm × 0.25 nm) in RTH framework and by the limitation of the pore connectivity. A MOR zeolites with 12 MR channel has a constrained and asymmetric 8 MR window (0.57 nm × 0.26 nm)^[A5], and is expected to work as a one-dimensional pore system for NH₃-SCR similar to RTH zeolite with 8 MR main channel. When the discussion is limited on the value of the reaction rate, the low reaction rate per Cu over MOR zeolites compared

with the CHA zeolite observed in this work has good agreement with the above explanation. However, it is reported in the other report^[A6] that turnover frequency (TOF) increases along with Cu content even over RTH zeolite with a low dimension channel system. Therefore, it is difficult to explain the behavior along with Cu loading over MOR zeolite only by one dimension channel system, and other factors are needed that inhibit the increase of reaction rate for NH₃-SCR along with the increase of Cu loading (= Cu ion space density) in MOR zeolite.

The transient response in the feed switch from dried N₂ to 500 ppm NO + 500 ppm NH₃ in dried N₂ at 473 K over 1.8 wt.% Cu loaded Cu-zeolites (36 % ion-exchange level of Cu²⁺) was conducted. In this process, the following stoichiometric reaction is assumed to take place:

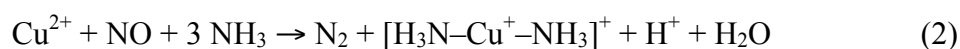


Therefore, the amount of Cu ion contributed to the NH₃-SCR can be estimated from the consumed amount of NO in this process, and the coordination state of Cu⁺, which is thought to be mobile during the NH₃-SCR at 473 K, can be estimated from the consumed amount of NH₃ in this process. In summary, this measurement was conducted to estimate the difference in amount of Cu ion contributed to the NH₃-SCR and the mobility of Cu⁺ on different zeolites. As the background, the profiles of the same transient response over parent sodium-form zeolites were used. Because of the preparation conditions described above, it was confirmed that the Cu-zeolites in this work have a small amount of H⁺ as the counter cation. Moreover, the transient response over parent zeolites at 473 K showed that they have little NH₃ adsorption capacity and almost all of adsorbed NH₃ are reversible. It was confirmed that equilibrated NH₃ concentration of breakthrough curve and the elution curve over the Cu ion-exchanged zeolites were almost the same as those over parent sodium-form zeolite. Therefore, it can be thought that quantification of the amount of consumed NH₃ in the process related to the Cu ion can be estimated by this method.

Table A1. Cu contained amount and consumed amount of reactants in the transient reaction at 473 K.

Entry.	Cu content / mmol/g	NO consumption / mmol/g	NH ₃ consumption / mmol/g	NH ₃ /NO
C902	0.29	0.25	0.56	2.3
M3	0.29	0.30	0.76	2.5

Table A1 shows the amount of Cu contained in the zeolites obtained by ICP-AES measurement, consumed NO, and consumed NH₃ in the transient reaction over 1.8 % Cu loaded CHA and MOR zeolites. In the case of MOR zeolite, consumed NO was almost equal to the amount of Cu, and consumed NH₃ was 2.5 times larger than NO. In the case of CHA zeolite, consumed NO was slight smaller than Cu, and consumed NH₃ was 2.3 times larger than NO. It is shown by the consumed amount of NO that the almost all of contained Cu on both zeolites is isolated species that can be reduced by NO + NH₃. Moreover, it is shown by the calculated molar ratio of NH₃/NO that the state of reduced Cu⁺ is almost equal on both zeolites. The observed NH₃/NO molar ratio is smaller than that predicted from the Eq. (1). This result can be explained by the contribution of the following two equations:



In summary, it is suggested that the amount of isolated Cu ion and the state of Cu⁺ complex during the NH₃-SCR at 473 K is similar on MOR and CHA zeolites from the transient response measurement. Nevertheless, it was observed that the reaction rate per Cu for the MOR zeolite is far smaller than the reaction rate per Cu for the CHA zeolites over whole Cu loading region. Moreover, the reaction rate per Cu for the MOR zeolites was almost constant with increase of the Cu loading while reaction rate per Cu for the CHA zeolites increased with Cu loading. In summary, it is suggested that there are some factors that inhibit increase in the reaction rate along with increase in Cu content (= increase in the density of Cu ion) on the MOR zeolites, and the factor is not due to the accommodation property of isolated Cu ion or the difference in the state of Cu⁺, which is thought to be the complex with high mobility.

A2. Effect of Si/Al Ratio on Reaction Rate for NH₃-SCR at 473 K – CHA, MFI, and *BEA Case

Figure A3 shows the correlation between the reaction rate for NH₃-SCR at 473 K and Cu loading over Cu ion-exchanged CHA, *BEA, and MFI zeolites with various Si/Al ratio. Note that it is revealed by ICP-AES measurement that Si/Al ratio is 17 after the sodium ion-exchange of *BEA zeolite with Si/Al = 14. As shown in Figure A3, the trend was observed that reaction rates per Cu over lower Si/Al ratio zeolites were larger than those over higher Si/Al ratio ones in the whole Cu loading. Note that reaction rate per Cu on FAU zeolite with Si/Al = 2.8 was far lower than those of any other zeolites with the same Cu loading. Then, it is shown that the high reaction rate for NH₃-SCR is not explained only by the low Si/Al ratio of zeolites. Over all of those zeolites, the reaction rates per Cu increased linearly with increase of the ion-exchange level of Cu. Interestingly, the behavior of the rates per Cu over the MFI and *BEA zeolites as the function of the Cu content were almost parallel to each other. Moreover, the effect of Si/Al ratio of parent zeolites was mainly observed in the extrapolation value at 0 on the plots of each zeolite. On the other hand, the effect of Si/Al ratio of parent zeolites were mainly observed in the slope of lines in the case for the CHA zeolites.

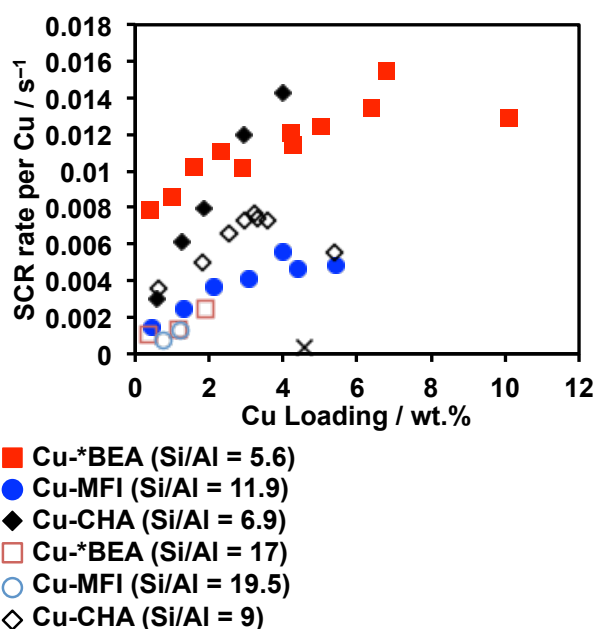


Figure A3. Correlation between the standard NH₃-SCR rate per Cu at 473 K and Cu loading over the MFI (●), *BEA (■), CHA(◆), and FAU(×) zeolites with various Si/Al. The filled symbols show the zeolites with lower Si/Al and the hollow symbols show the zeolites with

higher Si/Al.

Figure A4 shows the relationships between Na ion-exchange level and Cu ion-exchange level of the *BEA and MFI zeolites. The stoichiometric ion-exchange from Na to Cu was observed in the profiles shown in Figure A3, suggesting that almost all Cu is ionic. Moreover, both zeolites have a three-dimensional channel structure and there is no restriction on the pore connectivity. Therefore, it is difficult to explain the difference in the extrapolation value at 0 observed on the plots for *BEA and MFI zeolites under the understanding that the rates for NH₃-SCR are determined only by Cu loading or Cu volumetric density^[S7, 9] regardless of zeolite structures. However, it can be estimated that zeolites without enough Al content in the framework have some inhabitation effect on the reaction compared in the zeolites with the same topology, maybe due to the localized cation exchange site distribution.

In summary, it is suggested that the model zeolites from which the factors are avoided except zeolite topology that might limit the reaction rate should be selected toward the comparative study on the catalytic activity for NH₃-SCR. In this line of consideration, the “cation density in micropores” was defined.

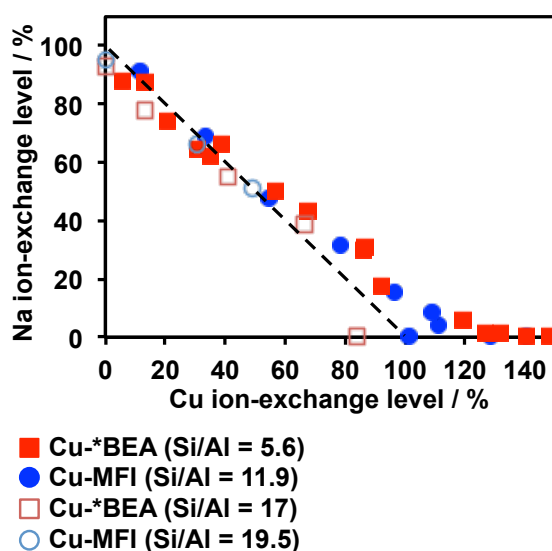


Figure A4. Correlation between the Na ion-exchange level and Cu ion-exchange level of the *BEA (Si/Al = 5.6; ■), *BEA (Si/Al = 17; □), MFI (Si/Al = 11.9; ●), and MFI (Si/Al = 19.5; ○) zeolites. Na ion-exchange level were calculated at Na/Al = 1 as 100 % because the sodium ion is monovalent. Cu ion-exchange level were calculated at Cu/Al = 0.5 as 100 % because the copper ion is divalent.

References

- [A1] C. Paolucci, A. A. Parekh, I. Khurana, J. R. Di Iorio, H. Li, J. D. A. Caballero, A. J. Shih, T. Anggara, W. N. Delgass, J. T. Miller, F. H. Ribeiro, R. Gounder, W. F. Schneider, *J. Am. Chem. Soc.* **2016**, *138*, 6028.
- [A2] F. Gao, D. Mei, Y. Wang, J. Szanyi, C. H. F. Peden, *J. Am. Chem. Soc.* **2017**, *139*, 4935.
- [A3] C. Paolucci, I. Khurana, A. A. Parekh, S. Li, A. J. Shih, H. Li, J. R. Di Iorio, J. D. Albarracin-Caballero, A. Yezerets, J. T. Miller, W. N. Delgass, F. H. Ribeiro, W. F. Schneider, R. Gounder, *Science* **2017**, *357*, 898.
- [A4] J. D. Albarracin-Caballero, I. Khurana, J. R. Di Iorio, A. J. Shih, J. E. Schmidt, M. Dusselier, M. E. Davis, A. Yezerets, J. T. Miller, F. H. Ribeiro, R. Gounder, *React. Chem. Eng.* **2017**, *2*, 168.
- [A5] Database of Zeolite Structures, <http://www.iza-structure.org/databases/>.
- [A6] Y. Shan, X. Shi, J. Du, Y. Yu, H. He, *Catal. Sci. Technol.* **2019**, *9*, 106.

List of Publications

Publications related to this thesis

- [1] **Yusuke Ohata**, Toshiki Nishitoba, Toshiyuki Yokoi, Takahiko Moteki, and Masaru Ogura, Effect of zeolite topology on Cu active site formation for NO direct decomposition, *Bull. Chem. Soc. Jpn.* **2019**, *92*, 1935–1944.
- [2] **Yusuke Ohata**, Hiroe Kubota, Takashi Toyao, Ken-ichi Shimizu, Takeshi Ohnishi, Takahiko Moteki, and Masaru Ogura, Kinetic and spectroscopic insights into the behaviour of Cu active site for NH₃-SCR over zeolites with several topologies, *Catal. Sci. Technol.* *in press*. DOI: 10.1039/d0cy01838d
- [3] **Yusuke Ohata**, Takeshi Ohnishi, Takahiko Moteki, and Masaru Ogura, High NH₃-SCR reaction rate with low dependence on O₂ partial pressure over Al-rich Cu-*BEA zeolite, *RSC Adv.* *submitted*. Manuscript ID: RA-ART-02-2021-000943

Other Publications

- [1] Takuo Minato, Kosuke Suzuki, **Yusuke Ohata**, Kazuya Yamaguchi, and Noritaka Mizuno, A modular synthesis approach to multinuclear heterometallic oxo clusters in polyoxometalates, *Chem. Commun.* **2017**, *53*, 7533–7536.
- [2] Takuo Minato, **Yusuke Ohata**, Kazuyuki Ishii, Kazuya Yamaguchi, Noritaka Mizuno, and Kosuke Suzuki, Exploring orientationally aligned anisotropic large spin molecules with unusual long-distance intermolecular ferromagnetic interactions, *J. Mater. Chem. C* **2019**, *7*, 12918–12925.
- [3] **Yusuke Ohata**, Takeshi Ohnishi, Takahiko Moteki, and Masaru Ogura, Catalytic Activities of Cu-Zeolite Catalysts for Several deNO_x Reactions, *Shokubai* **2019**, *61*, 353–359 (Review, Japanese).
- (大畠悠輔, 大西武士, 茂木堯彦, 小倉賢, 種々の NO_x 浄化反応に対する銅イオン交換ゼオライトの触媒特性, *触媒*, **2019**, *61*, 353–359.)